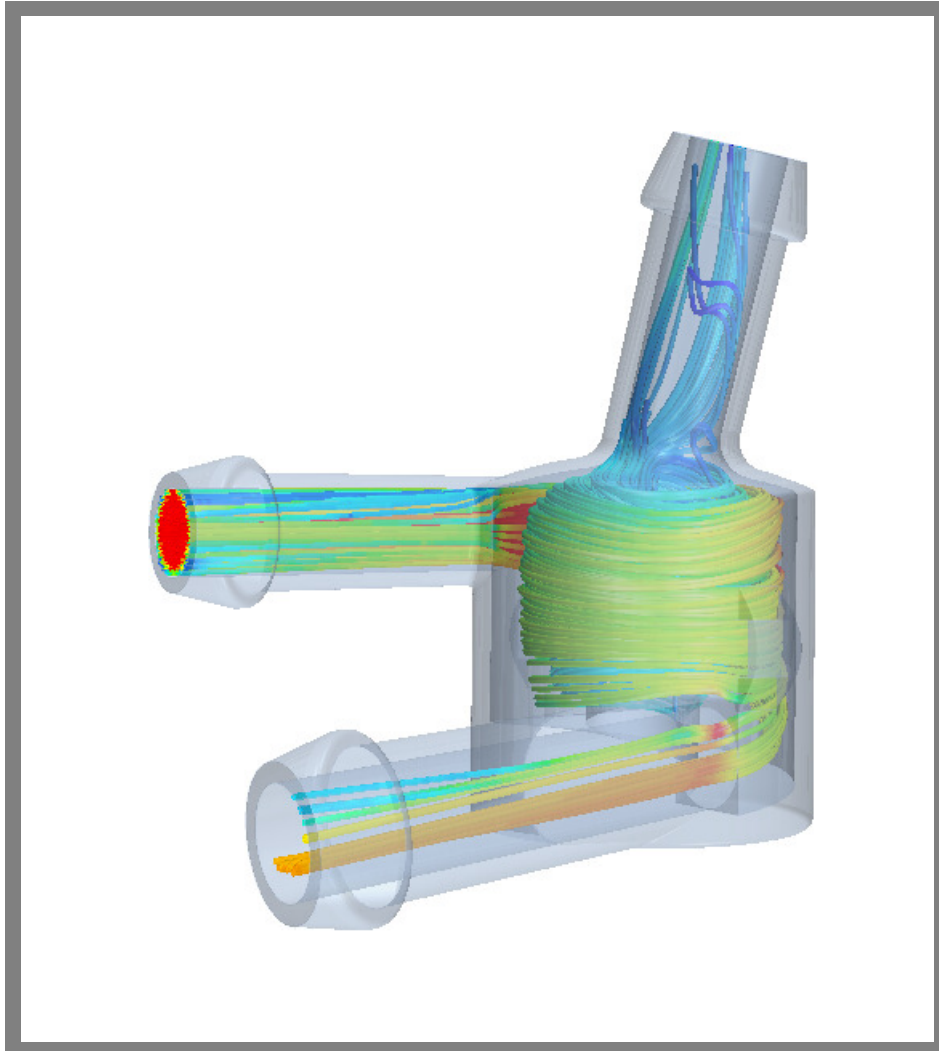




CHALMERS
UNIVERSITY OF TECHNOLOGY



Testing and Modeling of Air Elimination in Automotive Cooling System

Master's Thesis in Applied Mechanics

JOHAN FORSGREN
DAVID WINQVIST

Department of Mechanics and Maritime Sciences
CHALMERS UNIVERSITY OF TECHNOLOGY
Gothenburg, Sweden 2018

MASTER'S THESIS 2018:64

**Testing and Modeling of Air Elimination
in Automotive Cooling System**

JOHAN FORSGREN
DAVID WINQVIST



CHALMERS
UNIVERSITY OF TECHNOLOGY

Department of Mechanics and Maritime Sciences
Division of Fluid Dynamics
CHALMERS UNIVERSITY OF TECHNOLOGY
Gothenburg, Sweden 2018

Testing and Modeling of Air Elimination in Automotive Cooling System

JOHAN FORSGREN, DAVID WINQVIST

© JOHAN FORSGREN, DAVID WINQVIST, 2018.

Supervisor: Ulf Nilsson, 1st CAE Engineer, System development cooling system, Volvo Cars

Examiner: Prof. Lars Davidson, Mechanics and Maritime Sciences, Chalmers

Master's Thesis 2018:64

Department of Mechanics and Maritime Sciences

Division of Fluid Dynamics

Chalmers University of Technology

SE-412 96 Gothenburg

Telephone +46 31 772 1000

Cover: Air flow through the optimized design visualized with streamlines. The velocity magnitude of air is shown as scalar field.

Gothenburg, Sweden 2018

Testing and Modeling of Air Elimination in Automotive Cooling System
JOHAN FORSGREN
DAVID WINQVIST
Department of Mechanics and Maritime Sciences, Division of Fluid Dynamics
Chalmers University of Technology

Abstract

The increasing environmental awareness in modern society pushes various fields to become more energy efficient, not least the automotive industry. The emerging electrification and the increased complexity of vehicles brings high demands on temperature regulation and the cooling system. Studies have shown that entrapped air in the cooling system does have negative effects on its performance and also causes deterioration of its components. In order to relieve the system from this unfavorable air, different kinds of separators are commonly used.

This thesis investigated the use of cyclone separators in a vehicle cooling system. The aim of the project was to increase the knowledge regarding separators and provide Volvo Cars Corporation with a design suggestion. Simplified lab experiments on a transparent separator were used to validate a steady state, Eulerian-Eulerian CFD model in the computational software STAR-CCM+. The phases were evaluated using the Reynolds Stress Turbulence and turbulence response models. The computational model was utilized in combination with a parametric CAD-model to evaluate various design aspects which were found relevant based on a literature survey. A design of experiments was conducted and using the optimization toolbox of the commercial software modeFRONTIER, a final design suggestion was presented. A 3D-printed model was used for verification of the final design in the lab test rig.

The thesis has provided relevant information regarding different design parameters' effect on separation efficiency, pressure drop and volume of the separator. The work has also shown the significance of the flow structures and bubble size entering the separator. Finally, the optimized design of the separator shows clear performance improvements in comparison to the reference model.

Keywords: Cyclone separator, Cooling system, Air extraction, Degas, Bubble size, Multiphase, Eulerian-Eulerian, Optimization, DOE, CFD.

Acknowledgements

The work presented was performed at the Department of Mechanics and Maritime Sciences and the Division of Fluid Dynamics at Chalmers University of Technology, Gothenburg as a 30 ECTS Master's thesis. The project was started in February and presented in June of 2018. The main work of the thesis has been conducted in collaboration with the cooling system department at Volvo Cars Corporation (VCC) in Torslanda, Sweden.

During the process of this Master's thesis many people have been involved in one way or another and everyone of them deserves to know that we truly appreciate their support. First of all, we would like to acknowledge our supervisor, Ulf Nilsson (1st CAE Engineer, System development cooling system, Volvo Cars), for your support throughout the whole project. You have provided us with valuable information and guidance and despite being on parental leave for some period, helped us to reach the project goals. We would also like to extend our gratitude to Lars Davidsson (Professor, Head of Division Fluid Dynamics, Chalmers University of Technology) for taking the role as our examiner during this project. Further, we would like show gratitude to persons that, within their area of expertise, have guided us through the various parts of the work. Andre Larsson (Model and Design Prototypes, Volvo Cars) was of great help when constructing the test rig with extraordinary precision. Aristotelis Babajimopoulos (Technical Expert, Fluid Dynamics and Heat Transfer, Volvo Cars) instructed us in the usage of modeFRONTIER and within the field of optimization. Gustaf Granbom (Analyze Engineer, Volvo Cars) was very helpful during the experimental phase of our project. For the set up of our computational model, Huadong Yao (Researcher, Chalmers University of Technology) and Roman Thiele (Dedicated Support Engineer for Volvo Cooling Systems, Siemens) have been supportive and provided us with valuable information by sharing their knowledge. Andreas Folkesson (CAD GSI, Volvo Cars) provided us with a parametric CAD model of the separator which truly streamlined our project. Samuel Swedenborg (CAE Engineer Cooling System) helped us during the project and came with good advice. Rickard Camp (Volvo Cars) and Oskar Johansson provided help with prototype manufacturing. In addition we would like to thank Linda Bodforss (Manager, System development cooling system, Volvo Cars) for giving us the opportunity to perform this project.

Finally we want to thank the company of Volvo Cars Corporation and all its employees for having us. We were during our time at Volvo provided with all tools necessary to perform our work and have had nothing but a great experience.

Johan Forsgren, David Winqvist, Gothenburg, June 2018

Contents

Nomenclature	xi
1 Introduction	1
1.1 Background	1
1.2 Project Purpose and Definition	2
1.3 Project Delimitations	2
2 Theory	3
2.1 Vehicle Propulsion Cooling System	3
2.2 Air Introduction and Elimination	4
2.2.1 Cyclone Separators	4
2.3 Previous Work and Findings	4
2.3.1 Design Parameters of Interest	6
2.4 Multiphase Flow Theory	7
2.4.1 Fluid Motion	7
2.4.2 Eulerian-Eulerian	7
2.4.3 Eulerian-Lagrangian	8
2.4.4 Choosing Multiphase Model	8
2.4.5 Phase Interaction	9
2.5 Computational Theory	11
2.5.1 Meshing	11
2.5.2 Turbulence	13
2.5.3 Discretization Methods	15
2.6 Optimization Theory	16
2.6.1 Design of Experiments	16
2.6.2 modeFRONTIER	17
2.6.3 Optimization Algorithms	18
3 Method	20
3.1 Experimental Tests	20
3.1.1 Physical Separator Model	20
3.1.2 Test Rig Design and Test Execution	21
3.1.3 Measurements	21
3.2 Simulations	22
3.2.1 Meshing	22
3.2.2 Model Set Up	24
3.3 Parametric Study	29
3.3.1 Parametric Catia Model	29
3.3.2 Method of Evaluation	31
3.4 Optimization	33
3.4.1 Parametric Study Based Optimization	33
3.4.2 Design of Experiments	34
3.4.3 DOE Optimization	35
3.4.4 Manual Optimization	36
3.5 Optimized Design Evaluation	36

4 Results and Discussion	38
4.1 Experimental Tests	38
4.1.1 Pressure Drop	38
4.1.2 Coolant Temperature	38
4.1.3 Separation Performance	39
4.1.4 General Visual Findings	40
4.2 Simulations	40
4.2.1 Validation of CFD Model	40
4.3 Parametric Study	44
4.4 Optimization	48
4.4.1 Parametric Study Optimization	48
4.4.2 DOE Optimization	48
4.4.3 Manual Optimization	50
4.4.4 Choice of Design and Optimization verification	51
4.5 Improved Design Evaluation	52
4.6 Overall Discussion	54
5 Conclusion	57
6 Future Work	58
Bibliography	a
Appendix A	c

Nomenclature

Abbreviations

AER	Air Extraction Rate
AMUSIG	Adaptive Multiple Size-Group
CAD	Computer Aided Design
CAE	Computational Aided Engineering
CFD	Computational Fluid Dynamics
DNS	Direct Numerical Simulation
DOE	Design Of Experiments
ECTS	European Credit Transfer System
FVM	Finite Volume Method
GLCC	Gas Liquid Centrifugal Cyclone
LES	Large Eddy Simulation
MOPSO	Multi-Objective Particle Swarm Optimization
PBE	Population Balance Equations
RANS	Reynolds-Averaged Navier-Stokes
RSM	Response Surface Methodology
RST	Reynolds Stress Transport
SST	Shear Stress Transport
ULH	Uniform Latin Hypercube
VCC	Volvo Car Corporation
VOF	Volume Of Fluid

List of Symbols

α	Volume fraction
\bar{f}_k	Objective function
β	Volumetric thermal expansion
Δ	Delta
δ_{ij}	Kronecker delta
\dot{m}	Mass flow rate

η	Separation efficiency
λ	Thermal conductivity
μ	Dynamic viscosity
μ_t	Turbulent viscosity
∇	Nabla operator
ν	Kinematic viscosity
Φ	Importance factor
ϕ	Arbitrary variable
Π	Pressure strain term
ρ	Density
σ_h	Turbulent thermal diffusion Prandtl number
τ'_{ij}	Reynolds stress tensor
τ_{ij}	Viscous stress tensor
θ'	Temperature fluctuation
ε	Turbulent dissipation
a	Acceleration
A_D	Linearized drag coefficient
C_t	Turbulence response function
$C_{L,eff}$	Effective lift coefficient
C_{VM}	Virtual mass coefficient
D_t	Turbulent diffusion term
F	Force
f	Body force
g	Gravitational acceleration
h	Enthalpy
M	Sum of inter-phase forces
m	Mass
p	Pressure
Q	Inter-phase heat transfer
T	Temperature
u	Velocity
V	Volume
v_i	Relative drift velocity
y^+	Dimensionless wall distance

1

Introduction

In this chapter, an introduction to the project will be presented. The chapter will focus on providing information regarding the reasons for conducting the project and also give an understanding of its relevancy. Furthermore the project purpose and the delimitations will be presented.

This thesis was performed at the Cooling System Department at Volvo Cars Corporation (VCC) in Gothenburg, Sweden, during the spring of 2018.

1.1 Background

In recent years the importance of the environmental effects of the vehicle industry has continued to increase. This has led to higher demands on the final product and that every part of the vehicle needs to be properly designed for its purpose. The powertrain of the vehicle is thus pushed to its limits and also the need to keep all the parts at a suitable temperature. As cars become more technically advanced, additional parts such as computers are also in the need of temperature regulation. The emerging electrification of cars also brings increased demands on the cooling system. This is due to the less temperature resistant materials of electrical components in comparison to the parts of a conventional combustion engine. Also, the preferred working temperature of these new systems is closer to the ambient temperature which is challenging for a cooling system.

The cooling system is evidently an important part of a vehicle, both for electrified and conventional combustion engines. The systems are getting more complex with additional heat sensitive components and a wider range of optimal working temperatures. As cooling systems are getting more attention it has been found that entrapped air has strong negative effects on the performance of the cooling system as well as the lifetime of its components [1]. Locations where the air is trapped will suffer from hot spots which can lead to thermal stress, fatigue and eventually cracking. The entrapped air will also reduce the performance of the coolant pump which will lead to reduced flow rate and thus reduced capacity of the heat transfer. Also, if there is entrapped air in the system there is a risk that cavitation occurs which can cause deterioration of the pump [2]. Hence, to ensure durability and performance of the components and the vehicle, any improvements to reduce the risk of air in the system or improving the air extraction ability of the system are beneficial.

Traditionally, the elimination of air from the cooling system has been achieved by leading the flow through the expansion tank where the air is separated from the coolant due to the gravitational effect. Although, with the increased complexity and additional components of the modern car, multiple cooling circuits are required to account for the wide range of optimal working temperatures. The air elimination for each circuit could be achieved via the expansion tank but this would lead to an unwanted energy exchange between flows at different temperatures, which would result in reduced cooling performance. Also, the additional piping this would imply is disadvantageous with respect to cost and packaging [3]. To circumvent this problem, the solution at Volvo Cars is the usage of a separator which eliminates air from the low temperature circuit. The air is transported, via a one-way coupling, to the high temperature system where it is finally eliminated in the expansion tank. Even though the solution has solved the air elimination without risk of energy exchange between the cooling circuits, more knowledge about the separator performance is needed. In order to minimize the size, the pressure losses as well as maximizing the efficiency of the separator, a thorough investigation is of interest.

1.2 Project Purpose and Definition

The purpose and goal of this Master's thesis is to provide Volvo Cars with a deeper knowledge about separators and the importance of the various separator design parameters to facilitate future product development. The results are presented in terms of an effective calculation method to predict coolant pressure drop and air separation efficiency for the separator as well as a suggested improved separator design.

The problem can further be divided into a number of questions which are evaluated during the project. In this manner a simplified overview of the project is achieved. Note that the questions are not answered explicitly but were used as guidance in order to reach the project goal.

- How does the separator of the cooling system work today?
- What are the most important design parameters for the performance of a separator?
- How can a lab test be set up to replicate the most important features of the cooling system for evaluating the performance of the separator?
- How can a computational model be set up, using multiphase flow, to achieve the same or at least the same trends as the lab test?
- What effects does changing different design parameters have on the pressure drop, the size and the efficiency of the separator?
- How can optimization tools be used in order to find an optimum design of the separator?
- Does the optimum design, extracted from the computational models, also show improved results in actual lab testing?

1.3 Project Delimitations

To be able to perform the project within the given time frame, a few delimitations had to be made. The delimitations of the project are given as bullets below.

- This thesis focuses on the electric drive cooling circuit and its separator. Hence, flow rates and air volume fractions are adapted for these conditions.
- Only the flow through the separator and the pipes connected to it are evaluated. That is, the flow in the rest of the system is out of the scope.
- Only separators of cyclonic kind are evaluated.
- All the various designs tested in the simulations are not replicated in an actual lab test. Only an initial validation of the simulation method are performed, as well as an experimental test of the final design.
- Geometrical changes in the CAD model are performed in a parametric model, hence the configuration possibility is restricted to these parameters.

2

Theory

In this chapter, the relevant theory for understanding the project can be found. It starts with general information regarding cooling systems and separators. Thereafter the chapter treats multiphase flow modeling and finally some theory regarding design of experiments and optimization.

2.1 Vehicle Propulsion Cooling System

A cooling system works by exchanging heat between different medium to achieve a suitable temperature of the working parts of the engine. In modern cars, the most commonly used cooling method is a liquid based cooling system [4]. The cooling liquid, or coolant, is transported through the engine bay, extracting redundant heat from the engine. The warm fluid is thereafter transported to a thermostat which determines if the fluid needs cooling or can be circulated back to the engine. If the coolant temperature is above the optimal temperature limit it is transported to the radiator to be cooled down. In the radiator the flow is divided into a fine net of small tubes of a material with good heat transfer abilities. The increased wetted area improves the heat transfer abilities and the forced convection, applied via the motion of the car and/or a fan, cools the fluid and thus removes the heat from the system [4].

The electrification of cars results in different components of the car requiring different working temperatures. Therefore multiple cooling systems are needed to provide the various desired temperatures. An example of such a system can be found in Figure 2.1 where the layout of a cooling system in a hybrid electric vehicle is displayed. Two cooling circuits are shown in the figure, the high temperature circuit (black) and the low temperature circuit (yellow) which are used to cool the combustion engine and the electric drive components, respectively. The circuits are connected via the separator and this connection has two purposes. It is utilized to transport coolant to the yellow circuit during filling and is also used to let eliminated air escape the same circuit. Hence, there is no continuous flow of coolant between the two circuits.

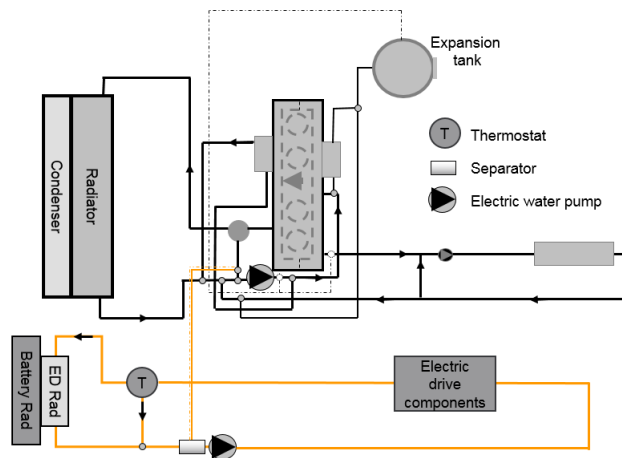


Figure 2.1: Cooling system layout for a hybrid electric vehicle. Note that some components have been left out from the figure for confidentiality reasons.

2.2 Air Introduction and Elimination

There are various reasons why air is introduced into a cooling system. One reason is that air enters the system while the engine is running, due to a leakage. Although, in a well functioning system this should not occur. Other sources of air which are much more difficult to avoid are in the filling process and the fact that air can be dissolved in the coolant. Getting entrapped air during filling is considered unavoidable and therefore there is a need to eliminate this as a post-fill process [1]. A standard engine cooling system uses the fact that air will rise to the highest points in the system due to buoyancy. One of these points is the top of the radiator from which the air is led to the expansion tank through a hose. If this air elimination is insufficient an additional device can be added to the system to help eliminate the air. This device is referred to as a separator.

There are two common types of separators: gravitational and centrifugal [1]. In a gravitational separator the flow is slowed down due to a relatively large separator volume. This leads to a buoyancy controlled motion of the gas, which can rise through the coolant and be evacuated through the top of the separator. A downside to the gravitational separator is the required volume. The engine bay of modern cars contain a large number of components and the packaging is crucial. The centrifugal separator is more suitable from a size perspective. Instead of slowing down the flow, the centrifugal separator creates a vortex which gives rise to a pressure gradient and the air is separated due to the density difference. With this method there is no need to have a large volume and hence it is more favorable when having packaging limitations. Centrifugal separators are also known as cyclone separators.

2.2.1 Cyclone Separators

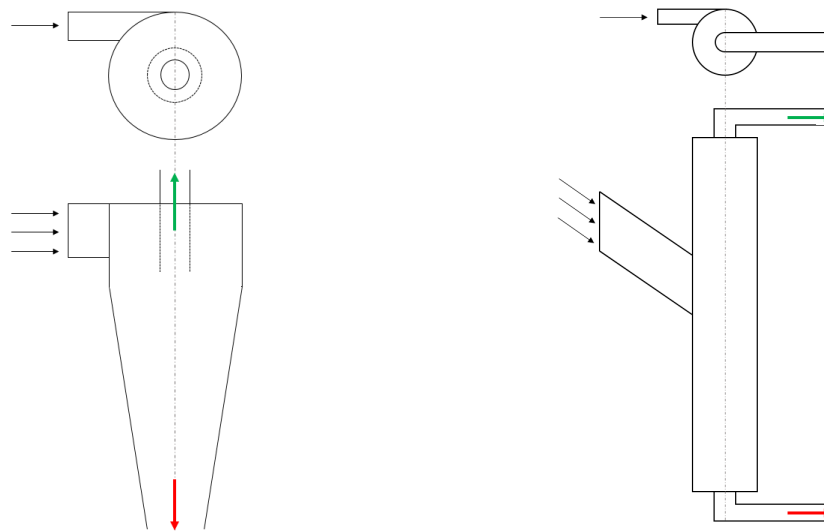
As the efficiency of various processes in close to all industries continues to receive more attention, the use of separators has grown [5]. The separation between solids and gas or liquid are widely used within mining industries etc. However, Gas Liquid Centrifugal Cyclones (GLCC) are mainly used within the petroleum industry. Cyclone separators are cheap and robust, since they do not have any moving parts. The fact that they are generally smaller than a conventional gravitational separator is another reason for cyclone separators becoming more popular [5][6].

The working principle of a cyclone separator is simple. The multiphase flow is tangentially injected into the circular cyclone. The curvature of the cyclone forces the flow into a centrifugal motion resulting in a favorable pressure gradient towards the centre of the cyclone. Separation of the phases is thus reached as the light weight phase is forced towards the centre of the cyclone and the heavier phase is pressed against the circumferential of the device. The goal is then to achieve an up moving vortex in the centre of the cyclone and a down moving vortex towards the edges, which separates the phases of the flow [6][7]. In addition, the inlet is generally placed in the upper part of the cyclone. This is in order to, apart from the centrifugal force, also take advantage of the gravitational force when separating the flow. An example of a generic design of a cyclonic solid-gas separator can be found in Figure 2.2a. The cyclone is slightly larger in the top in order to provide space for the interior up moving vortex. In the top it can be seen that the gas outlet goes down slightly into the cyclone. This design feature serves to shield the inner vortex from the fast moving inlet flow as well as to stabilize the swirling motion [7].

Figure 2.2b shows a general design of a gas-liquid separator in the petroleum industry. The inlet is placed slightly lower and the dimensional height to width ratio is larger than for a gas-solid separator. The gas-liquid separator is however less stable in its performance than the gas-solid separator, and the efficiency of the separation depends strongly on the flow velocity [6].

2.3 Previous Work and Findings

A literature study was continuously performed during the project to find information about similar studies which would give guidelines for the evaluation of separators. In the search for relevant



(a) Solid-gas cyclone separator.

(b) Gas-liquid cyclone separator.

Figure 2.2: Generic designs of separators. Black arrows are multiphase inlets, red arrows are high density outlets and green arrows are low density outlets.

literature it was found that very little publicly available research has been done in this area, which has also been confirmed by other authors [8]. Only a few papers regarding separators for automotive cooling systems have been found and most of the research lies in the oil industry for gas-liquid cylindrical cyclones. Although, even in this area the amount of studies is moderate [9]. Two papers were found relevant for this project and were evaluated further. These have been used as guidance for pre-processing, physics setup, post-processing and design. A brief summary of the two reports are given below.

The Characterisation of a Centrifugal Separator for Engine Cooling Systems

The study [8] treats both experimental testing and CFD simulations of a commercially available centrifugal separator. The objective was to perform a benchmark case for the separation efficiency as well as analyzing the flow characteristics. The simulations were performed in STAR-CCM+ and both Eulerian-Lagrangian and Eulerian-Eulerian models were evaluated, where the latter approach was deemed to be most suitable. The simulations were performed under steady state conditions for four different flow rates of coolant and three different volume fractions of air. The same conditions were used in the experimental rig tests. The results from the CFD simulations were presented as velocity, pressure and volume fraction fields and the separation efficiency was presented as a function of volume fraction and compared to the experimental data. The CFD simulations tended to predict the separation efficiency to the same order of magnitude as the experimental data but were unable to capture the same trends.

Numerical Analysis of Fluid Flow in a Compact Phase Separator

In [10] the objective was to perform a numerical investigation of a separator in the software FLUENT, in order to know how to design with respect to minimum pressure drop and maximum separation efficiency. Also this study was performed in a steady state condition but with a single volume fraction of 10 % and varying inlet velocities between 5 and 20 m/s. The study used a Eulerian multiphase mixture model. The results were presented as velocity, pressure and volume fraction fields. Also, the separation efficiency and the pressure drop are presented as functions of inlet velocity. Among the conclusions it can be found that the efficiency and the pressure drop increase with increasing inlet velocity.

2.3.1 Design Parameters of Interest

As mentioned, a low number of previous studies performed on separators in automotive applications have been found. However, slightly more information regarding gas liquid cyclone separators can be found from the petroleum industry. The reports contain information regarding design advice and the importance of different parameters for the performance of the separator. Below, various design parameters will be addressed and the major findings from previous studies regarding the relevance of the parameter will be given.

- **Size and shape of the inlet:** The inlet velocity of the mixture flow is of high importance for the performance of the separator. A low velocity means that a small centrifugal motion will be achieved and the separator will mostly act as a gravitational separator. A low flow rate can also in some cases cause mixing rather than separation in the separator [6]. The velocity of the flow also affects the size of the bubbles coming into the separator which is another important aspect [5]. Thus the inlet size is of great importance for the performance of the separator. The shape of the inlet should preferably be rectangular so that the gas liquid mixture is pushed close to the wall which increases the angular momentum [11][12]. The inlet can also have a converging shape in order to additionally increase the velocity of the flow. However, a too severe one causes high pressure losses [6]. In order to achieve the best separation in a cyclone, the flow regime should according to a study create a double flow reversal. This means that there is down flow in the centre of the cyclone as well as by the wall. In between the two there is a region with upward flow [13].
- **Separator inlet angle:** The angle of the inlet has proved to be of interest for the performance of the separator. It has been found that an inclined inlet can significantly increase the operational envelope of the separator [14]. An increased downward angle leads to higher flow velocities and thus a better separation to the vortex. A very high incline does however cause a large volume of air going into the liquid outlet [15][16].
- **Size and shape of gas outlet:** The efficiency is low for both a large gas outlet as well as a small one. The best alternative is thus somewhere in between [12]. A study also shows that for the separation of gas and oil, the most important aspect on the performance of the separator was the length of the tube to the gas outlet [17].
- **Size and shape of outlet:** Similar trends were shown as for the gas outlet size, a medium size outlet is preferred since a large one as well as a small one gives worse results [12]. The fact that the efficiency is increased with decreasing outlet diameter is verified by [16]. A study for a separator in an AC system of a vehicle shows that out of a few parameters, the gas and liquid outlet shapes and sizes were the most important. A slight change in those parameters can make large variations in the efficiency of the separator [17].
- **Position of inlet and outlet:** In order to maximize the air extraction ability of the separator the inlet position should be placed as high as possible on the separator body [16]. A study has also shown, that in order to create the best separation, one should use several tangential inlets. This would be the way to create double flow reversal which should be profitable for separation [13].
- **Separator shape:** One study shows that the height of a separator should be a minimum of a certain level but it is not beneficial to make it infinitely long [12]. Another study shows that the performance of the separator becomes better with an increasing main diameter [16].

The reports show that, even though the principle of a cylindrical separator is simple, the flow structure can be very complex and therefore hard to model. The number of possible design parameters are few but small differences can have a large effect on the separation ability. Since the inlet size and flow velocity have a great impact on the performance of the separator, it is difficult to design a separator for various particle sizes and flow velocities [6].



(a) Eulerian approach where the particles are monitored as they pass the control volume. (b) Lagrangian approach where every particle is continuously followed. t is time.

Figure 2.3: Eulerian and Lagrangian motion study, the black lines are stream lines.

2.4 Multiphase Flow Theory

Multiphase flow is a common phenomenon in nature and in industrial applications where several phases of different properties share the same domain. Thus, it is of high relevancy to understand and predict this type of behaviour. The phenomenon is generally complex and complicated to represent in a mathematical model due to the collective behaviour of a large number of interacting degrees of freedom [18].

2.4.1 Fluid Motion

The study of fluid motion is divided into two different approaches. These ones are the Eulerian and the Lagrangian frames of reference. In the Eulerian frame of reference the flow is studied from a stationary position while the Lagrangian approach continuously follows the flow [19]. A representation of the two methods can be found in Figure 2.3. For computational evaluation of multiphase flows the two reference frames can be combined into the Eulerian-Eulerian or the Eulerian-Lagrangian approach.

2.4.2 Eulerian-Eulerian

In the Eulerian-Eulerian approach, often referred to as a two fluid model, the carrier phase as well as the dispersed phases of the flow are modelled as a continuum for which the flow equations are solved. The method assumes that two or more phases cannot occupy the same space, and thus one can follow the volume fractions of the flow [10]. The advantages of Eulerian-Eulerian is that it covers a full range of volume fractions. Mean quantities such as volume fraction and velocity can be obtained directly and turbulence can be calculated in each phase with little extra cost. The negative aspects about the method is that modelling particles of various sizes can be complex and particle-particle and particle-wall interactions are not simulated directly [20]. For each phase the conservation equations for mass, momentum and energy are solved. The conservation of mass can be found in Equation 2.1, the momentum in Equation 2.2 and the energy equation is found in Equation 2.3 [18][20][21]. Note that for a single phase problem, all interaction terms are cancelled and $\alpha = 1$. For all the equations, the notations m and n refer to what phase that is evaluated.

$$\frac{\partial}{\partial t}(\alpha_m \rho_m) + \frac{\partial}{\partial x_i}(\alpha_m \rho_m u_{i,m}) = \sum_{m \neq n} (\dot{m}_{mn} - \dot{m}_{nm}) \quad (2.1)$$

α is the volume fraction, u is the velocity and \dot{m} is the mass transfer rate, index mn and nm is the transfer from m to n and vice versa. Note that the sum of the volume fractions is 1.

$$\frac{\partial}{\partial t}(\alpha_m \rho_m u_{i,m}) + \frac{\partial}{\partial x_j}(\alpha_m \rho_m u_{i,m} u_{j,m}) = -\alpha_m \frac{\partial p}{\partial x_i} - \alpha_m \rho_m g_i + \frac{\partial}{\partial x_j} [\alpha_m (\tau_{ij,m} + \tau'_{ij,m})] + M_{i,m} \quad (2.2)$$

p is the pressure and M is the sum of the inter-phase forces, i.e the drag, turbulent drag, lift, virtual mass and momentum transfer due to mass transfer. g is the gravity. τ and τ' are the viscous and turbulent stresses respectively.

$$\frac{\partial}{\partial t}(\alpha_m \rho_m h_m) + \frac{\partial}{\partial x_i}(\alpha_m \rho_m u_{i,m} h_m) - \frac{\partial}{\partial x_i} \left[\alpha_m \left(\lambda_m \frac{\partial T_m}{\partial x_i} + \frac{\mu_t}{\sigma_h} \frac{\partial h_m}{\partial x_i} \right) \right] = Q_m \quad (2.3)$$

λ is the thermal conductivity, T is the temperature and Q is the heat transfer between the phases. h is the enthalpy, μ_t is the turbulent viscosity and σ_h is the turbulent thermal diffusion Prandtl number.

2.4.3 Eulerian-Lagrangian

In the Eulerian-Lagrangian approach, also known as Lagrangian Particle Tracking, the carrier phase is treated as a continuum and the governing equations are defined in the Eulerian framework, just like in single phase flow. The dispersed phase is described as a discrete number of particles and each particle is tracked by solving the equation of motion in the Lagrangian framework [22]. The particles are smaller than the grid used for the Eulerian framework, hence the interaction between the phases has to be modeled. The phases interact through exchange of mass, momentum and heat. For flows with a small amount of particles, each particle can be tracked through the domain but many problems deal with larger amount of the dispersed phase. In this case a statistical approach can be used where particles are gathered in a cloud, a so called parcel, where every particle in the parcel shares the same properties. Instead of tracking individual particles the parcels are tracked to represent the full population of particles [23]. Depending on the characteristics of the flow, the choice can be made to model with a one-, two or four-way coupling. In a one-way coupling only the continuous phase affects the dispersed phase while in a two-way coupling both phases affect each other. In a four-way coupling there is also interaction between the dispersed particles. The advantage with the Eulerian-Lagrangian method is that it handles well polydisperse flows, heat and mass transfer problems and flows including chemical reactions [18].

The governing equations for the continuous phase are the Navier-Stokes equations, see Equations 2.1 - 2.3. The governing equation for tracking the particles is the linear momentum conservation equation, recognized as Newton's second law in Equation 2.4.

$$m_p \frac{du_{i,p}}{dt} = F_{i,s} + F_{i,b} \quad (2.4)$$

m_p is the mass of the particle, $u_{i,p}$ is the particle velocity, $F_{i,s}$ is the resultant of the surface forces and $F_{i,b}$ is the resultant of the body forces. The surface force can be divided into several forces such as drag force, pressure gradient force and lift force. Additional forces can be added depending on relevance for the problem.

2.4.4 Choosing Multiphase Model

Multiphase behaviour is an inherently difficult area and are in general complex to model. There are guidelines of how to define your problem even though they are often vague and open for interpretations. The choice of multiphase model and phase interactions is therefore not straight forward. Thus, finding the correct model and phase interaction often requires an iterative procedure where the correct settings are slowly built up [18].

In a computational software such as STAR-CCM+ a number of models exist where most are based on one of, or a mixture of, the models Eulerian-Eulerian or Eulerian-Lagrangian. Some of the models are simplifications of the previously mentioned models which, at the cost of some accuracy, might produce a less costly solution [23]. The choice of model and phase interaction properties comes down to the properties of the flow such as volume fractions, particle size and what aspects of the flow that are of interest to evaluate. An additional difficulty is that in a flow domain, many different flow regimes may exist, see Figure 2.4 [23].

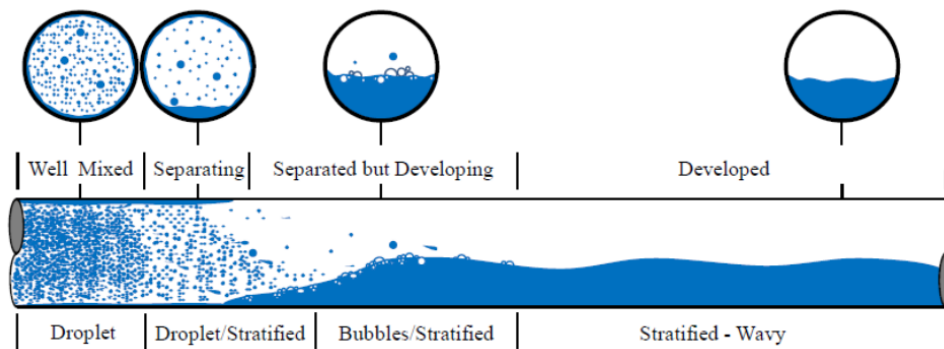


Figure 2.4: Display of various flow regimes [23].

There are several techniques for solving the different flow regimes. For stratified flows which can be seen in the right part of Figure 2.4, a distinct large scale interface is present. A typical choice would be to use an interface tracking/capturing method. Such methods are front-tracking, level set or volume of fluid (VOF), which are methods where the interface between phases is tracked [23]. For the droplet flow in the leftmost region of Figure 2.4 both Eulerian-Eulerian and Eulerian-Lagrangian approaches can be applied. Which one to choose is a matter of domain size, volume fractions, polydispersity, phase interactions, phenomena of interest etc. For flows in the mid region a combination of previously mentioned techniques might be suitable [23].

2.4.5 Phase Interaction

In addition to choosing the most suitable method for solving the problem, there are a number of phase interaction physics that are of importance in order to acquire a satisfactory solution. The choice of how to model the phase interactions affects the level of how the phases influence each other. In this section a number of the more crucial and mostly used interaction models are described. Note that these interaction models have been regarded from an Eulerian-Eulerian perspective. Similar phase interaction models exist for Eulerian-Lagrangian approach but are modeled with minor differences.

Drag Force

The drag force is the resistant force that a particle from the dispersed phase experiences due to its relative velocity to the continuous phase. The force is calculated as per Equation 2.5

$$F_i^D = \frac{1}{2} \rho_c C_D |u_{j,rel}| u_{i,rel} \frac{A}{4} \quad (2.5)$$

where $u_{i,rel}$ is the relative velocity between the continuous and dispersed phase and A is the particle area "seen" by the flow. Index c represents the continuous phase. The drag coefficient, C_D , can be modelled using a scalar value, neglecting the fact that a cluster of particles or bubbles experiences a different drag force than a separate one. A more sophisticated model such as Schiller-Naumann, Tomiyama or Bozzano-Dente takes cluster effects as these into account and are all suitable for gas-liquid flow. Each model has its specific qualities and one need to choose the most suitable one [23][24]. The Tomiyama drag coefficient model is suitable for a wide range of flow conditions. In a pure state, i.e. no contamination, the Tomiyama drag coefficient is computed as per Equation 2.6

$$C_D = \max \left[\min \left(\frac{16}{Re} (1 + 0.15 Re^{0.687}), \frac{48}{Re} \right), \frac{8 Eo}{3(Eo + 4)} \right] \quad (2.6)$$

where Re is the Reynolds number based on the relative velocity and Eo is the Eotvos number.

Lift Force

In cases of swirling flow or non uniform continuous flow, the dispersed phase is affected by a lift force in perpendicular direction to the flow velocity. The lift force is calculated as per Equation

2.7 where $C_{L,eff}$ is the product of the lift coefficient and the correction factor, depending on the interaction area density model in STAR-CCM+. The notation d represents the dispersed phase [23][24][25].

$$F_i^L = C_{L,eff} \alpha_d \rho_c [u_{j,rel} \times (\nabla \times u_{i,c})] \quad (2.7)$$

A Tomiyama model is also available for the lift coefficient and just like the Tomiyama drag coefficient it relates the coefficient to Reynolds number and Eotvos number.

Virtual Mass

The continuous flow affects the acceleration of a bubble or a particle from a dispersed flow through its inertia. In an inviscid flow, this force can be modelled as a virtual mass which is the mass of the continuous phase that the dispersed particle displaces multiplied with a constant. The feature of adding a virtual mass can make flow structures and the acceleration of particles more realistic. It is especially helpful in swirling flow and can in addition make convergence easier. The virtual mass added through the relative acceleration is calculated according to Equation 2.8. C_{VM} is the constant for the interaction and a represents the acceleration of the phases. In case particle mass is not changing throughout the flow, the acceleration can be calculated as per the material derivative [23].

$$F_i^{VM} = C_{VM} \rho_c \alpha_d (a_{i,c} - a_{i,d}) \quad (2.8)$$

Turbulent Dispersion Force

The turbulent dispersion force is of high importance for the distribution of the volume fraction of the dispersed phase. It can be explained as when a region of high concentration of the dispersed phase is affected by interphase drag from the continuous phase turbulent eddies. The force acts as the transfer of momentum in between the phases [23][24]. The turbulent dispersion force is calculated as

$$F_i^{TD} = A_D v_i \quad (2.9)$$

where F_i^{TD} is the turbulent dispersion force per volume, A_D is the linearized drag coefficient and v_i is a relative drift velocity due to volume fraction weighted definitions of phase velocity [23].

Particle Size

The particle size of the dispersed phase is an important factor of a multiphase problem set up. A simplification that can be made is to set the particle size to be fixed. In that case this parameter is set as the interaction length scale. In addition, interaction area density defines the effective area of which the different phases can affect each other. That is the approximate area which is available for heat, momentum and mass transfer between phases [23].

In multiphase applications the reality is however more complicated and a fixed particle size is seldom the case. Instead factors such as breakup, coalescence, nucleation and dissolution of bubbles or particles creates a wide range of sizes. This is especially common in cases where the dispersed phase is either liquid or gas which have a higher tendency of changing shape than a solid particle. Varying particle sizes are of importance since interfacial terms depend on the surface area and weight of the particles [23][24].

In computational software, models are available for accounting the various bubble or particle sizes of the dispersed phase. This is done by solving population balance equations (PBE) which are combined with the mass and momentum transport equations. The PBE keeps track of the amount of particles having the same size i.e. the particle number density. Simplified computational models reduce the number of different sizes for the moment calculation, making the computations less expensive. In STAR-CCM+ one such model is the S-Gamma which is adapting the particle size distribution to a shape function by accounting for the mean diameter and its variance. In combination, breakup and coalescence probability parameters are applied to set the probability of this

occurring at a bubble or particle collision. Another alternative is to use the AMUSIG method which works in a similar fashion [23][24].

Applying one of these models provides a more realistic representation of the multiphase flow where the dispersed phase exists in several particle or bubble sizes. Using such a model does however imply extra demands on the mesh. The mesh size is crucial for acquiring a reliable solution when modeling multiphase flow. A field of various particle sizes can thus cause divergence problems for a multiphase flow solver [18][23].

Wall Lubrication force

A force which for a rising bubble or particle close to the wall, prevents touching of the wall. This force acts due to the asymmetrical force created by the continuous flow on the dispersed particles where the asymmetry is due to the no slip conditions of the wall surface [23]. This force causes a slight offset from the wall of the peak volume fraction. In STAR-CCM+ this force is modelled as per Antal et al.

2.5 Computational Theory

As the results from a computational model is never better than the quality of the model, the computational set up is of great importance. A deep understanding of the physics of the real situation is necessary in order to represent the case by applying mathematical models. Mesh and solver settings are thus crucial for acquiring trustworthy results.

2.5.1 Meshing

This section explains the types of meshes that are available in the software STAR-CCM+ and the mesh requirements for a multiphase problem. In order to make use of the Finite Volume Method (FVM) the geometric domain must be discretized into a number of computational cells. Before discretizing the volume, a representation of the surface is required. When importing a CAD-model into the CFD software this representation usually comes as a so called tessellation which means that the surface is made up of triangles. These triangles are often skewed and not suitable to base a volume mesh upon, whereby a surface remesher is needed to produce triangles of better quality and a size suitable for FVM modeling. When a good quality surface mesh is obtained the volume mesh can be created with this as a base. There are three main types of volume meshers used in STAR-CCM+: tetrahedral, hexahedral and polyhedral. These are commonly used in combination with a prism layer mesher. Which mesh that is most suitable depends on the specific case but factors to take into account are mesh generation time, solution accuracy, convergence rate and amount of computer memory.

- **Tetrahedral:** The tetrahedral mesh is the fastest to generate and also the cheapest regarding computer memory. The mesh generation makes use of the Delaunay method to construct tetrahedral cells. It is strongly dependent on the quality of the surface mesh which makes the triangulation of the surface crucial to obtain a high quality volume mesh [23].
- **Hexahedral:** The hexahedral mesher, called trimmed mesher in STAR-CCM+, is not directly dependent on the surface mesh quality and is more likely to produce a good quality volume mesh compared to both tetrahedral and polyhedral meshers. The mesh is created by placing a template mesh of hexahedral cells over the computational domain. The input surface then trims the cells, resulting in a domain predominantly made up of hexahedral cells with the outermost cells having cut off corners and edges [23].

- **Polyhedral:** The polyhedral mesh generation is similar to the tetrahedral and requires the same surface preparation. In fact, the polyhedral mesh utilizes tetrahedrals as a base during the mesh generation. A simplified description is that a tetrahedral mesh is created after which cells are merged together, forming polyhedrals with an average of 14 cell faces. The cell count for a polyhedral mesh is approximately five times less than a corresponding tetrahedral mesh [23].
- **Prism layer:** The prism layer mesher is a meshing tool which can be combined with previously mentioned methods. It creates orthogonal prismatic cells along wall boundaries. The purpose is to, with a refined near wall mesh, resolve the boundary layer without decreasing the overall cell size in the domain. It is important to adapt the mesh according to the boundary layer to more accurately predict flow quantities.

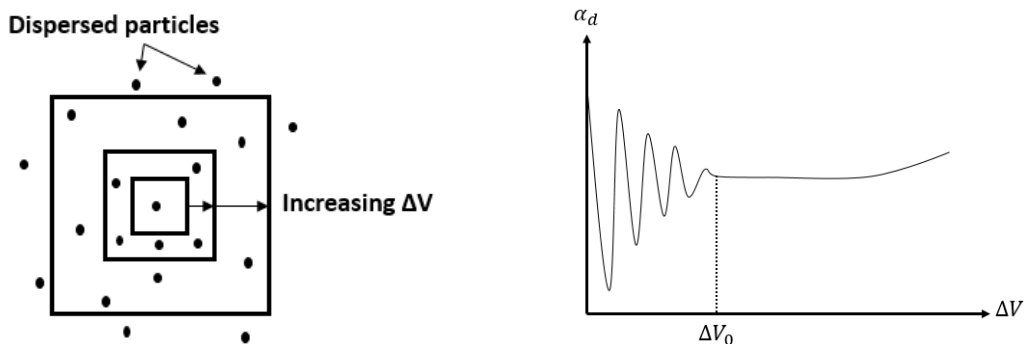
Compared to a single phase problem, the meshing for a multiphase problem comes with greater complexity. The reason is that a multiphase flow has a greater sensitivity to the cell size in the domain and is a consequence of the concept of continuum. Matter is regarded as a continuum if its properties vary continuously in space. The continuum approach is most often not a problem in a single phase flow since the spatial variations takes place at a molecular level which are far below the resolution of the domain. Although, in multiphase flows the variations no longer take place at a molecular level but at a level related to the size of the dispersed particles. An example is illustrated in Figure 2.5 where the volume fraction of the dispersed phase, α_d , is to be computed. The volume fraction is computed as per Equation 2.10

$$\alpha_d = \frac{\Delta V_d}{\Delta V} \quad (2.10)$$

where ΔV is the sampling volume over which the local volume fraction is calculated. As can be seen in the figure, an initial sampling volume contains only one dispersed particle but with an increase in volume the number of particles has grown to six. This leads to high spatial variations until a point, ΔV_0 , is reached where the variations are negligible [26]. The volume fraction can now be defined as per Equation 2.11

$$\alpha_d = \lim_{\Delta V \rightarrow \Delta V_0} \frac{\Delta V_d}{\Delta V} \quad (2.11)$$

However, this concern is more problematic when dealing with the Eulerian-Lagrangian approach where the dispersed phase consists of discrete particles. In the Eulerian-Eulerian framework a volume-averaged statistical approach is utilized, making it less sensitive to changing the mesh size. Although, with a finer mesh some cells can get heavily loaded where gradients are high which can cause problems [27].



(a) Increasing sampling volume.

(b) Sampling volume dependency.

Figure 2.5: The effect of increasing sampling volume.

2.5.2 Turbulence

Flow properties are divided into two large sub domains, laminar and turbulent flow, which can generally be identified using the Reynolds number. In close to all engineering applications turbulent flow is the most prominent [23]. Turbulent flow can be solved exactly using Direct Numerical Simulations (DNS) where all turbulent scales are solved for. The solution does however require large computational power and to mitigate this the smallest scales can be modelled using turbulence models. Various types of modelling methods exist where Large Eddy Simulation (LES) and Reynolds Averaged Navier-Stokes (RANS) are two of the most common ones. LES uses volume averaging where the smaller scales are modelled while scales larger than the grid size are solved. The solution tend to give more accurate transient solutions than the RANS method, but does also require larger computational power [19][23][28].

$$\phi = \bar{\phi} + \phi' \quad (2.12)$$

RANS turbulence models simplifies the Navier-Stokes equations by decomposing them into an averaged part and a fluctuating part respectively, see Equation 2.12. For steady state the averaging can be regarded as time-averaging while for transient solutions an ensemble averaging for repeatable transient solutions. Inserting these quantities into the Navier-Stokes equations results in the Navier-Stokes equations for the mean quantities, also known as RANS. The transport equations for the mean of mass and momentum can be found in Equation 2.13 and 2.14 respectively. Here ρ is the density, \bar{u} and \bar{p} are the mean quantities of velocity and pressure and f_i is the resultant body forces. The averaging procedure forming the RANS equations results in a closure problem due to the additional term τ'_{ij} . The term can be seen in Equation 2.15. The term is known as the turbulent stress tensor, also referred to as Reynolds stress tensor. To resolve this closure problem this term needs to be modeled [19][23].

$$\frac{\partial \rho}{\partial t} + \frac{\partial}{\partial x_i} (\rho \bar{u}_i) = 0 \quad (2.13)$$

$$\frac{\partial}{\partial t} (\rho \bar{u}_i) + \frac{\partial}{\partial x_j} (\rho \bar{u}_i \bar{u}_j) = -\frac{\partial \bar{p}}{\partial x_i} + \mu \frac{\partial^2 \bar{u}_i}{\partial x_j \partial x_j} - \frac{\tau'_{ij}}{\partial x_j} + f_i \quad (2.14)$$

$$\tau'_{ij} = \overline{\rho u'_i u'_j} \quad (2.15)$$

The method of modeling the Reynolds stress tensor can be done using eddy viscosity models where the stress tensor is described as a function of the mean flow quantities. This can be done using the concept of a turbulent eddy viscosity, μ_t . Here, the Boussinesq approximation is the most used. Commonly known eddy viscosity models are $k - \varepsilon$ and $k - \omega$ [23].

The stress tensor can also be solved for by calculating the specific Reynolds stress tensor $R_{ij} = -\tau'_{ij}/\rho$ through solving their governing transport equations. This method is known as the Reynolds Stress Transport (RST) model. It has the advantage that it is more accurate at predicting complex flows than the eddy viscosity models. The model naturally accounts for turbulence anisotropy, streamline curvature, swirl rotation and high strain rates [19][23].

Reynolds Stress Turbulence Model

As previously mentioned the RANS equations can be closed by solving the transport equations for the Reynolds stresses instead of applying eddy viscosity models. The transport equations for $u'_i u'_j$

are as per Equation 2.16.

$$\begin{aligned}
 & \frac{\partial \overline{u'_i u'_j}}{\partial t} + \overline{u}_k \frac{\partial \overline{u'_i u'_j}}{\partial x_k} = \\
 & -\overline{u'_i u'_k} \frac{\partial \overline{u}_j}{\partial x_k} - \overline{u'_j u'_k} \frac{\partial \overline{u}_i}{\partial x_k} + \underbrace{\frac{p'}{\rho} \left(\frac{\partial \overline{u}'_i}{\partial x_j} + \frac{\partial \overline{u}'_j}{\partial x_i} \right)}_{\Pi_{ij}} - \underbrace{\frac{\partial}{\partial x_k} \left[\overline{u'_i u'_j u'_k} + \frac{p' u'_j}{\rho} \delta_{ik} + \frac{p' u'_i}{\rho} \delta_{jk} \right]}_{D_{ij,t}} \\
 & + \nu \frac{\partial^2 \overline{u'_i u'_j}}{\partial x_k \partial x_k} - g_i \beta \overline{u'_j \theta'} - g_j \beta \overline{u'_i \theta'} - \underbrace{2\nu \frac{\partial \overline{u}'_i}{\partial x_k} \frac{\partial \overline{u}'_j}{\partial x_k}}_{\varepsilon_{ij}}
 \end{aligned} \tag{2.16}$$

For further explanation of the different terms, the reader is referred to [19]. In this equation the pressure strain term, Π_{ij} , and the turbulent diffusion term, $D_{ij,t}$, need to be modelled. Using the RST model means that seven equations need to be solved, instead of two as in eddy viscosity models like $k - \varepsilon$ and $k - \omega$. Since the Reynolds stress tensor is symmetric six equations are required and the seventh is the turbulent dissipation ε . The additional equations come with an extra cost in terms of extra computational time. Another disadvantage with this model is that it can be numerically unstable. The advantages are as mentioned previously that the model accounts for turbulence anisotropy, streamline curvature etc. [19][23].

RANS Eddy Viscosity Models

The most commonly used models in commercial CFD codes are the one equation model Spalart-Allmaras, the Realizable $k - \varepsilon$ and the SST $k - \omega$ model [29]. These models have during many years been tweaked and refined to provide robustness and accurate results. A general RANS linear eddy viscosity model does however sometimes have trouble coping with flow regions with separated or rotational effects as well as flows where a large adverse pressure gradient is present. As the RST model is expensive and can have the tendency to become unstable, a model that is both accurate for cases with strong stream line curvature and stable would be profitable [23][29]

The problems in regular linear eddy viscosity models occur in the previously mentioned regions since they cause misalignment of principal components of the stress and strain-rate tensors. This causes the eddy viscosity model to over predict the amount of turbulent kinetic energy. The standard $k - \varepsilon$ model only solves for the turbulent kinetic energy and the turbulent dissipation rate. The eddy viscosity model $k - \varepsilon$ Lag Elliptic Blending solves, apart from the general $k - \varepsilon$ equations, also a normalized wall-normal stress component ϕ and an elliptic blending factor. The Lag Elliptic Blending model solves the problem of misalignment in the principal components by incorporating an angle between those. It is therefore known to give more accurate results for flow with strong streamline curvature and rotational flow [23][29].

Choosing a final turbulence model comes down to computational power access and the need for robustness as well as accuracy. Among the commonly used two equation eddy viscosity models, the Realizable $k - \varepsilon$ model is known to give more accurate results than other two equation $k - \varepsilon$ models where separated flows or flows with complex secondary flows are present. The name comes from the fact that the mathematical model satisfies a physical constraint on normal stresses that the other $k - \varepsilon$ models do not [23][30].

Turbulence Response Model

In STAR-CCM+ there are two main alternatives for how to treat the turbulence for the continuous and dispersed phases. The turbulence of one phase can be treated independently from the other phase having its own set of equations for turbulence energy and dissipation. In this approach the formulation of the equations is the same as for single phase flows but scaled with the volume fraction of the regarded phase.

The other alternative is to use a turbulence response model where only the continuous phase turbulence equations are solved for. The turbulence properties for the dispersed phase are then related to the turbulence of the continuous phase via a response function. The response function is a function of the velocity fluctuations according to Equation 2.17.

$$C_t = \frac{|u'_{i,d}|}{|u'_{i,c}|} \quad (2.17)$$

The turbulence of the dispersed phase influences the continuous phase turbulence via its turbulence transport equations. In STAR-CCM+ one can choose between the Issa or the Tchen turbulence response models where the Issa model is preferable for bubbly flows [23].

2.5.3 Discretization Methods

In order to resolve flow structures numerically, finite volume solvers discretize the governing equations in space and time. The domain of interest are divided into a grid and the mathematical models for the flow are transformed into a set of linear equations which can be solved throughout the computational grid. Steady problems work without taking time into account and converge towards an equilibrium while unsteady problems are evaluated in time against a set time step [23].

A closed set of equations is attained by applying suitable relations into the conservation equations. The equations are combined into a generic transport equation which is integrated over the control volume. The Gauss's divergence problem then gives the integral form of the transport equation as can be found in Equation 2.18. Here the term ϕ represents flow scalar properties which are transported. The transient term represent the change over time of the fluid property ϕ . The convective flux and the diffusive flux is the net rate of decrease and increase respectively of the property ϕ over control volume boundaries. Finally the source term represents generation or destruction of ϕ inside the control volume. The set of flow properties ϕ , convection, destruction and source term parameters forms the final partial differential conservation equations for mass, momentum, energy and species which estimate the flow [23][31].

$$\underbrace{\frac{d}{dt} \int_V \rho \phi dV}_{\text{Transient term}} + \underbrace{\int_A \rho \mathbf{v} \phi \cdot d\mathbf{a}}_{\text{Convective flux}} = \underbrace{\int_A \Gamma \nabla \phi d\mathbf{a}}_{\text{Diffusive flux}} + \underbrace{\int_V +S_\phi dV}_{\text{Source term}} \quad (2.18)$$

The discretization scheme refers to the logic of how information is transported in between the various cells. Schemes should generally be conservative, which states that the flow that goes out through the east boundary of a cell, should go into the west boundary of the next cell. See Figure 2.6 for a visualization. Schemes should also be bounded, which refers to that, in a cell without source term, the value in the cell is bounded by its boundary values. The scheme should also be transportive which means represent the flow that it is resembling [31][32]. Simpler methods such as First Order Upwind scheme take information only from adjacent neighbouring cells. The method is unconditionally bounded which gives a stable solution. The method is also accurate in cases when the streamlines are aligned with the cell interfaces. However if the streamlines are not aligned, errors might occur. In order to solve this accuracy problem second order accurate schemes can be used. Two common methods are Second Order Upwind scheme and Central-Differencing scheme. A short explanation of these methods can be seen in Figure 2.6. The choice of scheme comes down to the accuracy against robustness of the scheme since more accurate schemes in some occasions can cause divergence in others. The general advice is therefore to use a simple First Order Upwind scheme to start with and thereafter apply a more advanced scheme when initial convergence is found [23]. When dealing with complex turbulent flow structures, Bounded Central-Differencing scheme generally is a good choice [23].

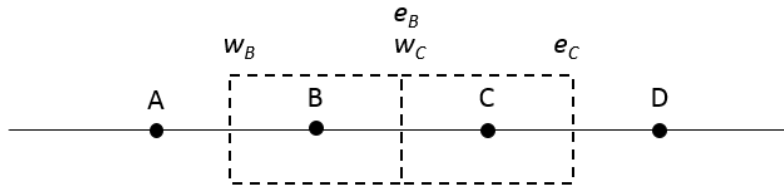


Figure 2.6: Computational discretization schemes: First-Order-Upwind, The value in face e_B/w_C is taken as B or C depending the direction of the flow. Second-Order-Upwind, The value in face e_B/w_C is taken as an interpolation from A,B or D,C depending on the direction of the flow. Central Differencing, The value in face e_B/w_C is taken as the mean value of B,C.

2.6 Optimization Theory

In engineering work, intuitively knowing what the "best" design or method is can sometimes be troublesome. The constantly growing capabilities of computational calculations have lately given the possibility to use computers in order to streamline decision processes. Instead of physically testing several prototypes or setting up parametric tests in simulations, it is possible to use optimization to find the most profitable solution to a problem [33].

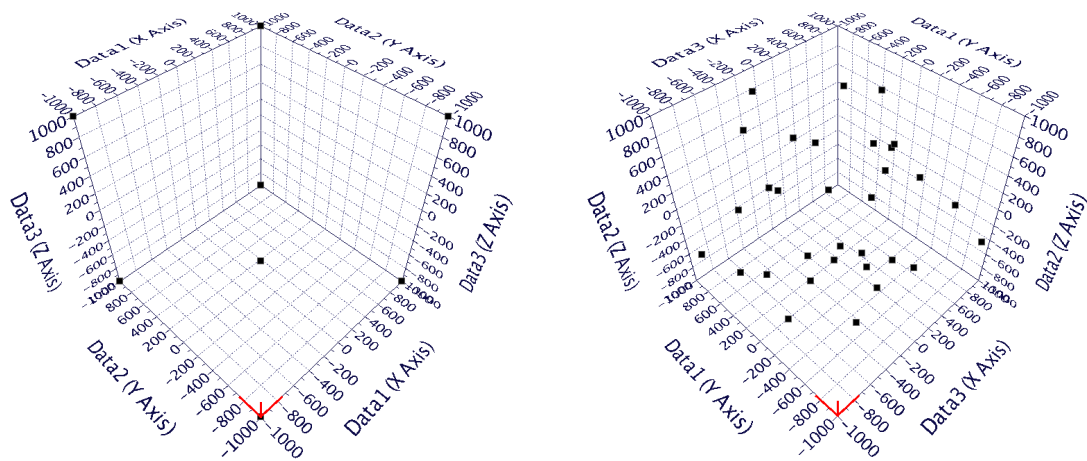
Optimization in design engineering implies formulating the design problem into a mathematical problem. A number of functions representing the problem are to be found and thereafter one of the functions is minimized subject to one or several constraints which are formed by the remaining functions. Depending on the number and the complexity of the provided functions, the difficulty of the optimization problem differs. Problems can alternate from simple ones such as linear or convex, uni-modal problems to multi-dimensional, non-convex problems with several local minimum. Therefore many different algorithms exist which are favourable for different levels of complexity problems [33][34].

Using optimization in design processes has the possibility to dramatically decrease the time and cost of finding a profitable design. However, the quality of the solution is only as good as how well the set of functions is representing the problem and the main objective as well as the accuracy of the optimization method in finding the global minimum and not just a local one [33].

2.6.1 Design of Experiments

Design of experiments (DOE) is a general name for using a systematic approach to perform experiments. Lab tests and simulations are commonly time consuming and expensive. Therefore, this method implies that you try to extract as much information as possible about a design space without performing a large number of experiments or simulations. The general idea is, where the traditional approach only tests one parameter at the time, this tests several parameters at the same time. DOE is especially interesting when the correlation between the parameters are of interest [35].

Design of experiments can be used for several different reasons. For example in order to get a statistic view over the design space, to find a meta model over the design space or to give input for an optimization. Depending on the reason for the study, the fashion of how to spread the experiments in the design space differs. In Figure 2.7 two different approaches are visualized. Note that the design space could be spread in many more dimensions than three, but in order to visualize the theory a three parameter design space is shown. When searching for a good statistical analysis, one should use a factorial approach which is evaluating the boundaries of the design space, see Figure 2.7a. If you on the other hand want to create a meta model, using for example a Response Surface Methodology (RSM), utilization of an explorational or space filling algorithm is a better approach. An explorational approach is shown in Figure 2.7b [35][36].



(a) Factorial DOE.

(b) Explorational DOE.

Figure 2.7: Design of experiments design space evaluation types.

Uniform Latin Hypercube

The Uniform Latin Hypercube (ULH) is a stochastic explorational DOE algorithm which distributes the experiments uniformly in the design space. The design space is constrained by the minimum and maximum of the various parameters. The algorithm works by dividing the design space into sub volumes. The amount of sub volumes depends on the number of parameters and the algorithm tries to spread the volumes as well as possible and thus minimizing correlations [37]. When the volumes have been set, the algorithm takes one design in each of the volumes and tries to maximize the distance between the chosen designs. In this fashion the algorithm assures a quite well uniformly distribution of the designs in the design space [35].

2.6.2 modeFRONTIER

modeFRONTIER is a commercial software which enables the possibility to use optimization tools to acquire a profitable design. The tool does so by providing a work flow model where it can couple other software together and perform optimization on extracted results. With modeFRONTIER it is possible to optimize for one aspect as well as several through multi-objective optimization. Opposing objectives are evaluated by the program by taking applied cost functions into account to find the most optimal solution. The modeFRONTIER toolbox allows usage of several different optimization methods. The method of choice can be adapted to fit the size and type of problem at hand [34].

An optimization in modeFRONTIER can be fully automated where the designs are created and evaluated iteratively without intervention. However, the software can also be used as an optimization tool for an imported data set. By importing a table with parameter values as well as the objective result for each combination, modeFRONTIER has the ability to use Response Surface Methodology (RSM) to map a surface in the design space for each parameter against an output value. These surfaces are thereafter used in combination with an optimization algorithm in order to acquire an optimum value. modeFRONTIER contains various methods to create the response surfaces by fitting the surfaces to the imported data. Examples of RSM methods are Polynomial SVD, Stepwise Regression and Kriging. The best fit can be found by comparing the error of the various methods and in such way it is easy to find the best response surface for your data [38]. Among the tools to evaluate the quality of the fit modeFRONTIER presents the R^2 value. The R^2 is expressed as a value between 0 and 1, where 1 is the best, and is a measurement of the percentage variance of the dependent variables which the independent variables explain [39].

Kriging RSM method

Kriging RSM method is based on a Bayesian Methodology. It is a statistical surface fitting method which is especially well suited for prediction of highly non-linear responses. The algorithm tries to fit the given data points by minimizing the standard deviation of the errors between real and predicted designs. The Kriging method is producing a complete probabilistic representation of the whole design space. The main disadvantage of the method is that it is expensive and might be time consuming to perform. However, if using a low number of design inputs this is not a major concern. In modeFRONTIER one can also use variants of Kriging. For example Anisotropic Kriging which makes it possible to use different importance factors for different input variables. Another one is DACE-Kriging which is especially designed for "Design and Analysis of Computer Experiments" [35].

2.6.3 Optimization Algorithms

There are a large number of optimization algorithms which have all been developed for fitting different types and sizes of problems. Some methods are extremely efficient on one type of problem while it will not be able to find an optimum for others. Some methods are on the other hand very general but might in some cases be highly inefficient. The choice of algorithm is therefore of importance for acquiring trustworthy and inexpensive results.

An iterative optimization algorithm is based on two main steps: finding a search direction and thereafter performing an optimization in the chosen direction. The choice of search direction can be performed using the gradient of the function. These methods are generally fast, but in some cases the gradient can be too expensive to calculate or for some other reason not ideal to use. In these cases, other methods such as perpendicular search methods can be used to find a direction [33].

When the direction has been found, or in cases where the function is just one line, a line search is to be performed in order to find the local minimum. There are several different methods to find this minimum. One such algorithm is the golden section search method. The choice of method comes down to a trade off between speed, accuracy and algorithm availability [33].

Many optimization problems are however complex and can contain several local minimum and various objectives and constraints that need to be accounted for. The problem might also be containing variables that can only take integer values which additionally complicates the optimization. In some cases an iterative optimization algorithm, as described above, can be part of the solver. For example it can be used in a multi-start optimization method which performs the optimization from various starting points and thus with some reliability will find the global optimum [33].

There are also algorithms which are specifically suitable for complex problems and global optimum search. One of these methods which is commonly used is a genetic algorithm. This method is based on an evolutionary approach where an initial number of solutions will be generated. Thereafter the objective function is used to rank the quality of the solutions. Based on a biological approach the best solutions will be combined and create an offspring. In addition, mutations are randomly created and inserted in the process [33].

Golden Section Search Method

The Golden section search method is a line optimization method and is explained by the use of Figure 2.8. The function f_k is assumed to be unimodal, only have one minimum, within the given section $[a_1 d_1]$. The function is thus strictly decreasing on the left side of the minimum and strictly increasing on the right side. The function f_k is divided into three subsections by applying b_1 and c_1 according to Equations 2.19 and 2.20. $f_k(b_1)$ and $f_k(c_1)$ are then evaluated and if $f_k(b_1) > f_k(c_1)$ the minimum must be in the interval $[b_1 d_1]$. For the next iteration the new sections can be set as $a_2 = b_1$, $d_2 = d_1$, $b_2 = \lambda a_2 + (1 - \lambda) d_2$ and $c_2 = (1 - \lambda) a_2 + \lambda d_2$. If instead $f_k(b_1) < f_k(c_1)$, the

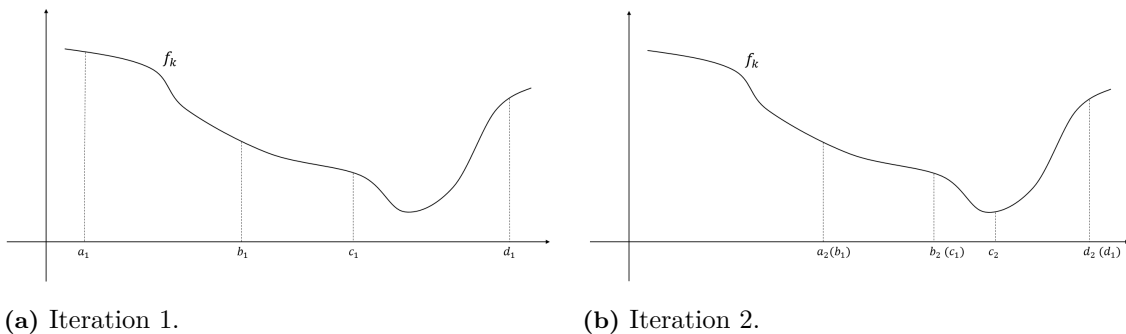


Figure 2.8: Golden Section Search Method.

minimum is known to be in the interval $[a_1 \ c_1]$. The values for the next iteration can then easily be calculated in a similar fashion as previously explained [33].

$$b_x = \lambda a_x + (1 - \lambda) d_x \quad (2.19)$$

$$c_x = (1 - \lambda) a_x + \lambda d_x \quad (2.20)$$

$\lambda = \frac{1}{2}(\sqrt{5} - 1)$ is the golden section constant. This implies that it preserves certain ratios and thus if $\bar{f}_k(b_1) > \bar{f}_k(c_1)$ then $b_2 = c_1$ or vice versa. Resulting in only one new value has to be calculated between the iterations [33].

HYBRID Optimization Method

In modeFRONTIER the HYBRID method is as the name suggests a mix between different types of optimization algorithms. It is based on a genetic algorithm for global search and a sequential quadratic programming algorithm for refined local search. The two algorithms do however pass information between each other during the whole optimization process in order to make the search more efficient. It can handle mixed integer and multi-objective optimization problems [35].

Multi-Objective Particle Swarm Optimization Method

The method is based on the behaviour of bird flocking and has many similarities with a genetic algorithm. Multi-objective particle swarm optimization (MOPSO) does not have any evolutionary steps and is therefore not as robust as the genetic algorithm. It does however have the quality of being much faster and can therefore evaluate more designs. The method is based on an elitism strategy where all points which are dominated by another one get replaced. They are replaced in such a fashion that the currently best solution acts as a guide which the remaining particles are following. The method can handle mixed integer and multi-objective optimization problems [35].

3

Method

This chapter will treat the methods used during the project. The main goal of the project was to accumulate more knowledge about the separator and its performance. The performance of the separator was quantified in terms of separation efficiency and pressure drop. In addition, the volume of the separator was included among the performance parameters. The project was performed in a sequential manner following a common thread. In order to make the process easy to follow, this chapter will follow the same outline. To further clarify the process the project was divided into two consecutive parts.

Part 1

- Information gathering through literature survey and meetings with Volvo Cars employees.
- Construction of test rig.
- Experimental testing.
- Computational model set up in STAR-CCM+.
- Analysis and comparison of experimental and simulation results.

Part 2

- Parametric study of design parameters.
- Design of experiments and optimization process.
- Evaluation of improved design.

3.1 Experimental Tests

An experimental test was performed in order to validate the reliability of the computational model. The test rig was designed to resemble an actual cooling system. However, the focus was to replicate the separator part of the circuit and the rig was therefore simplified by not adding all components to the circuit. The construction of the rig was performed in collaboration with the precision engineering department at Volvo Cars.

3.1.1 Physical Separator Model

For the experimental tests a separator model made of transparent plastic was used. The model, which can be seen in Figure 3.2b, shares the same main features of the currently produced separator but has a few differences, such as height and width. For further reading the currently produced separator will be referred to as design X. The model used in the experimental test is divided into three separate parts: a bottom part, a mid part and a top part. The inlet is found in the bottom part and consists of a pipe with an inner diameter of 13 mm, in which the flow enters tangentially to the cylindrical body of the separator. Inside the separator the flow is lifted via a ramp, pushing it upwards towards the outlet. An interior cone in the bottom part forces the flow to follow the outer wall. The outlet is located in the mid part and is a pipe with an inner diameter of 15 mm. The mid part is basically a cylinder with the outlet letting the flow exit the separator in a tangential direction. The top part consists of a slightly bell shaped lid and the gas outlet is located at the top of the lid. The gas outlet is a pipe with an inner diameter of 13 mm and an inclination angle

of approximately 7° . The outer dimensions of the separator main body are 65 mm in height and 90 mm in diameter.

3.1.2 Test Rig Design and Test Execution

A schematic image of the test rig can be found in Figure 3.1 and a picture of the physical test rig in Figure 3.2a. The rig consisted of two circuits, an inner one where the separator is connected and an outer one. The inner circuit could be disconnected by the use of valves. This function was applied when inserting a known volume fraction of air into the system and for mixing of the air and liquid. When the two phases were sufficiently mixed, the inner circuit was connected. As liquid a 50/50 mix of water and ethylene glycol was used, which is the same coolant as is utilized in Volvo cars.

Two test series were performed. In each test series, the velocity of the flow was the only parameter alternating. In test series A, the inlet and outlet were placed according to design X, i.e. the outlet altitude being higher than the inlet altitude. In test series B the inlet and outlet changed place. This change gave the opportunity to find the effects of a geometrical change which was of great interest for later parts of the project. A and B will further be used as design references for these two configurations. The initial air volume fraction at each test was 4% which represented 0.14 l of the total system volume of 3.5 litre. In Tables 3.1a and 3.1b the properties of each test are shown. The volume flow rates were chosen with the rate of 8.4 l/min as starting point which was deemed relevant for the system in which the separator is used today. This volume flow rate is referred to as 1. For example A1 representing design A at a flow rate of 8.4 l/min. To get a wider range of flow rates and investigate the trends, flow rates below and above 8.4 l/min were chosen. Note that these other flow rates are defined by different numbers. As the flow rates were deemed of different importance, different number of tests were performed for the various flow rates. In Table 3.1 the number of the test are marked by .x, for example A1.1. The reason for various tests was to evaluate how well the tests could be repeated. For a complete description of the test set up and performance, see Appendix A.

3.1.3 Measurements

The pressure was measured and recorded right before and right after the separator to be able to calculate a pressure drop. A temperature sensor measured and recorded the coolant temperature to ensure no large variations occurred. To reach the different volume flow rates a flow meter was used and the flow rate was monitored via a display, although no data was recorded. To measure the separated air a camera was placed to record the decreasing level of coolant in the measurement cylinder. The recordings were later on manually processed to collect the data. For visualization of the flow a camera was placed to record the flow structures inside the separator.

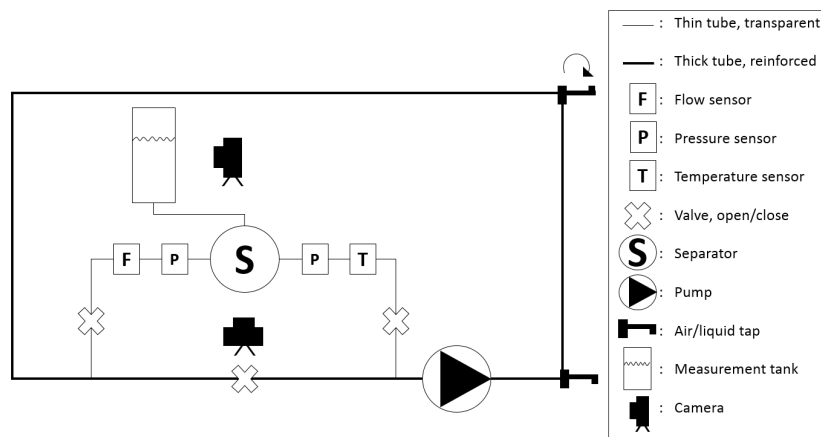
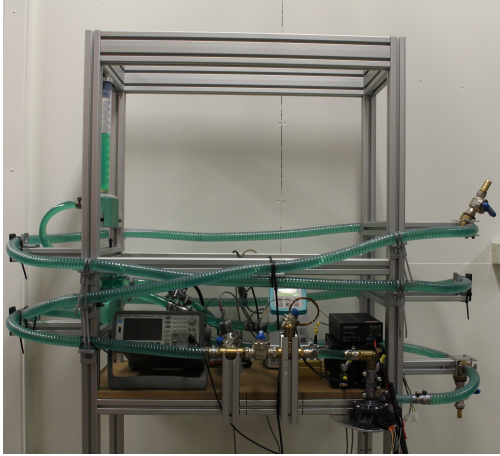


Figure 3.1: Schematic image of test rig.



(a) Test rig.



(b) Transparent separator model used in the experimental tests.

Figure 3.2: Test set up.**Table 3.1:** Test specification for lab experiments.

(a) Test series A.

Test ID	Volume flow rate [l/min]
A1.1	8.4
A1.2	8.4
A1.3	8.4
A2.1	12.6
A2.2	12.6
A3	16.8
A4	4.2
A5	2.5

(b) Test series B.

Test ID	Volume flow rate [l/min]
B1.1	8.4
B1.2	8.4
B1.3	8.4
B2.1	12.6
B2.2	12.6
B3	16.8
B4	4.2
B5	2.5

3.2 Simulations

In this part of the report the process of acquiring a trustworthy computational model of the performance of the separator will be presented. The results found in the experimental test were to be analyzed and replicated in simulations. The main objective was not to get the exact same values as in the experiment, but to be able to follow the same trends. This in order to through later evaluation of the computational model, with some degree of confidence, be able to validate the results for a physical model.

The computational model was initially set up using information found in literature as well as information gathered from supporting professors, STAR-CCM+ support and experienced personnel at Volvo Cars. Using the result from the test, the model was analyzed and tuned in order to obtain the best resemblance.

3.2.1 Meshing

In any type of CFD studies, the type and design of the mesh is of great importance and can have large effects on the results. The general rule is to use a mesh which is as coarse as possible in order to reduce the amount of computational power needed. In multiphase flow the meshing is however slightly more complicated than for a single phase flow. Depending on the multiphase model used, the mesh must not be too fine and neither too coarse in order to represent the flow. Due to the fact that the mesh was to be used in various geometries and still give trustworthy results, a lot of effort was put into acquiring a well performing mesh.

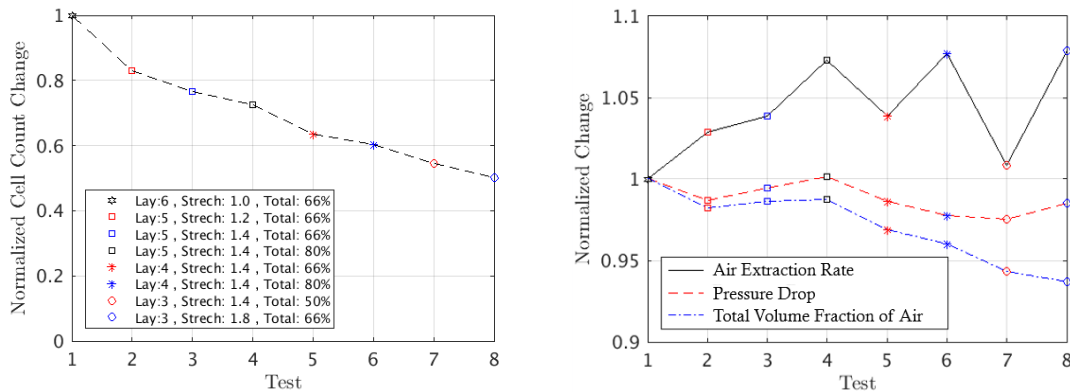
Mesh Type

There are various types of meshes as pointed out in Section 2.5.1. The most suitable type to use is case dependent. If possible, a simpler mesh type such as hexahedral or tetrahedral is usually profitable in order to reduce computational expenses. A more advanced mesh can on the other hand improve the accuracy of the model. The choice was to use a hexahedral mesh since this was the recommended approach by [23] in which the argument for this mesh type is that the cells are aligned with the circumference of the separator.

y^+ and Wall Treatment

The wall treatment was chosen according to [23] where the authors claim that it is preferable to use a "All y^+ Wall Treatment" whenever this is available. Especially so when the geometry and velocities are varying throughout the domain. Although the name suggests otherwise you are advised to stay out of the buffer layer if possible, which implicates that the first cell should not be located in the region $1 < y^+ < 30$. However, if needed, going as high as $y^+ = 5$ is acceptable. Due to the importance of resolving the wall flow structures, $y^+ < 1(5)$ was preferred.

A thorough investigation was performed in order to find the most suitable prism layer approach. Since the usage of prism layers can radically increase the cell count it was of interest to select a prism layer approach that would give valid results at a low computational cost. Close cooperation with STAR-CCM+ support [27] and STAR-CCM+ documentation [23] was used in the process. In Figure 3.3 an evaluation of the cell count of the mesh as a function of various prism layer approaches can be found. The first prism layer was always set to a height where the y^+ value did not go above 5, since setting the first prism layer lower gave unstable results. It can be seen that the mesh cell count drastically decreases with changed prism layer settings. There are also some variations in the performance parameters when changing the settings but no clear trends could be identified. Also variations in the total volume fraction of air in the domain can be seen. Since no converged value was obtained the most theoretically correct prism layer approach was chosen, implying an acceptable y^+ and a good resolution of the boundary layer. This approach gave stable solutions and a reasonable cell count. The fact that the solution is dependent of the wall treatment was however verified.



(a) Cell count as function of prism layer settings.

(b) Performance parameters as function of prism layer settings.

Figure 3.3: Prism layer dependency study. "Lay" represents the number of prism layers, "Stretch" is the stretching factor and "Total" is the total prism thickness as a percentage of the base cell size.

Mesh dependency study

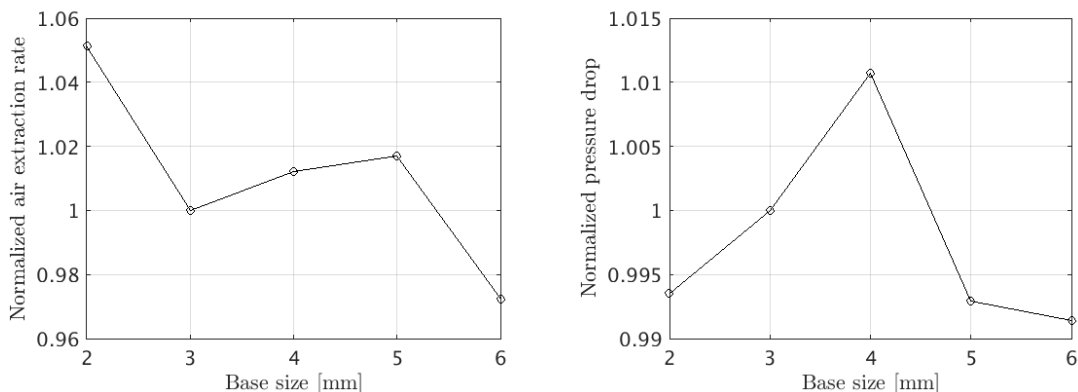
The sensitivity for mesh size and quality is, as per Section 2.5.1, higher for multiphase applications. A long time was therefore spent on finding an initial mesh giving results that correlated with the experiments. The initial mesh was built with an element base size of 3 mm and the simulations showed a good correlation with experimental results. A mesh dependency study was yet performed to investigate the opportunity to decrease the cell count and thereby save computational time, which was of importance since numerous simulations were to be run in the parametric study and during the optimization. The mesh was altered by changing the base size without jeopardizing the geometrical representation of the domain. The results of this can be found in Figure 3.4. The values from the 3 mm mesh were used to normalize corresponding values during the mesh dependency study to check the deviation. As can be seen there is no trend indicating any asymptotic behaviour but the decision was made to use a base size of 4 mm. The decision was based on the fact that a fairly good correlation with the test results had been reached for the 3 mm mesh and the deviation in air extraction rate for the 4 mm mesh was rather low. The pressure drop results tended to be more stable when changing the mesh size and a maximum deviation of about 1 % was found.

To assure a good mesh quality was achieved, checks were made for cell quality, skewness angle and cell volume change. The chosen mesh parameters are presented in Table 3.2 and a visual representation of the mesh can be seen in Figure 3.5. The figure shows the cell surfaces of the cells in the vicinity of plane sections cutting through the separator geometry.

3.2.2 Model Set Up

In this section the physics applied in the computational separator model will be presented. The choice of models were carefully performed in cooperation with STAR-CCM+ support [27] and by the use of literature [23]. For the physics model some assumptions were made:

- Air and coolant have constant densities
- The flow is isothermal
- There is no mass transfer between the two phases
- The air enters the separator at a constant volume fraction

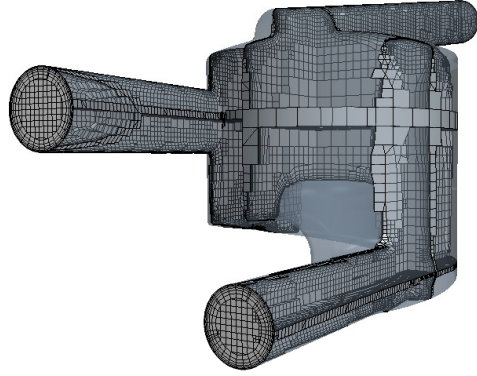


(a) Air extraction rate depending on mesh size. (b) Pressure drop depending on mesh size.

Figure 3.4: Mesh dependency study.

Table 3.2: Mesh parameters.

Base size	4 mm
Target surface size	100% of base size
Minimum surface size	10% of base size
Surface curvature	72 points/circle
Surface growth rate	1.5
Number of prism layers	6
Prism layer stretching	1.4
Prism layer total thickness	100% of base size

**Figure 3.5:** Mesh.

Multiphase Model

The case was chosen to be solved using the Eulerian-Eulerian approach since tracking the exact paths of the bubbles was not of interest but rather the collective behaviour. If using the Eulerian-Lagrangian approach the estimated bubble size of the flow would result in a large number of particles which could have affected the computational time. Also, the Eulerian-Eulerian approach was the recommended one in [8] which treats a similar case. It was also used in [16] in the investigation of a GLCC. Using the Eulerian-Lagrangian model would however been valid and there was no obvious reason for using one or the other.

The selected physics model in STAR-CCM+ is presented in Table 3.3. For the velocity convection a second order upwind scheme was applied and a first order upwind scheme for the volume fraction convection. The case was solved in a steady state condition to decrease the computational time when running the optimization part which required a high number of simulations.

Phase Model Set Up

The choice of phase models was based on findings from literature as well as discussions with STAR-CCM+ support [27]. In order to best represent strong rotational flow it is of importance to use a model which can account for this. The RST model is particularly suitable for such cases and even though it can sometimes have a tendency to produce unstable results, it is in theory the most accurate model and has been used in several previous separator studies [12][16]. The RST model was therefore chosen as it was known to be the model which would best represent the flow in the separator. In addition, a turbulence response model was chosen to represent the dispersed phase in the computational model. The model was applied since it reduces the computational time and often gives comparable solutions to running a full turbulence model for the dispersed phase [23]. The settings for the phase models can be found in Table 3.4a and 3.4b, representing the continuous and dispersed phase respectively. If no other information is added, the settings were kept to default.

Table 3.3: Physics model.

Cell Quality Remediation
Gravity
Turbulent
Gradients
Multiphase Equation of State
Multiphase Segregated Flow
Multiphase Interaction
Eulerian Multiphase
Steady
Three Dimensional

Table 3.4: RST model set up.

(a) Continuous phase.

Constant Density
Exact Wall Distance
Flow
Liquid
◦ $\rho = 1070 [kg/m^3]$
◦ $\mu = 0.003653 [Pa \cdot s]$
Turbulent
Reynolds-Averaged Navier-Stokes
Reynolds Stress Turbulence
Elliptic Blending
All y+ Wall Treatment

(b) Dispersed phase.

Constant Density
Exact Wall Distance
Flow
Gas
◦ $\rho = 1.18415 [kg/m^3]$
◦ $\mu = 1.85508E-5 [Pa \cdot s]$
Turbulent
Reynolds-Averaged Navier-Stokes
Turbulence Response
Issa Turbulence Response Model

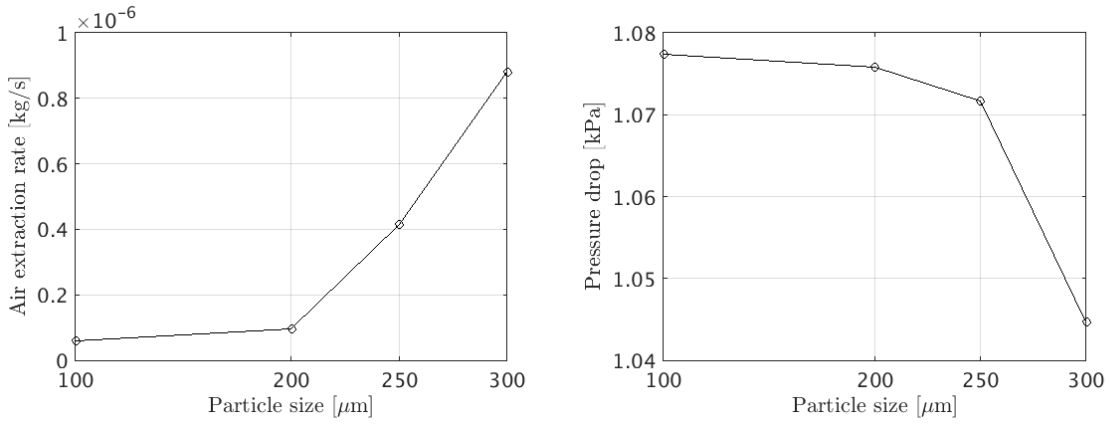
Phase Interaction Models

The used phase interaction models are listed in Table 3.5. The particle size was set as the interaction length scale and represents the diameter of the bubbles. Ideally a model for particle size distribution and coalescence and break up would have been implemented but due to convergence issues for the S-Gamma and AMUSIG models a constant particle size was assumed. Instead a study was performed in order to know how the particle size affected the performance of the separator. This could later be used to compare against experimental results in order to find a plausible bubble size. Although, the assumption of a constant bubble size is evidently a limitation and a possible source of error which had to be regarded throughout the study. An example of the limitation is that the model disregards changes in particle size due to change in flow velocity.

The graph in Figure 3.6a shows how the amount of air through the gas outlet increases exponentially with increasing particle size. Figure 3.6b shows that the particle size also affects the pressure drop but the effects are relatively small and were considered as negligible when deciding upon which particle size to use. Models were chosen to account for lift force, virtual mass force and wall lubrication force which are typically forces affecting bubbles dispersed in a liquid. To account for the turbulent eddies' impact on the bubbles, a turbulent dispersion force model was used.

Table 3.5: Phase interaction models.

Phase interaction	Additional selection
Continous-Dispersed Phase Interaction	Continuous Phase: Coolant Dispersed Phase: Air
Drag Force	Drag Coefficient: Tomiyama Drag Correction: Volume Fraction Exponent
Interaction Area Density	Symmetric
Interaction Length Scale	Constant
Lift Force	Lift Coefficient: Tomiyama
Multiphase Material	Surface Tension: Constant (0.055763 N/m)
Turbulent Dispersion Force	Turbulent Dispersion Prandtl Number: Constant
Virtual Mass Coefficient	Spherical Particle
Virtual Mass Force	
Wall Lubrication Force	Wall Lubrication Coefficient: Antal



(a) Air extraction rate as function of particle size. (b) Pressure drop as function of particle size.

Figure 3.6: Particle size dependency.

Boundary Conditions

For the separator inlet a velocity inlet boundary condition was used. The air was assumed to enter the domain at the same velocity as the coolant and the entering volume fraction of air was defined at the boundary. The outlet was treated as a pressure outlet with a gauge pressure of 0 kPa, implying an atmospheric absolute pressure. The gas outlet was treated as a degassing boundary which means that the boundary was treated as a wall for the coolant but for the air a permeable wall option was applied. This boundary condition was thought to most properly mimic the behaviour in the experimental test and the situation in the vehicle where an almost quiescent fluid was standing between the gas outlet and measurement tank. The rest of the domain boundaries were treated with a wall condition. The boundaries can be seen in Figure 3.7. The inlet and outlets were also treated with a surface and volume extrusion operation. For the inlet and outlet this was done since the pressure sensors in the experimental test were located at this distance from the separator. Also, for the inlet the extrusion meant that the flow had a distance to develop before reaching the main domain. For the gas outlet the extrusion was performed in order to minimize the impingement from the gas outlet boundary condition.

Convergence Criteria

In this type of simulations it is difficult to achieve stable residuals in a low order of magnitude and it is therefore even more important to check convergence against engineering quantities. In these simulations three different quantities were used to check the convergence: average volume fraction of air in the domain, separation efficiency and pressure drop. The separation efficiency was computed in two different ways:

$$\eta = \frac{\dot{m}_{air,GO}}{\dot{m}_{air,I}} \quad (3.1)$$

$$\eta = 1 - \frac{\dot{m}_{air,O}}{\dot{m}_{air,I}} \quad (3.2)$$

The index GO stands for gas outlet, I for inlet and O for outlet. For a converged solution the graphs for the two efficiencies should correlate. The pressure drop was calculated as $\Delta p = p_I - p_O$ where the pressures were computed as surface averaged pressures on the boundaries. Since the case is solved in a steady state condition but the actual physics are unsteady, the monitored quantities tended to oscillate. Although, the simulations were considered as converged when the solution showed periodic oscillations around the same value.

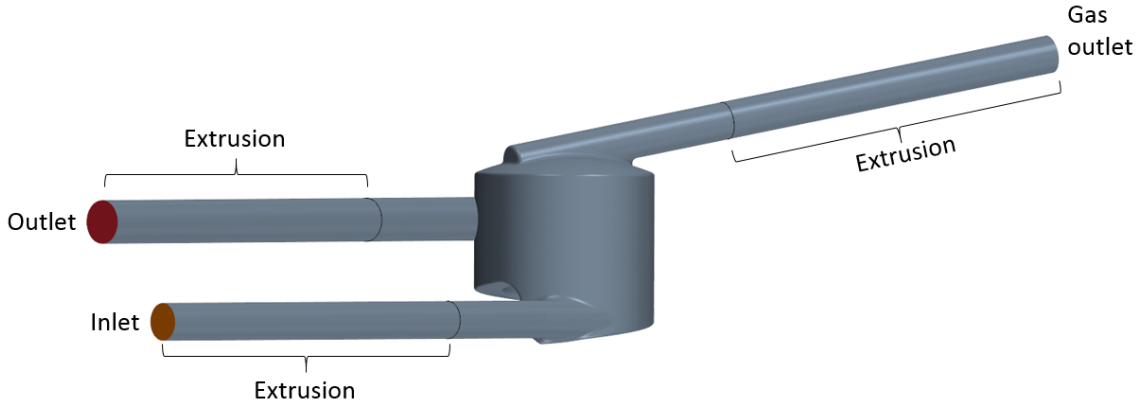


Figure 3.7: Fluid domain with boundaries and extrusions.

Validation of CFD Model

The RST computational model was validated against the experimental tests by comparing the measured quantities, i.e. the pressure drop and the amount of extracted air per unit time. The reason for not validating against the separation efficiency, η , was the uncertainty of this for the experimental data. The incoming air could not be measured during the tests, thus the efficiency could not be computed according to Equation 3.1. To ensure that the CFD model was able to predict the correct pressure drop for varying flow rates, simulations for every flow rate were performed and compared to the experiments. These simulations were performed with a constant volume fraction of air. The air separation performance was compared for the three highest flow rates and since the simulations were performed in steady state, four different volume fractions were used in the validating simulations to match the transient experiments.

In addition, scalar plots of the flow structures in the domain were compared to movies recorded during the experimental tests. The comparison was performed visually. The scalar plots were also examined extensively to find if there was any conspicuous nonphysical behaviour that could be identified.

Streamlining the Computational Process

As during the optimization process, a large number of simulations were to be performed there was a need to make the process as efficient as possible. After acquiring a computational model in form of the RST set up, it was of interest to find if a more simple model could be used to show correct output trends when changing the input variables. Since the geometries in the parametric study and optimization were only to be compared to each other the exact data was here of less importance. From literature and discussions with STAR-CCM+ employees it was found that especially two models were of interest to test. The Realizable $k - \varepsilon$ model and the Lag Elliptic Blending $k - \varepsilon$ model which both are more simple than the RST but are still able to predict flow regions with strong rotational effects. Note that in theory, the Lag Elliptic Blending $k - \varepsilon$ model should be a middle ground between the RST and the Realizable $k - \varepsilon$ model. This goes for computational expenses as well as accuracy. In [11] the Realizable $k - \varepsilon$ model correlated with theory and showed better resemblance to experimental results than other RANS models. The Lag Elliptic Blending $k - \varepsilon$ model was recommended by [27]. The settings for the two models can be found in Table 3.6a and 3.6b.

In order to additionally streamline the parametric study and optimization process a macro was written such that STAR-CCM+ was only needed to be opened when evaluating the results. Hence STAR-CCM+ automatically replaced the separator, meshed the geometry, initialized and ran the solution and finally displayed the relevant output.

Table 3.6: Simplified continuous phase model set up.**(a)** Realizable $k - \varepsilon$ model

Constant Density
Exact Wall Distance
Flow
Liquid
◦ $\rho = 1070 [kg/m^3]$
◦ $\mu = 0.003653 [Pa \cdot s]$
Turbulent
Reynolds-Averaged Navier-Stokes
K-Epsilon Turbulence
Realizable K-Epsilon Two-Layer
Two-Layer All y+ Wall Treatment

(b) Lag Elliptic Blending $k - \varepsilon$ model

Constant Density
Exact Wall Distance
Flow
Liquid
◦ $\rho = 1070 [kg/m^3]$
◦ $\mu = 0.003653 [Pa \cdot s]$
Turbulent
Reynolds-Averaged Navier-Stokes
K-Epsilon Turbulence
Lag EB K-Epsilon
All y+ Wall Treatment

3.3 Parametric Study

The parametric study was performed based on information from the literature survey. The survey aimed to evaluate what the most important design aspects might be in order to improve the performance of a separator. Thereafter, a number of the design parameters were tested using the computational model to find the trends of how a design change influences the separator performance.

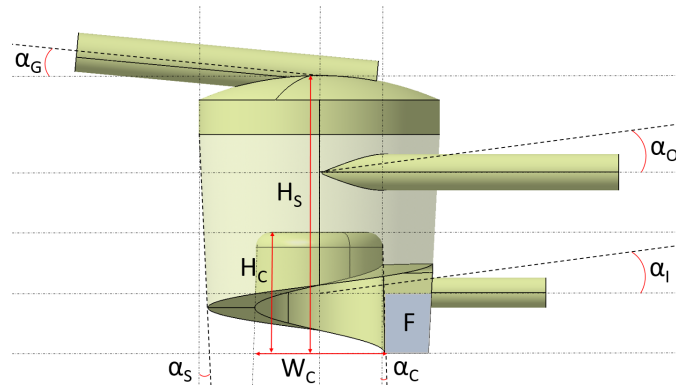
Evaluation of the results from the experimental study showed that the bubble size and the velocity of the flow was of great importance for the performance of the separator. For low volume flow rates, the separator worked well for all configurations tested. However, it was also evident that all air in the system was not brought along with the flow at the low velocities but got stuck along the tube walls. It was therefore found that any design of separator would work sufficiently at low flow velocities and thus the important flow velocity was the higher ones. For these flows the most air would reach the separator and thus this is where the design of the separator would be of highest importance. All the studies and design optimization steps were therefore from this point on, performed on a similar volume flow rate as the maximum that can be found in the system. This volume flow rate was 8.4 l/min, which is as previously explained referred to as 1.

3.3.1 Parametric Catia Model

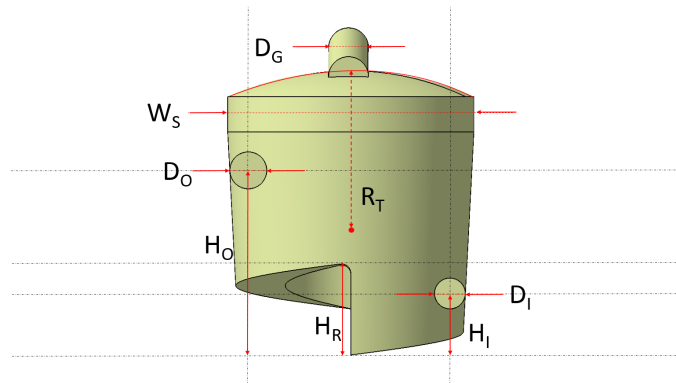
To evaluate the concepts from the parametric study a parametric CAD model of the separator was provided. The model had been made earlier at Volvo Cars to be able to create a generic separator to generate technical data-prerequisites to CAE, try various concepts and ensure packaging [40]. The model was made as a template where parameters easily could be changed to generate new concepts. The CAD model can be seen in Figure 3.8.

As the parametric model gave the possibility to change a large number of design parameters, a few general design aspects were fixed for all different designs. These design aspects were based on findings in literature as well as logical reasoning for fluid dynamics, see Section 2.2.1 and 2.3.1. The parameters are listed below.

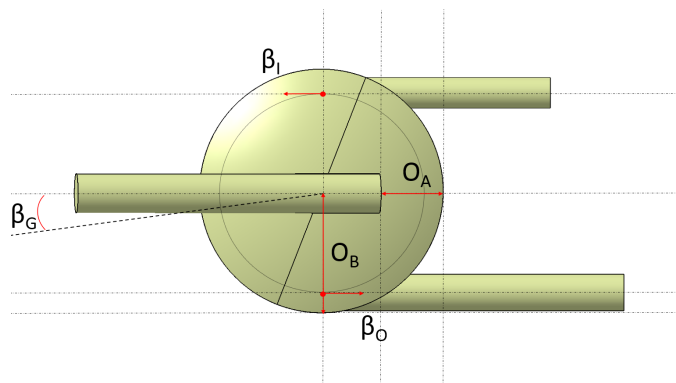
- The inlet and outlet were set to be tangential to the separator wall.
- The separator designs were to be kept free from design details causing stagnant flow zones. This includes minimizing sharp edges.
- In cases where a cone with a ramp was part of the design, the bottom connection was attached so that it followed the direction of the bottom of the ramp. That is, connected through face F in Figure 3.8a. This feature was adapted to reduce the risk of a stagnant or re-circulation zone close to the connection.



(a) Front view.

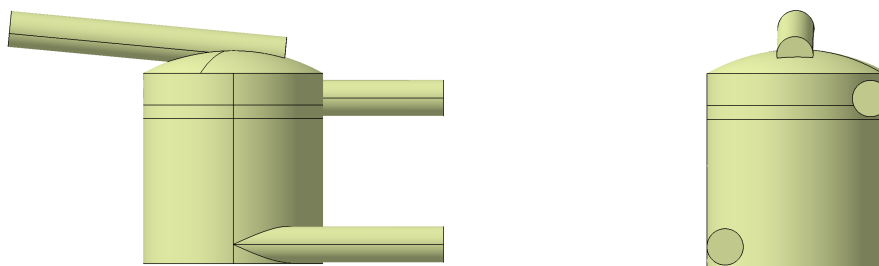


(b) Right view.



(c) Top view.

Figure 3.8: Parametric CAD model.



(a) Side view.

(b) Front view.

Figure 3.9: Base line separator design.

3.3.2 Method of Evaluation

An initial design was set up as a reference for the rest of the study. This design was called the base line design and can be seen in Figure 3.9. This model was designed to be highly generic and facilitate the possibility to vary one design parameter at the time. In Table 3.7 the different design parameters of the separator found in Figures 3.8 are explained and the base line values are presented. Observe that in the base line design the inlet is placed in the top and the outlet in the bottom as in design B. Also, note that the table is divided into different sections where every section represents one "type" of change to the geometry. The first one represents the main body of the separator, the second one is inlets and outlets and the third one stands for separator interior changes. A base line simulation was performed on the base line design. For every parameter design change, two simulations were performed when varying the chosen parameter to different magnitudes. Two separate studies were performed resulting in trends for the separation performance depending on the different design parameters. Note that no information regarding the combined effects of the parameters could be extracted. The first study focused on the first two design sections (separator body and inlet/outlet) and the second study focused on the third section (separator interior).

In order to give the best overview when looking at all the parameters combined, a given magnitude of change was not ranked the same for all the parameters. It was believed that making a straight comparison of changing parameters or using the same percentage change would not give the best overview of the effect. Instead, for every design parameters, an estimate of the maximum and minimum value possible was set to accompany the base line value. This method was used in order to give an intuitive feeling of the importance of the various parameters from a quick look at the resulting plots. The parametric study resulted in information regarding the air extraction rate, the total volume, the pressure drop and the air collection ability trends which every design change contributed with. Note that the air collection ability was of interest in cases when the flow velocity altered. At higher velocities the separator would collect the air and when flow velocity is decreased, the separator would extract the air collected inside. The parametric study test tables can be found in Tables 3.8 and 3.9.

Table 3.7: Base line design set up.

Parameter ID	Design Parameter	Parameter Value
H_S	Separator Height [mm]	65
W_S	Separator Width [mm]	65
R_T	Separator Crowning Radius [mm]	66
α_S	Separator Angle	0°
α_I	Inlet Angle	0°
H_I	Inlet Height [mm]	60
D_I	Inlet Diameter [mm]	13
β_I	Inlet Rotation	0°
α_O	Outlet Angle	0°
H_O	Outlet Height [mm]	7
D_O	Outlet Diameter [mm]	13
β_O	Outlet Rotation	180°
α_G	Gas Outlet Angle	7°
D_G	Gas Outlet Diameter [mm]	13
β_O	Gas Outlet Rotation	90°
O_A	Gas Outlet Offset A [mm]	20
O_B	Gas Outlet Offset B [mm]	32.5
H_C	Cone Height [mm]	0
W_C	Cone Width [mm]	0
α_C	Cone Angle	0°
H_R	Ramp Height [mm]	0

Table 3.8: First parametric study schedule.

Test ID	Design Parameter	Parameter Value	
		Test #1	Test #2
Base	Base line design	-	-
H_S	Separator Height [mm]	97.5	32.5
D_S	Separator Width [mm]	97.5	32.5
R_T	Top Crowning Radius [mm]	99	33
α_S	Adding Separator Angle	7.5°	15°
α_I	Inlet Angle	-20°	20°
H_I	Lowering Inlet Height [mm]	34	7
D_I	Inlet Diameter [mm]	15	10
β_I	Rotating inlet	120°	240°
α_O	Outlet Angle	-20°	20°
D_O	Outlet Diameter [mm]	16	10
α_G	Increasing Gas Outlet Angle	35°	70°
D_G	Gas Outlet Diameter [mm]	16	10
β_G	Rotating Gas Outlet	120°	240°

Table 3.9: Second parametric study schedule.

Test ID	Design Parameter	Parameter Value		
		Test #1	Test #2	Test #3
Base	Base Line Design	-	-	-
Base*	Base with Mirrored Flow	-	-	-
H_C^*	Inserting Cone	$H_C = 15$ $W_C = 35$ $\alpha_C = 85^\circ$	$H_C = 25$ $W_C = 35$ $\alpha_C = 85^\circ$	$H_C = 35$ $W_C = 35$ $\alpha_C = 86^\circ$
H_R^*	Fixed Cone with Varying Ramp Height	$H_C = 25$ $W_C = 35$ $\alpha_C = 85^\circ$ $H_R = 16$	$H_C = 25$ $W_C = 35$ $\alpha_C = 85^\circ$ $H_R = 24$	-
H_{CR}^*	Fixed Ramp Height with Varying Cone	$H_C = 17$ $W_C = 35$ $\alpha_C = 85^\circ$ $H_R = 16$	$H_C = 25$ $W_C = 35$ $\alpha_C = 85^\circ$ $H_R = 16$	$H_C = 35$ $W_C = 35$ $\alpha_C = 85^\circ$ $H_R = 16$
Base**	Base with Mirrored and Reversed Flow	-	-	-
H_C^{**}	Inserting Cone	$H_C = 25$ $W_C = 35$ $\alpha_C = 85^\circ$	-	-
H_R^{**}	Inserting Ramp	$H_C = 25$ $W_C = 35$ $\alpha_C = 85^\circ$ $H_R = 16$	-	-

3.4 Optimization

In this section the work of finding an improved design of the separator will be explained. The work was performed using different methods. The first one is based on the parametric study and is a fast and simple method which makes a few simplifications in order to quickly find improved designs. The other method is based on the computational software modeFRONTIER which is a more sophisticated optimization tool. The software can among other things continuously create and evaluate designs or perform optimization on a given data set. Using modeFRONTIER results in a better coverage of the real performance of the separator, but is also more time consuming and expensive since it requires a large number of simulations.

3.4.1 Parametric Study Based Optimization

In the parametric study a number of different design parameter changes were evaluated by changing them separately. For every design parameter, a total number of 3 data points were extracted. The data points were all normalized against the base line design and could therefore be compared easily. By assuming that these three points gave a rough indication of the design parameters' effect on the performance of the separator, an initial optimization was performed.

As a function is needed to perform an optimization, all the sets of three data points were fitted to a second order polynomial function by the use of the computational software MatLab. As every design parameter was evaluated against pressure drop, air extraction rate, total volume of the separator as well as the ability to collect the air in the separator, this gave a total of four functions per design parameter. In order to weigh the importance of the different parameters against each other, the four functions were combined into one function while adding a factor in front of every different initial function. This factor could easily be alternated and was used in order to set the different importance of the parameters relative to each other. In a general optimization the aim is to minimize the function. Therefore the air extraction rate and the air collection ability functions were multiplied by -1 to turn the maximization into a minimization problem. The function of minimization can be found in Equation 3.3. Here, the constants A-D are given by the curve fit function in MatLab and the constants Φ are the ones specified to set the relative importance.

$$\begin{aligned} \bar{f}_k &= \Phi_{Pressure} * (A_1x^2 + A_2x + A_3) \\ &+ \Phi_{Tot_vol} * (B_1x^2 + B_2x + B_3) \\ &- \Phi_{Air_vol} * (C_1x^2 + C_2x + C_3) \\ &- \Phi_{Air_Extract} * (D_1x^2 + D_2x + D_3) \end{aligned} \quad (3.3)$$

The optimization was thereafter performed on all the parameters from the parametric study using a golden section search method. The objective function in the optimization was \bar{f}_k , Equation 3.3. The function was also defined by constrains of minimum and maximum values that each parameter could take. The result of the optimization depended on the relative importance input as well as the maximum and minimum constraints. After discussions with concerned employees at Volvo Cars, a few different rates of importance were found and evaluated. The constraints as well as the different set up of importance can be found in Table 3.10b and 3.10a respectively. The optimization loop finally resulted in a table suggesting an optimum value for each of the design parameters. The estimated value of the performance parameters was also given by the optimization loop.

As this method was only based on the trends of each of the parameters separately, it was known that combining the parameter changes might give large deviations from the estimated results. The goal was therefore to find if the optimization gave trends that coincided with a simulated result with all the parameters changed. A verification of the optimization method was performed by taking suggested designs from the loop and performing simulations in STAR-CMM+. It is worth noticing that the fact that only three data point per parameter change was the base of this optimization and can therefore strongly affect the accuracy.

Table 3.10: Parametric study optimization input.

(a) Different set up of the importance factor.				(b) Constraints for parametric study based optimization.		
Parameter	Importance Factor [%]			Parameter ID	Minimum	Maximum
$\Phi_{Pressure}$	10	38	9	H_S [mm]	30	70
$\Phi_{Tot-vol}$	30	38	61	W_S [mm]	30	70
$\Phi_{Air-vol}$	10	8	0	R_T [mm]	33	100
$\Phi_{Air-Extract}$	50	16	30	α_S	0°	20°
				α_I	-45°	-45°
				H_I [mm]	0	65
				D_I [mm]	12	16
				β_I	0°	359°
				α_O	-45°	-45°
				D_O [mm]	10	16
				α_G	0°	90°
				D_G [mm]	10	16
				β_G [mm]	0°	359°

3.4.2 Design of Experiments

Evaluation of the results from the parametric study and the initial optimization gave information regarding the relative importance of changing the different parameters. It was clear that some parameters were of greater importance than others. It could also be seen that some parameters showed clear trends regarding what the setting of the parameter should be while others were more unclear.

When performing an optimization, the computational power and time at hand made it impossible to perform a study of all the parameters. Therefore, the most important parameters were chosen and a design of experiment method was conducted. The information of which ones were used was taken from the parametric study as well as logical reasoning. The parameters evaluated also correlated well with previous optimization studies performed in [16]. The other parameters were set to a fixed value. Note that some of the parameters, which in the optimization were set to fixed values, were to be evaluated further at a later stage of the design process. These were the β -rotations and the position of the gas outlet. These factors did not affect the pressure drop or the size of the separator namely and therefore a more simple, single objective optimization could be used for these parameters. In addition, as the inlet and outlets can be rotated 360° a large number of simulations were to be required in order to find the best solution. Therefore, these parameters could be more efficiently evaluated and optimized from visually inspecting the simulations and adapting the values.

Using the same logic regarding the complexity of the optimization, the number of performance parameters was reduced. In the DOE study, no attention was taken to the air collection ability. It was found from the optimization based on the parametric study that this factor had the worst correlation between test and evaluation. Also, since this was a factor introduced only after the lab testing, it was not deemed of same importance as the other performance parameters. Thus, the three performance parameters used in the DOE study were pressure drop, air extraction rate and volume of the separator.

The output from the DOE optimization were to be trained on response surfaces and therefore the DOE method was chosen to Uniform Latin Hypercube. More information regarding this can be found in Section 2.6. In Table 3.11 the parameters included in the DOE as well as the other parameters and their respectively set value are listed. Note that the cone and ramp was included as an on and off feature where it was always applied in the same way, just covering the outlet.

Table 3.11: DOE set up, shows fixed parameters and min/max for included ones.

Parameter ID	Note	min:	max:
H_S [mm]	DOE	30	70
W_S [mm]	DOE	30	70
R_T [mm]	Set to 70		
α_S	Set to 0°		
α_I	DOE	-30°	0°
H_I [mm]	Set to max height		
D_I [mm]	DOE	11	14
β_I	Set to 0°		
α_O	DOE	-30°	0°
D_O [mm]	DOE	12	16
α_G	Set to 70°		
D_G [mm]	Set to 13		
β_G	Set to 180°		
H_{CR}	DOE	On	Off

3.4.3 DOE Optimization

The ULH DOE tool gave a matrix spanning the design space. Using these values a number of 32 different designs were built in the CAD software CATIA V5 and were thereafter evaluated in STAR-CCM+. The pressure drop and the air extraction rate were taken from the simulations as output. In addition, the volume of the separator was calculated as the cylindrical body of the separator. Inlet, outlets, extrusions, top radius volume and the cone with ramp were thereof not taken into consideration for the separator volume. The three performance parameters were included into the DOE table in additional columns. The table was thereafter once again imported into modeFRONTIER.

In modeFRONTIER, using the "Data wizard", the table could easily be cleaned so that only the relevant data was imported. Thereafter the input and output variables were marked and constraints as well as functions to minimize and maximize were applied. In addition to the boundaries of the design space, constraints were set onto the objectives. The objectives and their constraints can be found in Table 3.12.

Once the data was imported into modeFRONTIER the seven dimensional design space data was fitted to surfaces using RSM. For every objective a response surface was created, giving a total of three response surfaces. In order to validate the quality of the response surfaces, the training of the surfaces was performed on 29 data samples, while an evaluation was performed on the remaining 3. This gave the opportunity to see what method for fitting the data to the surface was the most appropriate for the different objectives. The evaluation resulted in two types of response surface fitting types being used. The ones chosen for the various objectives can be seen in Table 3.12.

Using the response surfaces, an optimization could be performed in order to find optimum design points. Due to the usage of RSM surfaces, optimization algorithms could process the data fast and a large number of optimized designs could be generated. The importance when choosing the algorithm was to use one that could work with multiple objectives and also had the possibility to handle mixed integer optimization. Therefore, the algorithms applied were the HYBRID method as well as the MOPSO method.

In the optimization, no importance factor were set for the different objectives. Therefore the optimization gave a 3D shell with Pareto optimum points taking the pressure drop, the air extraction rate and the volume of the separator into consideration.

Table 3.12: modeFRONTIER boundary condition and response surface settings.

Parameter	Objective	Constraint	RSM method
Air Extraction Rate	Maximize	min: 1E-7 [kg/s]	Anisotropic Kriging
Pressure Drop	Minimize	max: 2 [kPa]	Anisotropic Kriging
Volume	Minimize	max: 0.15 [l]	DACE Kriging

3.4.4 Manual Optimization

In the DOE optimization, a number of 7 parameters were investigated. As previously stated some other parameters were very hard to evaluate in the DOE optimization study due to the high number of simulations needed. Therefore, the inlet rotation and the gas outlet position were chosen to be optimized manually after the DOE optimization.

After having identified a good geometry of the main separator, the inlet was rotated to take seven additional angles. This gave a 360° view of how the the separator inlet position changed the performance of the separator.

In addition, a number of simulations were performed while tweaking the gas outlet position. Both placing it in the centre of the separator and in the centre of the vortex. The result from this study was evaluated visually as well as looking at the performance parameters.

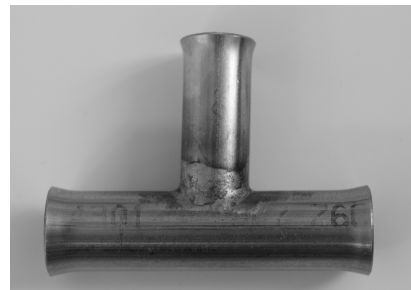
3.5 Optimized Design Evaluation

After having performed the parametric study and the various parts of the optimization it was of high relevance to find how well the process had predicted the performance of the separator. It was therefore of importance to perform validation testing on the optimized product. This validation was performed in three consecutive steps. The initial one was to create a CAD model which was possible to 3D print. This model was based on the optimized parametric separator but in addition some features were added which could not be achieved in the parametric model. These additional changes, such as adding a radius to sharp edges, were based on literature findings and reasoning regarding the visual observations from all the simulations performed. The RST model had proven to be more accurate than the Realizable $k - \varepsilon$ model. Therefore the following stage was to evaluate the final design using the RST computational model.

The final stage of the evaluation of the optimized design, was to use 3D printing to generate a model of the final design and test it in the previously built test rig. In addition to comparing the optimized design to design A and B, it was also to be compared to design X and a T-connection design. Design X is the separator which is currently used in the vehicle and a T-connection was examined in order to evaluate the relevancy of using a separator at all. Design X and the T-connection can be seen in Figure 3.10.



(a) Design X.



(b) T-connection.

Figure 3.10: Test objects for final tests.

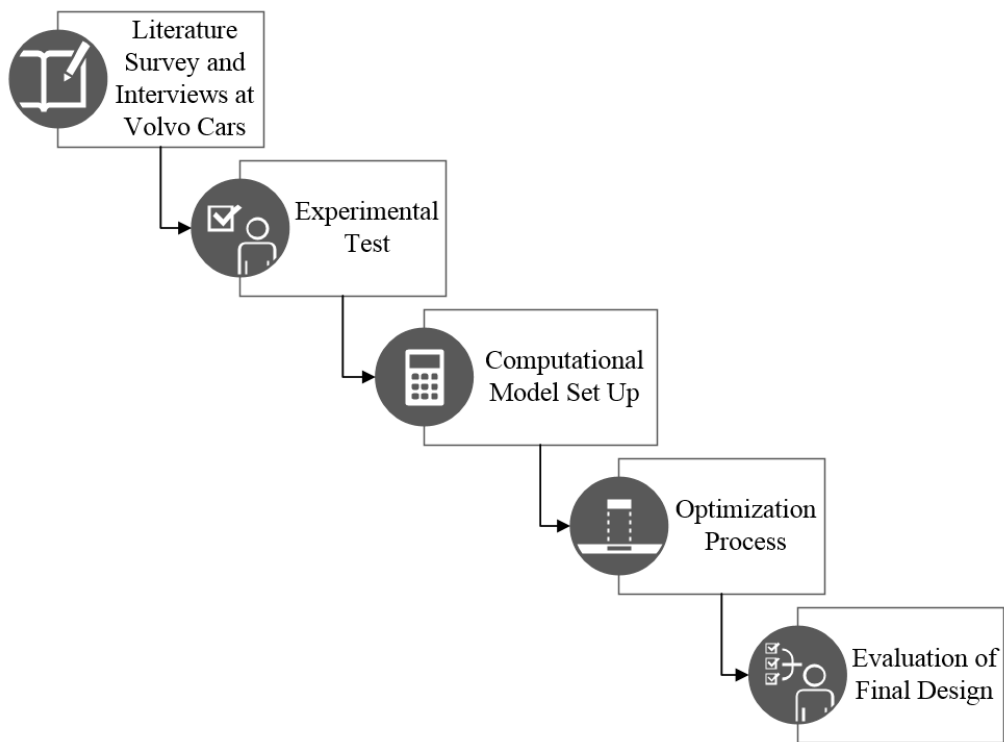


Figure 3.11: Schematic work flow.

In Figure 3.11 a schematic work flow is presented. The work flow is summarizing the Method chapter and clarifies the work order which was performed during the process.

4

Results and Discussion

In this chapter all relevant results are presented and the findings are discussed. First the experimental test results are presented, followed by simulation results and a comparison of simulated and experimental data. Further, the findings from the parametric study are treated and the results from the optimization process are presented. Finally a suggested improved separator design is presented along with its validation results from experiments.

4.1 Experimental Tests

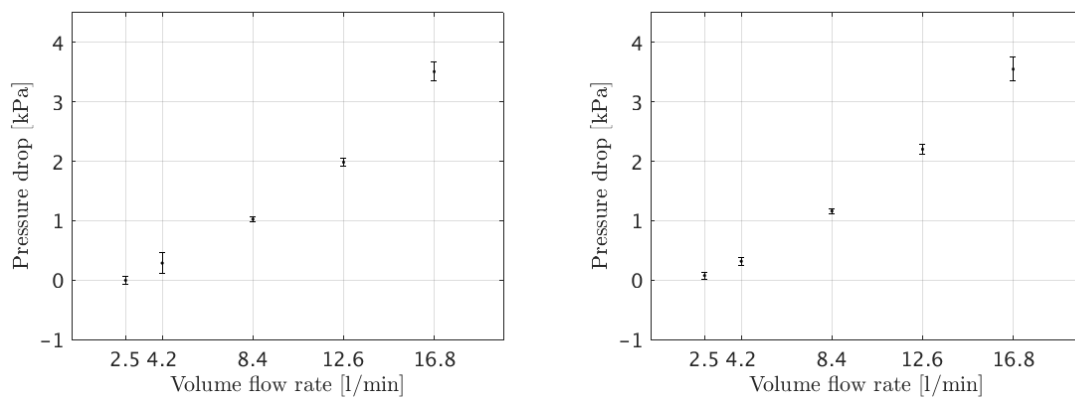
The collected test data including pressure drop, coolant temperature and separation performance are presented in Figure 4.1-4.3. Also, the general visual findings are presented.

4.1.1 Pressure Drop

In Figure 4.1 the pressure drop are shown for each test, both for A and B tests. Note that during the 10 minute long tests the pressure drop fluctuated. As suspected, the pressure drop increased with increasing volume flow rate. The graphs show that the pressure drop is similar between the tests, although slightly higher for design B. However, swapping the inlet and outlet does not affect the pressure drop to a great extent according to the experimental tests.

4.1.2 Coolant Temperature

In Figure 4.2 the mean temperature of the coolant for each test is shown. The temperature was kept at an almost constant value of approximately 23 °C and the variations in coolant properties were therefore deemed as negligible.



(a) A tests.

(b) B tests.

Figure 4.1: Pressure drops from the experimental tests. The presented values are the mean pressure drops and the error bars show the standard deviation.

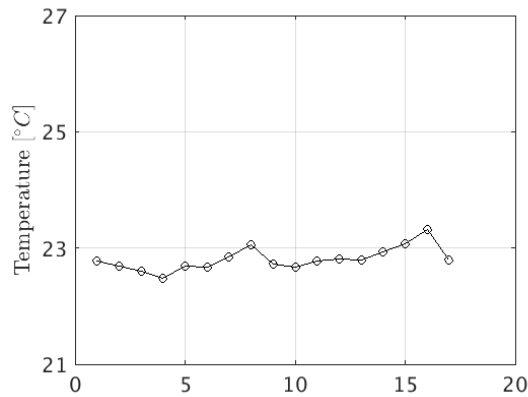
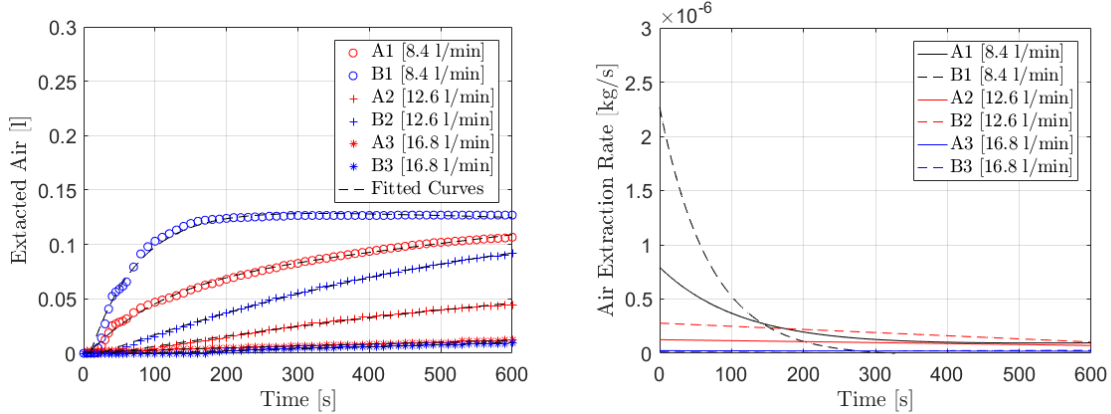


Figure 4.2: Coolant temperature throughout the test runs.

4.1.3 Separation Performance

The extracted amount of air from the system can be found in Figure 4.3a. The extraction rate of air is found in Figure 4.3b. Only data from the three highest flow rates are treated since for the lowest flow rates air got stuck in the system making the collected data unreliable. Note that design B shows an overall improved separation performance in comparison to design A. It was shown that the best separation occurred at a volume flow rate of 8.4 l/min. Since this was a relevant flow rate for the cooling system, this volume flow rate was chosen as a fixed parameter for further improving the separator.



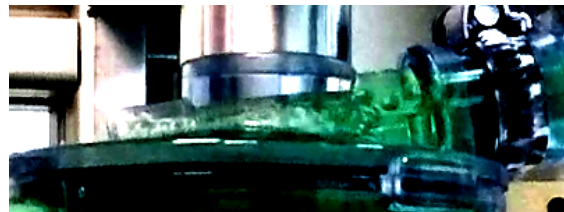
(a) Extracted air as function of time.

(b) Air extraction rate as function of time.

Figure 4.3: Test results for separation performance.



(a) Design A.



(b) Design B.

Figure 4.4: Pictures of the gas outlet taken during the lab experiments for visual evaluation of flow structures. The volume flow rate is 8.4 l/min.

4.1.4 General Visual Findings

- For the lowest volume flow rates, the air had time to coalesce into larger bubbles and since the velocity was low, air got stuck in some parts of the system. Although, for the larger bubbles that did reach the separator the air elimination worked very well due to the buoyancy effect on the larger bubbles.
- A problem was found when opening the inner circuit after running the flow only in the outer circuit. After mixing air and coolant in the outer circuit, the pump got affected by the sudden change in volume fraction when connecting the inner circuit. In addition, the pump had to accelerate the previously still fluid. A combination of these factors probably lead to the decreased flow velocity for some seconds which allowed the air to gather into larger bubbles. Therefore the first few seconds in the tests probably gave misleading results.
- For all tests the air had a tendency to collect in the top of the separator, much likely due to the inclination angle of the gas outlet pipe being low. See Figure 4.4 which visualizes the separators at 8.4 l/min. The collected air did however leave the separator when the pump was switched off. Hence, the air collection ability could be of interest to evaluate since the more air that is collected, the more air is extracted when the system is shut off.
- The ability for the air to reach the gas outlet was strongly dependent on flow velocity. At higher velocities, the flow in the separator became chaotic and the buoyancy force was too weak in comparison to rotational forces to make the air rise to the gas outlet. The air was instead caught by the swirling flow and flushed out through the outlet.
- The bubble size clearly decreased with increased flow velocity. Also, the pump significantly reduced the bubble size.
- The vortex in the separator seemed to be standing in a diagonal position and did not align perfectly with the central axis for test A. A slightly improved position was found in the B tests where the top centre of the vortex correlated better with the gas outlet.
- For the A tests, the ramp seemed to guide the air directly to the outlet instead of contributing to a beneficial swirling motion.
- Large improvement in separation efficiency was found for the B tests which can be seen in Figure 4.3.

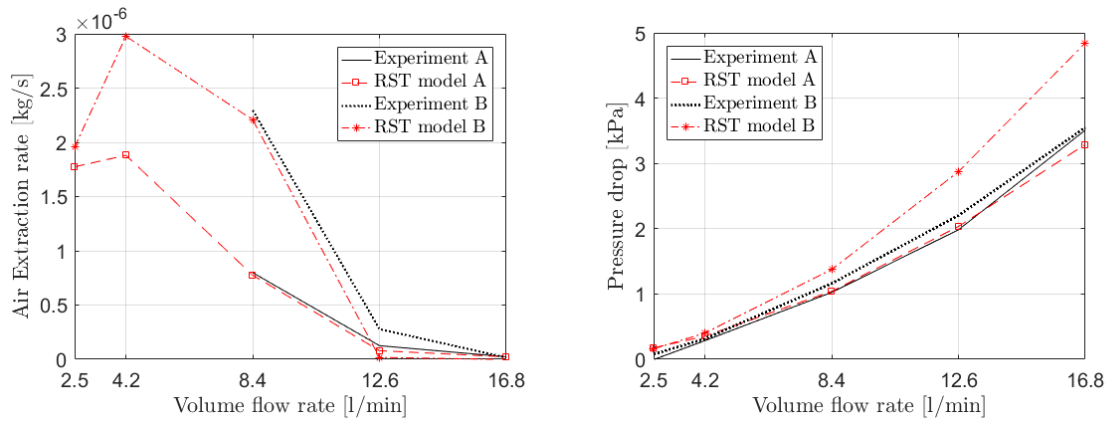
4.2 Simulations

This section treats the comparison between the experimental testing and the computational model. Various computational set ups are compared, evaluating the performance parameters as well as visual correlation.

4.2.1 Validation of CFD Model

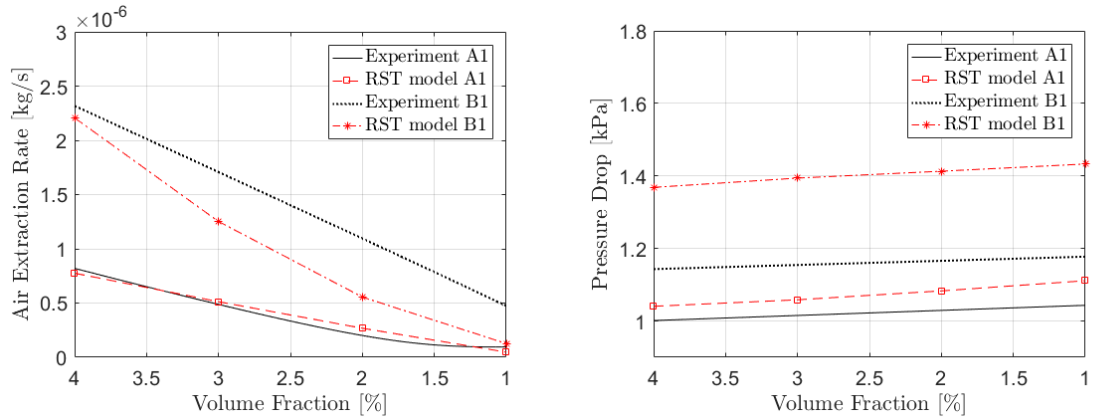
The quality and reliability of the CFD model were evaluated as described in Section 3.2.2. The results for pressure drop and separation performance were examined against the lab test both as a function of volume flow rate and volume fraction of air. The results can be found in Figure 4.5 and 4.6. It can be seen in Figure 4.5a and 4.6a that the trends of the computational model correlate well with the trends of the lab results for different flow rates and volume fractions of air. In Figure 4.6a it is evident that the simulation results deviate a bit from the test results for lower volume fractions, especially for the B tests. The exact reason for this could not be established. The results show that the CFD model is able to predict the outflow of air through the gas outlet to the correct order of magnitude although the absolute values do not match exactly. An important aspect is that similar trends are captured.

As was mentioned in Section 3.2.2 the simulations were limited to the assumption of a constant particle size. Since the actual size could not be measured in the experimental tests another method had to be used in order to find a reasonable bubble size. From the particle size dependency study, presented in Figure 3.6 in Section 3.2.2, it was known that the air extraction rate increased with increasing bubble size. This correlation was used to compare with experimental results for air extraction rate to find a matching particle size. From this comparison it was decided to apply a



(a) Air extraction rate as function of volume flow rate. (b) Pressure drop as function of volume flow rate.

Figure 4.5: Comparison between tests and CFD models for different volume flow rates.

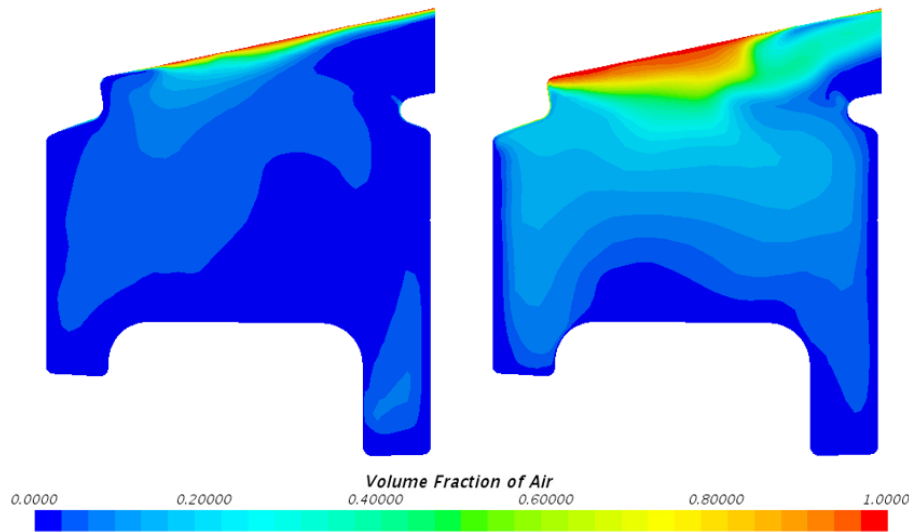


(a) Air extraction rate as function of volume fraction of air. (b) Pressure drop as function of volume fraction of air.

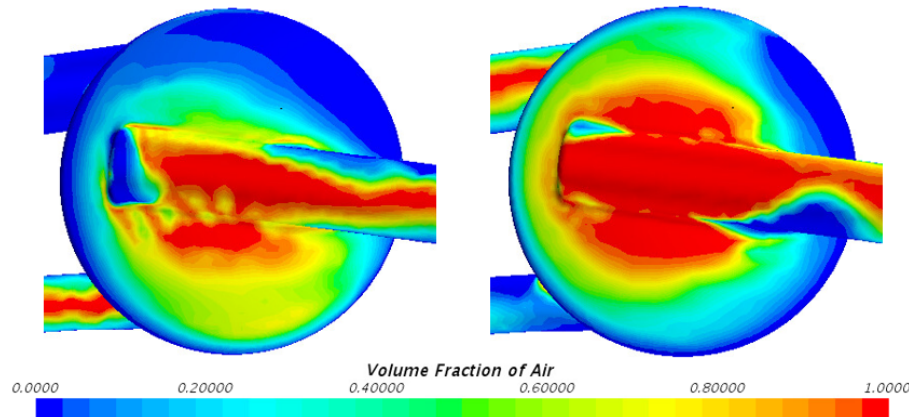
Figure 4.6: Comparison between tests and CFD models for different volume fractions.

particle size of $290 \mu\text{m}$. This method was not used in order to predict the exact particle size but rather to find a plausible size according to available data. Due to the limitation of a constant particle size, and the chosen remedy, the possibility is that the well matching trends with respect to air extraction rate partly is a result of this "tuning" of an important parameter in the computational model. However, the size was deemed reasonable and its effect on the trends in performance when changing geometry, which is the main focus in the current study, will be discussed in Section 4.6.

When looking at the pressure drop, Figure 4.5b shows a good correlation between experimental tests and simulations for the A case. Although, for the B case there are discrepancies. The reason for this could not be fully concluded. Note that in the experimental test, the inlet and outlet pressure was measured at the same tube diameter. However, in the simulation the pressure was measured at the tube diameter corresponding to the inlet and outlet respectively. This difference is highly likely to affect the result. Since the correlation is still rather good for a volume flow rate of 8.4 l/min and this was the flow rate to be used in the optimization part, the decision was to proceed with this CFD model. In Figure 4.6b one can see that the pressure drop is slightly increasing for a decreasing volume fraction of air. It is here of importance to point out that the changes in pressure drop are the same for both case A and B. These results are expected since moving a heavier phase should require more energy than moving a more light weight phase. Note



(a) Side view of design A (left) and B (right). The scalar fields are shown on a plane cutting vertically through the mid section of the separator.

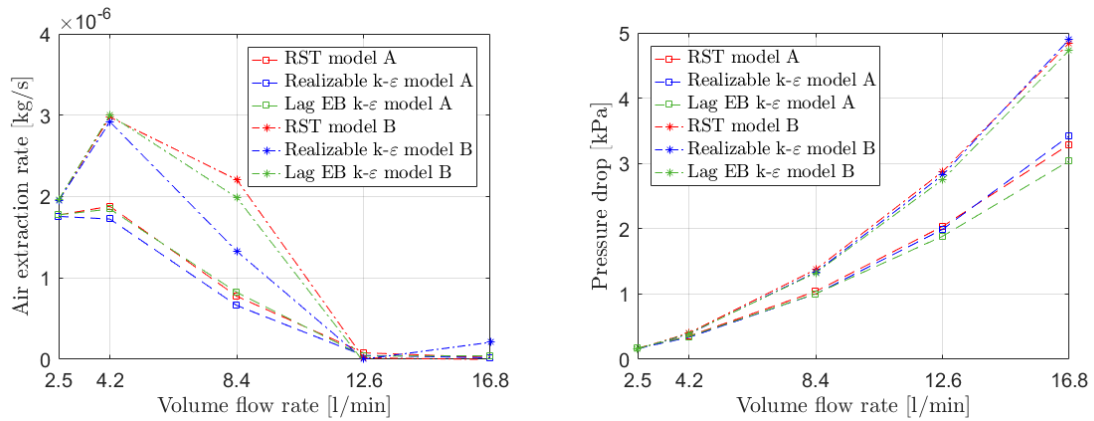


(b) Top view of design A (left) and B (right). The scalar fields are shown on the separator top surfaces.

Figure 4.7: Scalar plots of the air distribution in the separator at a volume flow rate of 8.4 l/min.

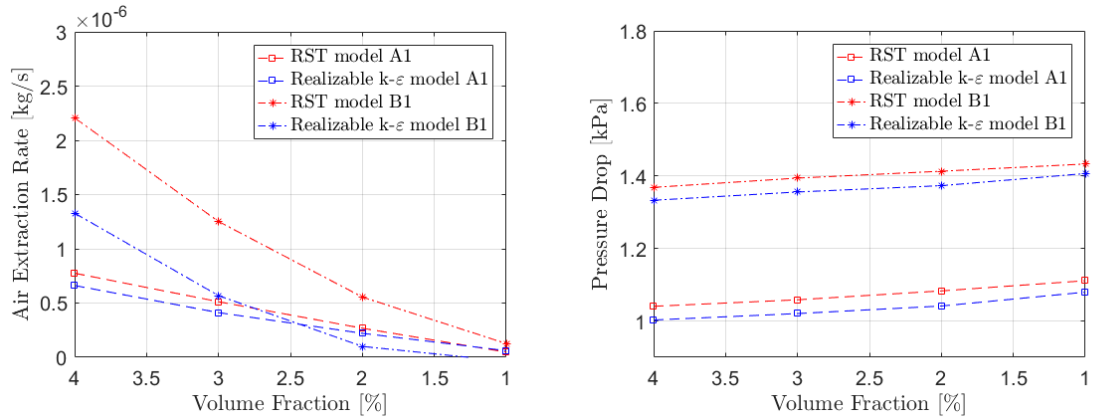
that this increase in pressure drop with a decreasing volume fraction of air is correlating with experimental data.

The simulations were also visually validated against the experiments by comparing the video recordings against scalar field views. The comparison was mostly focused on finding regions in which the air seemed to gather and comparing these findings with the scalar field of air volume fraction in the simulations. Starting with the side view in Figure 4.7a, it can be noticed that for case B the air seems to gather more towards the back of the gas outlet than it does for case A. This could be noticed visually during the experimental tests, see Figure 4.4. The reason that the air is gathered differently in the top is most likely due to the position of the vortex, which collects the air in its top centre. Another phenomenon which was also captured in the experimental tests is that in the B case there seems to be a "liquid pocket" right before the air leaves the gas outlet. In Figure 4.4b this phenomenon can be seen and compared with the B design in Figure 4.7a. The reason for this feature seems to be that the flow structures causes a rotation of the fluid in the gas outlet, pushing the gas towards its middle. By comparing design A and B in Figure 4.7b it can be seen that for design B, the air is more evenly distributed around the centre axis of the separator. This indicated that the vortex stands more straight and thus collects the air closer to



(a) Air extraction rate as function of volume flow rate. (b) Pressure drop as a function of volume flow rate.

Figure 4.8: Comparison between turbulence models for different volume flow rates.



(a) Air extraction as a function of volume fraction of air. (b) Pressure drop as a function of volume fraction of air.

Figure 4.9: Comparison between turbulence models for different volume fraction of air.

the gas outlet. This was also noticed during the experiments and is probably partly the reason to why design B had a better separation performance. However, the most evident reason for the increased separation performance of design B is the elevated position of the inlet in combination with the outlet position being further away from the gas outlet.

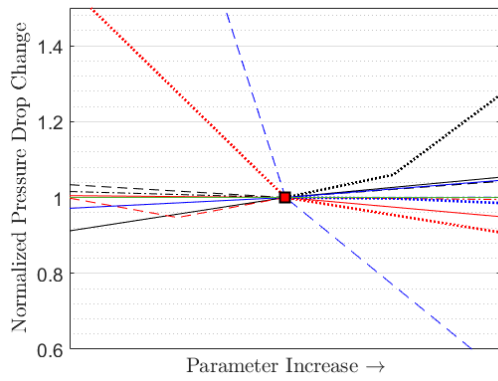
As mentioned in Section 3.2.2, the Realizable $k - \epsilon$ turbulence model as well as the Lag EB $k - \epsilon$ model was evaluated. This study was performed to see if there was an opportunity to use any of these in the following parametric study and optimization, as the RST model is expensive and can have a tendency to be unstable. Figure 4.8 and 4.9 shows the same graphs as in Figure 4.5 and 4.6 but comparing the RST model with the other turbulence models. Note that the Lag EB $k - \epsilon$ model was only evaluated for different volume flow rates. Looking at Figure 4.8b and 4.9b one can see that the pressure drop in the models are similar, apart from some small differences. The air extraction rate does however show larger differences between the models as can be seen in Figure 4.8a and 4.9a. The Realizable $k - \epsilon$ model has a lower level of agreement with the RST model than the Lag EB $k - \epsilon$ model. The reason for using another model would however be to minimize the computational time needed and increase the stability and simplicity of the model. It was found that the computational time of the Realizable $k - \epsilon$ model was lower than for the Lag EB $k - \epsilon$ model. It is also known that Realizable $k - \epsilon$ model is a more simple model and should

be the more stable alternative. Since the Realizable $k - \varepsilon$ model follows the same trends as the RST model this was deemed sufficient for the parametric study and optimization process. This choice was made based on the importance of computational time as well as the fact that only the relative values are relevant in the comparisons between different geometrical configurations.

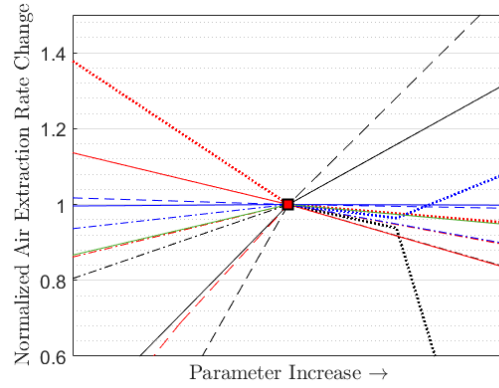
4.3 Parametric Study

The design changes presented in Table 3.8 were performed one by one to isolate the impact from each one of the input parameters. The results are found in Figure 4.10. The graphs show how changing each parameter affected the pressure drop, air extraction rate, air collection ability and the total volume of the separator. The air collection ability was chosen as an additional performance parameter to study since this was found interesting during the experimental tests. It is measured in volume of air in the domain. On the y-axis the change in performance is shown as a value normalized with the base line value. The x-axis represents an increase of the altered design parameter. It should be emphasized that the trends shown in the graphs are based on only three values for each design parameter, namely the base line value and two altered values.

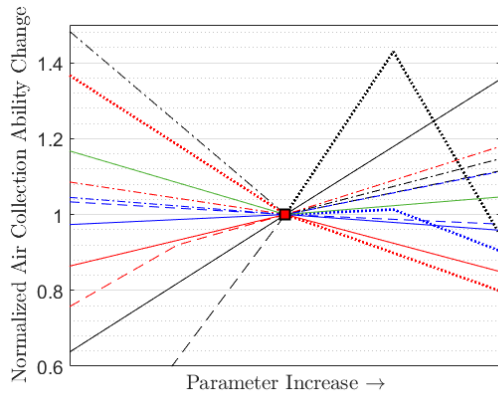
Similarly, an investigation of the internal parameters of the separator was performed, see Table 3.9. The results from this study can be seen in Figure 4.11. Note that below each of the two studies, the main findings effecting the various performance parameters have been pointed out. Visual findings from the two studies are also commented. In addition, in Table 4.1, a summary of the results are given for each parameter separately. It is of interest when looking at this table to compare it with the information found from previous studies which can be found in Section 4.1. It is clear that a lot of the trends correlate well with literature.



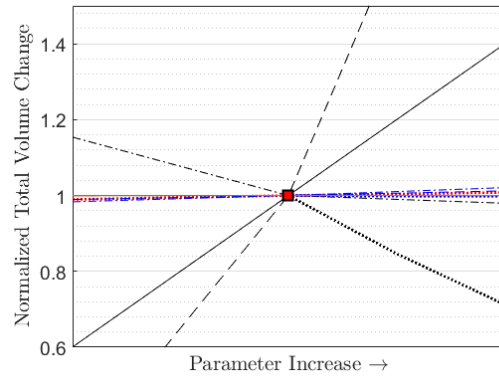
(a) Pressure drop.



(b) Air extraction rate.



(c) Air collection ability.



(d) Total separator volume.



Figure 4.10: First parametric study results. Only the y-axis is normalized, see Section 3.3.2

The main findings from the first parametric study of the separator are found below:

- The pressure drop is found to be mostly dependent on inlet and outlet diameter. A larger diameter gives a reduced pressure drop and particularly the outlet diameter shows large effects. In addition, the separator body angle is also of interest for the pressure drop. Smaller but yet interesting parameters are the outlet angle as well as the separator height.
- The air extraction rate of the separator does for most geometrical changes from the base line show negative results. However, making the separator higher, wider, decreasing the inlet diameter as well as adding a negative angle to the inlet proves to give an improved air extraction rate. Additionally, increasing the gas outlet angle and decreasing the outlet diameter also show tendencies of an improved efficiency. The most obvious negative effect on the air extraction rate is found for making the separator smaller in size as well as lowering the inlet height.
- The air collection ability is positively affected mostly by decreasing the separator crowning radius, adding a small angle to the separator body, decreasing the inlet diameter as well as making the separator higher. Negative effects are most evident when making the separator smaller.
- The total volume of the separator is affected by the outer parameters which are width, height, top radius and angle of the separator body.

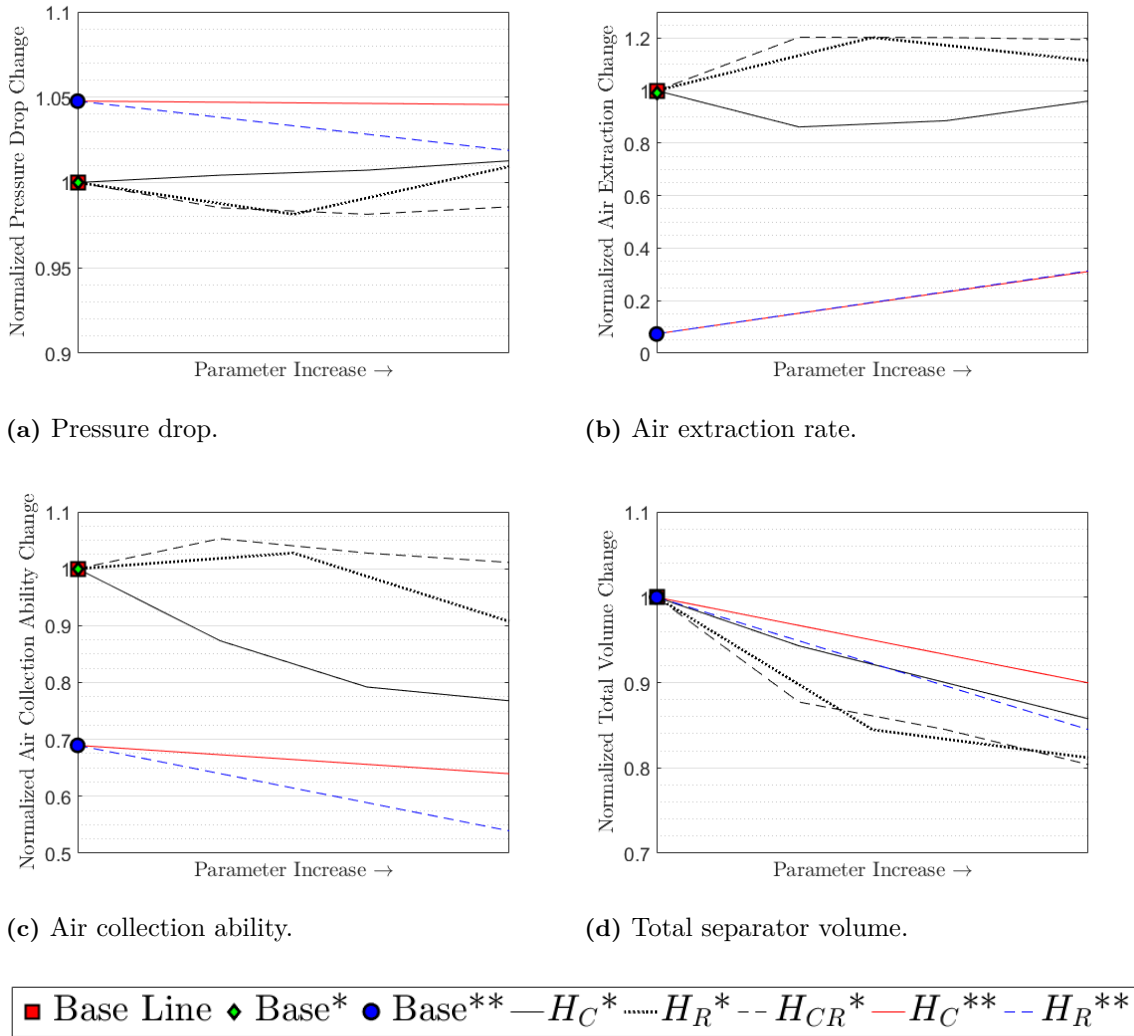


Figure 4.11: Second parametric study results. Only the y-axis is normalized, see Section 3.3.2

The main findings from the second parametric study of the separator are found below:

- It is clear that changing place of inlet and outlet, placing them as in design A, only gives negative results.
- Mirroring the separator, that is changing direction of the flow shows as expected small to no changes in abilities.
- The total volume change is not much of interest in this test since the outer parts of the separator are still measuring the same.
- Pressure drop and air extraction rate are both showing best results for a ramp just high enough to cover the outlet and the cone only slightly higher than this.
- The air collection ability is best for a ramp just covering the outlet.

Additional findings from the parametric studies:

- The gas outlet position is of importance. It seems like the best efficiency is found when the gas outlet position coincides with the position of the centre of the vortex. The angle of the gas outlet seems of less importance as long as it is above a certain level, approximately 70° .
- β -rotations and gas outlet properties do only seem to be influencing the air extraction rate. The inlet rotation also seems to strongly influence the position of the vortex. A mathematical optimization on these parameters might be difficult, and a visual one might be preferable.

Table 4.1: Comments on the various design parameters.

Design Parameter	Comment
Separator Height & Width	The most important parameters. Affect all values of interest and are the two parameters that set the size of the separator.
Separator Body Angle	Increasing this parameter affects both the pressure drop and the air extraction rate negatively. However, it does show effect on the volume. It is worth noticing that this decrease in volume can be deceiving since the upper part still has the same size and therefore packing wise this volume decrease might not be of interest.
Separator Crowning Radius	Marginally affects the pressure drop while making the air extraction rate worse for both increasing as well as decreasing its value. It appears that the current value is OK. However, most probably should the top lid be redesigned in order to achieve the best air extraction rate abilities.
Inlet Angle	Shows a relatively linear trend where a negative inlet angle gives improved efficiency. Increasing the inlet angle gives a slight decrease in pressure drop.
Inlet Height	A clear trend that shows that the inlet should be placed as high as possible to achieve the best air extraction rate.
Inlet Diameter	Gives "false" effects on the total volume, i.e does not effect the main body of the separator but only the connections. Decreasing the inlet size gives improved air extraction rate performance but at the same time it also increases the pressure drop. The size of the inlet is therefore a trade off between air extraction rate and pressure drop.
Inlet Rotation	Rotating the inlet changes the air extraction rate due to its effect on the vortex position. However, only looking at three data points is not sufficient. It is important to note that this parameter mainly affects the air extraction rate.
Outlet Angle	Barely affects the air extraction rate but has some significance on the pressure drop where a negative outlet angle gives a decreased value.
Outlet Diameter	The single most important parameter for the pressure drop. However, for the air extraction rate, a smaller outlet is profitable. In comparison, it is important to note that the effect on the pressure drop is significantly larger. Note that this parameter gives "false" effects on the total volume.
Gas Outlet Angle	Does not show significant effects on other aspects than the air extraction rate. The result is however not clear but the most probable outcome is that a higher angle is preferable.
Gas Outlet Diameter	This parameter, similarly to all other inlet/outlet diameters gives "false" effects on the total volume. It additionally gives no effect on the pressure drop. It can be seen that it has the most profitable outlet size for the base line value (13 mm) for air extraction rate.
Gas Outlet Rotation	Shows very small effects on other performance parameters than air extraction rate. It seems profitable to have its position correlating with the one of the vortex.
Cone and Ramp	It is found that using a cone and ramp is profitable for the air extraction rate. The cone and ramp should be so high that they are just covering the outlet. It is important to note that changing these parameters gives "false" effects on the total volume.

4.4 Optimization

In this section all the relevant results from the optimization process of the separator design will be presented. The section will start with the simplified optimization which is based on the parametric study and can quickly give recommendations regarding how to design the separator in order to reach certain values for the performance parameters. Thereafter the results from the more thorough optimization are presented and finally how a design was chosen and evaluated will be described.

4.4.1 Parametric Study Optimization

A few simulations were performed in order to evaluate how well the optimization based on the parametric study estimated the outcome. In Table 4.2 the findings of this comparison can be found. It can be seen that the values do show correlation between the estimated values and the simulated values, even though the exact numbers mismatch. There are differences between the various design parameters of interest. The one that shows the worst correlation is the air collection ability. It is found that this optimization tool can be used as a rough starting estimation. It gives the opportunity to quickly go through various importance ratios and find corresponding design values. These design values can thereafter be used as for example an input starting position for a fully automated optimization. Making a good initial guess can considerably decrease the time and cost of an optimization.

Table 4.2: Parametric study optimization results.

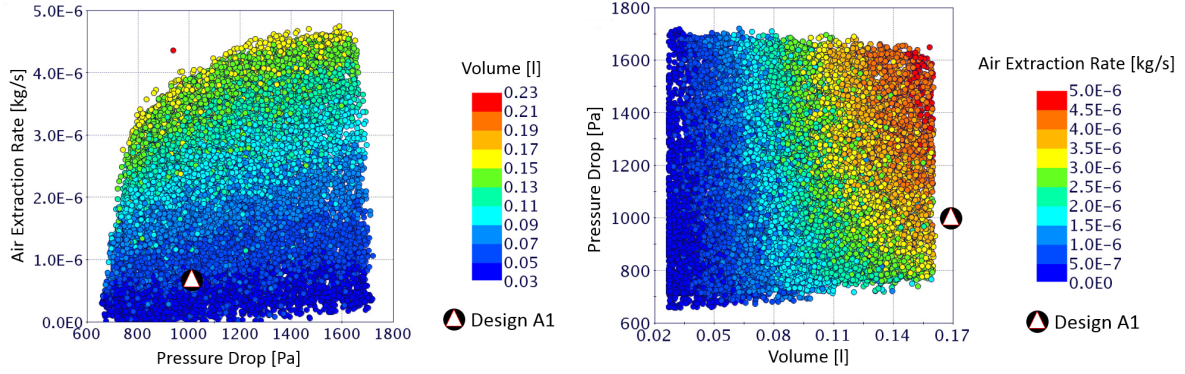
Importance Ratio [%]	Performance Parameter of Interest	Base Value	Estimated Value	Simulated Value
9	Pressure Drop [Pa]	1593	879	1178
30	Air Extraction Rate [kg/s]	3.52E-6	3.81E-6	3.41E-6
61	Total Volume [l]	0.270	0.172	0.178
0	Air Collection [l]	0.0194	0.0045	0.0167
10	Pressure Drop [Pa]	-	945	1145
50	Air Extraction Rate [kg/s]	-	9.32E-6	5.02E-6
30	Total Volume [l]	-	0.297	0.298
10	Air Collection [l]	-	0.0011	0.0023
38	Pressure Drop [Pa]	-	725	872
16	Air Extraction Rate [kg/s]	-	4.1E-8	6.75E-7
38	Total Volume [l]	-	0.0878	0.0978
8	Air Collection [l]	-	0.0080	0.0062

4.4.2 DOE Optimization

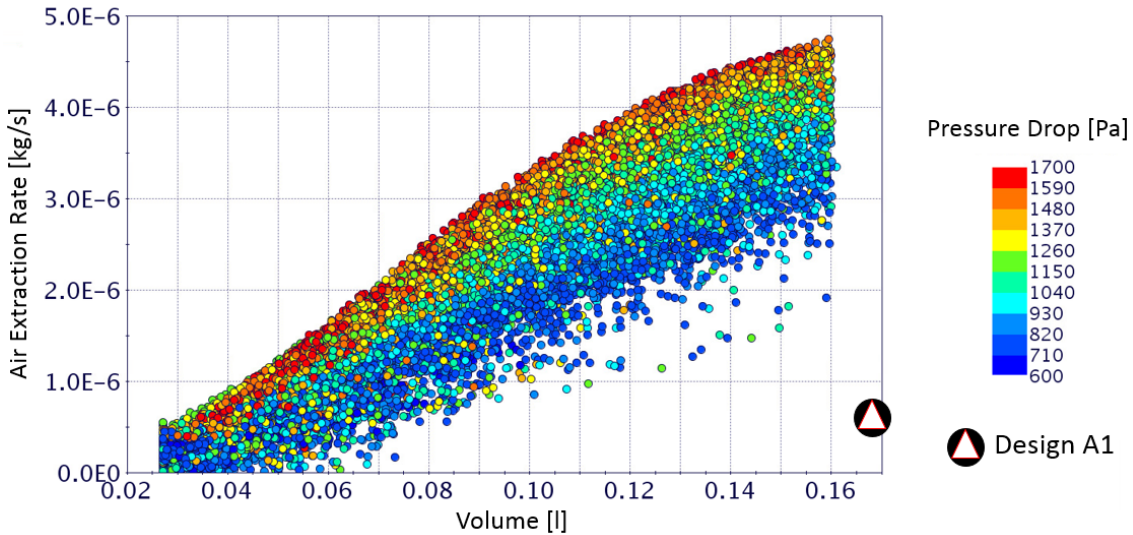
The optimization was performed on the response surfaces created from the DOE table. The quality of the surfaces was evaluated and the results can be found in Table 4.3. Here the mean absolute error and the R^2 values are presented. It can be seen that the volume and the air extraction rate give good values which indicates that the output from these two performance parameters will be trustworthy. The pressure drop however shows significantly worse results. This provides the information that the pressure drop is probably highly non linear and the estimation of the pressure drop will be less trustworthy. This information is of interest when evaluating the results and are also not very surprising. The pressure drop is depending on the flow structures in the separator and how smooth they are. Small changes in the interior domain can affect the flow structures and therefore also the pressure drop.

Table 4.3: Response surface quality.

Measurement	Volume	Air Extraction Rate	Pressure Drop
Mean Absolute Error	1.7E-5 [m^3]	1.7E-7 [kg/s]	43.8 [Pa]
R^2	0.999	0.976	0.148



(a) Air Extraction Rate as function of Pressure Drop and Volume as colour. (b) Pressure Drop as function of Volume and Air Extraction Rate as colour.



(c) Air Extraction Rate as function of Volume and Pressure Drop as colour.

Figure 4.12: Optimization results.

In Figure 4.12 the result of the optimization is visualized. The solution of the three objective functions are creating a shell which spans the optimal solutions. The choice of the best solution now comes down to what performance parameter is of highest interest to maximize or minimize. It is found that the pressure drop is not very high for any of the designs, compared to the overall pressure drop in the cooling system. In addition, response surface quality indicated that the pressure drop is the least trustworthy. Therefore, in Figure 4.12c the volume and the air extraction rate are visualized against each other. The best trade-off between the two performance parameters can be chosen along the top line. Note that the performance of design A1 is added into the three plots as a reference.

Note that in Figure 4.12, there are some distinct outliers. These are especially clear in Figures 4.12a and 4.12b. The reason for this is that from the DOE, these design alternatives were used to span the design space. However, when running the optimization the constraints on volume,

Table 4.4: Evaluation of the quality of the optimization prediction.

Output	Mean Error [%]	Max Error [%]
Air Extraction Rate	8.7	12.7
Pressure Drop	7.1	14.1
Volume	0.1	0.4

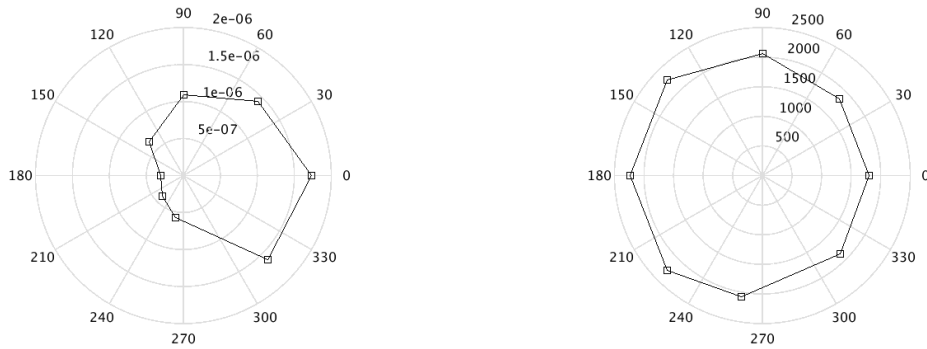
pressure drop and air extraction rate made the optimization algorithm not create geometries in these sections.

In Table 4.4 the quality of the optimization prediction is given. A total of five random designs given from the optimization tool were evaluated by creating simulations in STAR-CCM+. The mean error as well as the maximum error of the five evaluation runs are given in the table.

4.4.3 Manual Optimization

In Figure 4.13 the results from rotating the inlet position can be found. It is clear that changing the inlet position around the separator has large effects on the air extraction rate of the separator but also some effect on the pressure drop. From visual findings it was seen that the inlet position strongly altered the position of the vortex. Having the inlet at the original position gave the best results for both the pressure drop and the air extraction rate. These results coincided well with the visual findings that the bottom of the vortex was as far away from the outlet of the separator as possible. It is worth noticing that during this evaluation the outlet and the gas outlet were kept fixed. However, the gas outlet was placed in the centre of the separator and had a high inclination, i.e. 70° . The contribution from the gas outlet to these results is therefore regarded as small.

Placing the gas outlet in the correct position showed to be an important factor for the air extraction rate of the separator. A visualization of these results can be found in Figure 4.14. Note that the angle of the gas outlet is directed into the paper in Figure 4.14a and thus the strange shape of the outlet. Visual findings showed the importance of the gas outlet being in the highest position of the separator in order to not have any pockets where gas can be gathered. It was also seen that the placement of the gas outlet should be in the centre of the vortex which improves the air extraction rate of the separator. Changing the angle of the gas outlet was known from the parametric study to give results on the air extraction rate. It was found in the study that placing the gas outlet in the same angle as the vortex gave improved results on the air extraction rate. It is of importance to note that the angle of the gas outlet is still of high importance and should be kept above a value of approximately 70° .



(a) Air Extraction Rate [kg/s].

(b) Pressure Drop [Pa].

Figure 4.13: Properties as function of rotating the inlet.

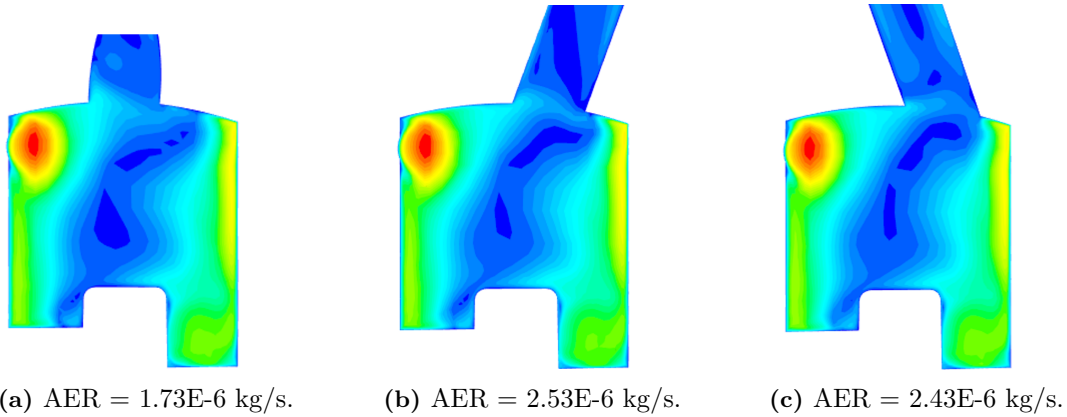


Figure 4.14: Air Extraction Rate (AER) for different positioning of gas outlet. The figures are velocity scalar plots where the red areas with high velocity correlate with the inlets. Blue color indicates lower velocities.

4.4.4 Choice of Design and Optimization verification

After performing the optimization process, a design with an interesting mix of the various properties was chosen. As the goal was to minimize the size and the pressure drop while maximizing the air extraction rate, the choice was a trade-off between these parameters. It is worth noticing that this design was chosen after some discussions with Volvo Cars employees. However, if other properties are of interest it is possible to go back to the optimization result and find a more suitable design suggestion.

The improved design can be seen in Figure 4.15. This design is for further reference called design C. The design was evaluated both in STAR-CCM+ and after 3D-printing, in the lab. The comparison between the results can be found in Table 4.5. It can be seen that the simulation is slightly underestimating the air extraction rate, which is however correlating with the previous verification performed in Section 4.2.1. The simulation is also underestimating the pressure drop. However, this error is more significant. It is important to remember that the tubes connecting the separator with the test rig was not replaced to accommodate for the lower inlet and outlet diameters in test C. This results in a more distinct edge for the flow to pass when entering the separator which might have affected the pressure drop. Also, remember the difference between the simulations and experiments for measuring the pressure drop discussed in Section 4.2.1. These factors could explain the difference between the experiments and simulations.



Figure 4.15: 3D-print of design C.

C is similar to but slightly better than design B. If looking in Table 4.6 one can see that the pressure drop of design C is considerably higher than for the other designs. As previously found, the pressure drop is mostly a result of the inlet and the outlet diameter. In designs A and B, the inlet and outlet is 13 mm and 15 mm while in design C, the inlet is 11 mm and outlet 13 mm. The increase in pressure drop is therefore no surprise and worth pointing out is that the inlet and outlet diameters are the same as for design X. It should also be pointed out that these levels of pressure drop which reached for design C, are regarded as small in comparison to other components of the cooling circuit [3]. Looking at the last column of Table 4.6 one can see the volume of the separator. It is here noticed that the volume of design C is less than half of the volume of designs A and B.

Finally, a comparison between design X and the optimized solution was performed. As can be seen in Table 4.6, design C does show improvements in air extraction rate and volume while the pressure drop of the two is similar. This correlates well with the previous discussion regarding the pressure drops dependence on inlet and outlet diameter. Looking in Figure 4.17 one can see that the air extraction of design X is very irregular and not as smooth as other tests. It was noted during the test that air was mainly extracted in situations where the pump stalled a bit, slowing down the flow for a brief period of time. When a continuous flow through the design X separator was achieved, barely any air was extracted via the separator. It can thus be stated that design C is an improvement compared to design X.

Additionally, it was interesting to evaluate the performance of design C at other volume flow rates. Previous evaluations of the separator designs A and B showed decreased air extraction ability for an increased volume flow rate. Noticeable is that when increasing the volume flow rate for design C, the separator seemed to be able to extract additional air. These findings were however discovered late in the project and therefore no data can be presented. Nonetheless it can be stated that design C works as a cyclone separator should, the strong rotational motion of the flow "pushes" the air towards the center where the air can be extracted by buoyancy effects. As previously discussed, design A and B work mostly as gravitational separators.

Table 4.6: Experimental results of design C and other geometries for comparison.

Design	Pressure Drop [kPa]	Extracted Air [l]	Volume [l]
A1	1.025	See Figure 4.17	0.1778
B1	1.162	See Figure 4.17	0.1778
C1	2.17	See Figure 4.17	0.0615
X1	2.16	See Figure 4.17	0.1024
T-Connection	-	See Figure 4.17	-

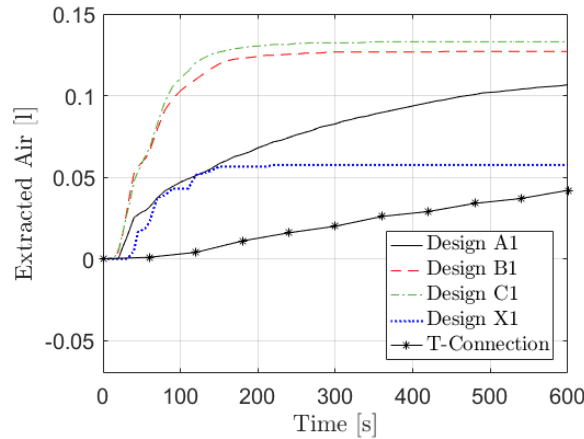


Figure 4.17: Air extraction experimental results.

4.6 Overall Discussion

Initially, it is worth emphasizing that errors could have occurred due to imprecise measurement tools in the lab experiments. The air extraction rate was evaluated using a camera and there were instabilities in the pressure drop measurements. More sophisticated tools could have been used to get more precise values. However, it is worth pointing out that it is believed that the accuracy of the test method is sufficient for the evaluation performed.

The test rig was designed to replicate the real, in vehicle, cooling system as well as possible. However, no other devices of the cooling system circuit were attached and a fairly large tube diameter was used in parts of the system in order to make the system reasonable in volume. It is known that both devices and tube diameter might affect the coalescence and break up of air bubbles. It was discovered that the bubble size had a great effect on the separator efficiency, especially when the separator was designed such that the buoyancy effect was more dominant than the cyclone effect. It would therefore be of interest to evaluate the flow in the cooling system just before the separator, in order to better be able to estimate the bubble size and flow properties entering the separator and thus replicating this in the lab test set up. Additionally, the findings show the importance of the separator positioning. The separator, independent of the type, should be located where the inflow fluid has been disturbed as little as possible. Preferably after a long, straight and wide tube section.

It was also found that the velocity of the flow had a strong influence on the bubble size. Decreasing the inlet diameter can therefore be counterproductive. The increased separation efficiency due to a fast flow and a stronger vortex production, might result in an even stronger negative effect due to the break up of the bubbles. Most likely, the ideal design would be to keep the inlet and outlet diameter to the same as the tube connecting to the two branches respectively. This since any abrupt change in the flow domain will increase turbulence and thus also break up of bubbles. However, it is also worth pointing out that a large inlet diameter results in a low inlet velocity which results in a weak vortex. In design A, the inlet and outlet size were 13 mm and 15 mm. This design showed some effects of the vortex gathering the bubbles, but the gravitational effect definitely seemed to be more dominant for the separation. Hence it can be stated that if one wants the separator to work as a cyclone separator and not just as a gravitational one, an inlet velocity above a certain level is required.

In order to find a reliable computational model for the separator performance, a large part of the project time was consumed. As previously has been mentioned, a multiphase problem is not as straight forward as a single phase one and this dilemma was especially encountered when selecting a suitable mesh. There were tendencies of fluctuating results when changing the size of the mesh, especially the prism layer size. Trying an even coarser mesh would have been of interest but this lead to a worse representation of the geometry and was therefore disregarded. Another problem was that a simple generic mesh suitable for different geometries was desired. Thus, a more thorough study on how to adapt the mesh for one single geometry was not done. However, the utilized mesh gave results which correlated rather well with experimental results and the model could therefore be regarded as acceptable to use for the study.

It is of importance to note that due to the time frame of the problem, the mesh set up of the problem could not be fully evaluated. Eventually the mesh was set up in accordance with general guide lines for meshing and boundary layer representation, information from literature regarding similar projects as well as by the help of experienced personnel at STAR-CCM+ support and Chalmers employees. However, even though it would probably be of interest to evaluate this part of the problem further it is most likely the case that finding a perfect mesh is very difficult. Multiphase problems are inherently difficult and acquiring a mesh set up that gives stable and accurate results for any geometry is both cumbersome and time consuming. Therefore the project went along without being fully confident with the mesh set up and it is therefore of importance to note that the estimation of the separator performance is only as good as the computational model set up.

Regarding the particle size, which was discussed previously in this section, it would have been

desirable to treat this in a different manner. From the experimental tests it was clearly visible how an increase in flow velocity lead to a decrease in particle size and obviously this should also be captured in the simulations. Attempts were performed to account for this physical aspect using the S-Gamma model. The usage of the model did however result in severe convergence problems. The alternative was to assume a constant particle size, which was also done in the studies in [8] and [10]. Due to the fact that the model had to be stable for a variety of geometries, the choice was taken to use a fixed particle size in order to represent the flow. It is thus of importance to remember that when changing, especially the inlet diameter of the model, the computational model might not be fully reliable. It is worth pointing out that when performing the study to find a suitable particle size, some additional interesting information could be extracted. It could for example be seen that using a smaller particle size would give similar trends as using a larger one, only that the levels of extracted air were smaller. This would indicate that in order to just evaluate the trends, the particle size is not of highest importance. However, no extensive study was performed and this assumption is solely based on a few simulations. Therefore, this would be of interest to investigate further to provide information regarding the reliability of this method.

Another alternative on how to treat the particle size could be to completely change from an Eulerian-Eulerian approach to an Eulerian-Lagrangian, which is known to handle a wide range of particle sizes well. At an early stage of the project there was a will to include a comparison between the two approaches but this was later rejected due to time limitations. However, there was never a definite answer on which method being the most suitable. Perhaps, with all facts on hand, the Eulerian-Lagrangian method might have been the better choice and it could be of interest to try in further studies.

When performing the optimization to find the most suitable design of the separator this was performed using a computational model which was less accurate than the best one found. The chosen set up was based on a Realizable $k - \varepsilon$ model due to this model's advantages regarding speed and stability. Even though the results of this model were not as close to the test data as the more expensive RST model, it is important to point out that the trends of the results were correct. That implies that the air extraction values found from the computational model might not be trustworthy, but the model should be able to find the best design relative to each other. It is therefore of importance, when looking at the results from the parametric study and the optimization, to remember that the values are most probably not completely correct. However, the trends and the parameters importance relative to each other should be of great interest.

Regarding the final choice of design, it is of importance to emphasize that this combination between the design parameters is taken by persons without full insight in the cooling system design process. Therefore the optimization performed in this study are to be used as a tool to give guidelines in how to design a future separator and should not be seen as a definite design. The goal was initially to create a fully automated optimization but unreliability in the parametric CAD model and lack of time resulted in this not being performed. However, due to the fact that the relative importance of the different performance parameters are currently unknown, the method used is probably very well suited for the case at hand. The study gives a great overview of the effect which each input parameter have on the output and information regarding how they affect each other.

If a fully automated optimization is to be done in the future the work in this study is still of great importance. The study gives a general knowledge regarding the design aspects which can be used as an initial guess of where the optimum might be. In addition, this study can give information regarding applying constraints to the optimization. In summary this would result in a much faster, easier and less expensive automated process. Worth pointing out is that the final result is never better than the quality of the computational model. The accuracy of the model used in this study should be sufficient to give general design advice but in order to give definite trustworthy design values, some more time should be spent on improving the computational model.

When evaluating the final design it could be seen that it does show an improvement in comparison to design X. It also showed positive changes relative to design A apart from the pressure drop.

However, it has been found from discussions with Volvo employees that in comparison to other devices along the electric drive cooling system circuit, the separator pressure drop can almost be neglected. That is the reason for choosing this design despite the relatively high pressure drop. In a similar fashion it is recommended when settling for a final design to make some adjustments to the model. The lower the amount of variable parameters are, both input and output parameters, the easier it is to find an optimum design. It is therefore suggested to for example specifying the amount of space which is available in the engine bay and thereafter setting this as the volume of the separator. This will result in a smaller amount of parameters to optimize for and an easier and faster process. It is of importance to note that an assumption made here is that the efficiency gets better the larger the separator is, which is a result that can clearly be seen in this study. However, if one want the separator to work as a cyclone separator and not just as a gravitational one the size cannot be too great.

This thesis has solely treated the study of a separator of cyclone type with the aim to better understand and improve the currently produced separator. Although, it is still relevant to question this type of separator and if it is the most appropriate solution for the given task. In the experimental tests it was found out that for lower flow velocities no vortex was produced and the separator worked more like a gravitational type. Since the velocity was low the air gathered into large bubbles which created a strong buoyancy effect and the separation performance was good. Thus, it comes down to under which conditions the separation of air is thought to take place. If the system can be completely free from air under low pump speed a gravitational separator is probably sufficient. If there is still need for air elimination for high pump speed, then a cyclone separator is probably the most appropriate choice.

It is important to note that at low flow velocities, not all air in the system seemed to be brought along with the flow but got stuck in higher places or as small bubbles along the tube walls. In essence this says that a relatively high flow velocity is required to bring all the bubbles along with the flow. As a gravitational separator works by slowing the flow down, this results in the necessity to have a large separator. As this is not a very good alternative, there are basically two ways to go. Either one uses a cyclone separator or alternatively, no separator at all. In this case, one could apply a simple T-connection or an air extraction possibility in the radiator. A system as this does not control the air elimination as the usage of a separator is, but it would probably result in a much less significant pressure drop and take less space than a separator. As seen in the tests, a T-connection does extract air from the system. However, the time it would take or if it actually would eliminate all the air from the system is not known. It is worth pointing out that a more precisely designed T-connection than the one tested in this study could probably give higher air extraction rates.

In addition one can argue about the importance of the efficiency of the separator. Since the separator will stay in the car for the lifetime of the vehicle, the separator does indeed have a long time to empty the system from gas. However, it seems like when the separation performance is too low, it will basically never fully empty the system from air and small bubbles will always stay in the system. Hence, removing the separator might result in decreased air extraction abilities and possibly over heating of components. Nonetheless, it is still an interesting factor and a certain air extraction rate value necessary for eventually emptying the system from air has not been discovered in this project. The decision whether a T-connection is sufficient or a separator is needed and in that case what kind, is highly relevant. However, this all comes down to a further discussion regarding what aspect is the most important for the design of the cooling system and the separator.

5

Conclusion

The main findings from this thesis are summarized below:

- The bubble size is of great importance for the air extraction ability of a separator. Therefore, the positioning of a separator should preferably be where the flow is as undisturbed as possible. For example after a long straight tube having the same diameter as the inlet of the separator and preferably just upstream of the pump.
- Making the separator too big makes the centrifugal effect in the separator very small and the separator will only work as a gravitational separator.
- Removing the separator and applying a simple T-connection does eliminate air from the system. The rate of extraction or how much of the air that will be extracted can however not be guaranteed. If a controlled air extraction is deemed necessary, a separator should be used.
- When designing the separator with respect to separation efficiency, pressure drop and size, the optimal design is a trade-off between different design parameters since their effects counteract each other.
- The pressure drop over the separator is mainly affected by the inlet and outlet diameters. A wider diameter gives a lower pressure drop.
- The simplest and most evident design change to improve the air extraction rate of the separator is to have the inlet placed high and the outlet placed low.
- The air extraction rate is in addition positively affected by making the separator higher, wider, decreasing the inlet diameter as well as adding a negative angle to the inlet. Decreasing the outlet diameter also shows tendencies of an improved air extraction ability. The most obvious negative effect on the air extraction rate is found for making the separator smaller in size, having non tangential inlet and outlet as well as lowering the inlet height.
- The inlet and outlet should be rotated such that the bottom of the vortex is as far from the outlet as possible.
- The gas outlet should have a high angle and be placed at the highest position of the separator and angled to correlate with the vortex.
- Findings regarding what parameters that are important for the performance of the separator correlate well with literature. Also the preferred settings of the parameters correlate rather well.
- The RST turbulence model showed best correlation with experimental results but the Realizable $k - \varepsilon$ model is computationally cheaper and predicts the correct trends.
- Optimization tools have shown capable of finding an improved design. The quality of the design suggestion is however only as good as the models used to retrieve it. Further improvements to the method should result in a better design suggestion.
- A prototype design based on the study has been built and evaluated and shows significant improvements to the current separator.

6

Future Work

The study has shown that there are several improvements that can be made to the separator. Opportunities to make simple changes to the separator which would improve the air extraction solution exist as well as more complicated and time consuming alternatives. Therefore the future work has been divided into three groups where the first one is the most simple. The second group needs some more work but would give significant additional improvements compared to the first group. The third group will be more complex and take the most time. This should in theory give the optimum results but it all comes down to the quality of the work.

1. Direct Changes

- (a) Change place of inlet and outlet.

2. Simple and Fast Procedure [Using the Method of This Study]

- (a) Go back to the DOE optimization results and decide on a trade-off between pressure drop, air extraction rate and separator volume. Possibly extend the DOE table using more designs.
- (b) Refine this geometry by adding changes from the manual optimization and add features such as smooth corners to the separator.
- (c) Make the separator possible to manufacture while changing the interior geometry as little as possible.

3. More Complex Procedure [Refining the Methodology]

- (a) Perform testing on the actual cooling circuit using transparent tubes. This would give a better idea regarding the flow structures and velocities along the system and when entering the separator. The flow structures should thereafter be replicated in the simplified rig and the knowledge could be used to find an optimum position for the separator.
- (b) Use thinner tubes in the rig to reduce the risk for stagnant pockets of air.
- (c) Improve the computational model. Use information retrieved in 3(a) and improve the correlation between experiments and computational model. It would be of interest to make the model more generic using a feature such as S-gamma which allows for variable bubble size.
- (d) Constrain the parametric CAD model so that it can be used efficiently in an optimization. Also, it can be relevant to add a feature which enables a rectangular shaped inlet, which was advocated in literature.
- (e) Discuss the relevant importance of the performance parameters and set all but one of them to desired values. Alternatively, set relative importance factors for the various performance parameters.
- (f) Make an initial guess about the optimal design and/or set relevant constraints based on the performed DOE optimization and perform an automated optimization using modeFRONTIER to acquire an optimum design.
- (g) Perform steps 2(b) and 2(c).

In addition, it is of interest to discuss the air extraction rate and quality needed in the vehicle. A T-connection has proven to be able to extract air even though the rate or the quality of the extraction cannot be guaranteed. If the time it takes to reach a lower level of air content and the system does not need to be fully free from air, a T-connection or perhaps an air extraction valve from the radiator might be sufficient.

Bibliography

- [1] P. Wollen. “Gas in engine cooling systems: occurrence, effects and mitigation”. In: *Ph.D. thesis, Mechanical Engineering Department, Loughborough University*, (2012).
- [2] B. Went. “Pump cavitation and how to avoid it”. In: *FLYGT a xylem brand* (2014).
- [3] U. Nilsson. *Cooling system analyst, Volvo Cars Corporation*. Interview and Discussions. 2018.
- [4] The Editors of Encyclopædia Britannica. *Cooling system*. URL: <https://www.britannica.com/technology/cooling-system>.
- [5] S. M. Mousavian and A. F. Najafi. “Numerical simulations of gas–liquid–solid flows in a hydrocyclone separator”. In: *Springer-Verlag* (2008).
- [6] R. Hreiz et al. “On the effect of the nozzle design on the performances of gas–liquid cylindrical cyclone separators”. In: *International Journal of Multiphase Flow* 58 (2013), pp. 15–26.
- [7] R. Utikar et al. “Hydrodynamic Simulation of Cyclone Separators”. In: *International Journal of Multiphase Flow* 58 (2013), pp. 15–26.
- [8] M. Allen et al. “The Characterisation of a Centrifugal Separator for Engine Cooling Systems”. In: *SAE Technical Paper 2015-01-1693* doi:10.4271/2015-01-1693 (2015).
- [9] Ovadia Shoham Srinivas Swaroop Kolla Ram S. Mohan. “Structural Integrity Analysis of Gas–Liquid Cylindrical Cyclone (GLCC) Separator Inlet”. In: *Journal of Energy Resources Technology* (2018).
- [10] Panagiotis I. Kefalas and Dionissios P. Margaris. “Numerical Analysis of Fluid Flow in a Compact Phase Separator”. In: *The Open Mechanical Engineering Journal* 2 (2008), pp. 21–31.
- [11] R. Hreiz, C. Gentric, and N. Midoux. “Numerical investigation of swirling flow in cylindrical cyclones”. In: *Chemical Engineering Research and Design* 89 (2014), pp. 2521–2539.
- [12] P. Chang et al. “Numerical Simulation on Structure Optimization of Liquid-Gas Cylindrical Cyclone Separator”. In: *International Journal of Chemical Engineering* 2016.Article ID 3187631 (2016).
- [13] R. Hreiz et al. “Hydrodynamics and velocity measurements in gas–liquid swirling flows in cylindrical cyclones”. In: *Chemical Engineering Research and Design* 92 (2014), pp. 2231–2246.
- [14] Gene E. Kouba, Ovadia Shoham, and Siamack Shirazi. “Design and Performance of Gas Liquid Cylindrical Cyclone Separators”. In: *BHR Group 7th International Conference on “Multiphase 95”, Cannes, France*, 1(3) (1995).
- [15] Le Van Sy. “Influence of inlet angle on flow pattern and performance of gas-liquid cylindrical cyclone separator”. In: *Journal of Manufacturing Technology Research* 8.1-2 (2017), pp. 61–82.
- [16] A. Ghasemi, M. Shams, and M. Mahdi Heyhat. “A numerical scheme for optimizing gas liquid cylindrical cyclone separator”. In: *Journal of Process Mechanical Engineering* 231.4 (2017), pp. 836–848.
- [17] Thundil Karuppa Raj R. et al. “Parametric Study of a Phase Separator used in A/C Automotive System using CFD Tool”. In: *Research journal of engineering Sciences* 1(3) (2012), pp. 15–21.
- [18] S. Sasic. *TME160 - Multiphase flow, Lecture Slides*. University Lecture. 2017.
- [19] L. Davidson. “Fluid mechanics, turbulent flow and turbulence modeling”. In: *Division of Fluid Dynamics, Department of Applied Mechanics* (2018).
- [20] A.Read and R.Piccioli. *Introduction to Multiphase Flows*. June 2015.
- [21] H.-J. Kim. *Multiphase Modelling in STAR-CCM+*.

-
- [22] M. Chrigui. “Eulerian-Lagrangian Approach for Modeling and Simulations of Turbulent Reactive Multi-Phase Flows under Gas Turbine Combustor Conditions”. In: *Dissertation, Vom Fachbereich Maschinenbau An der Technische Universität Darmstadt* (2005).
- [23] STAR-CCM+. *STAR CCM+, Documents, Theory*. URL: https://documentation.theesteveportal.plm.automation.siemens.com/starccmplus_latest_en/index.html?param=RtUNa&authLoc=https://theesteveportal.plm.automation.siemens.com/AuthoriseRedirect.
- [24] K.J. Josefsson and M. Lind. “A CFD Method for Simulation of Gas-Liquid Flow in Cooling Systems - An Eulerian-Eulerian Approach”. In: *Master Thesis, Department of Management and Engineering - Division of Applied Thermodynamics and Fluid Dynamics, Linköping University* (2016).
- [25] M. B. Graf E. M. Greitzer C. S. Tan. *Internal Flow: Concepts and Applications (Cambridge Engine Technology Series)*. Cambridge University Press; 1 edition, 2007.
- [26] Martin Sommerfeld Clayton T. Crowe John D. Schwarzkopf. *Multiphase Flows with Droplets and Particles*. Taylor & Francis Group; 2 edition, 2012.
- [27] Roman Thiele. “STAR-CCM+ Support”. In: *Mail contact* (2018).
- [28] E. Ljungskog and U. Nilsson. “CFD for Underhood Modeling - Development of an Efficient Method”. In: *Master Thesis, Department of Applied Mechanics, Division of Fluid Dynamics, CHALMERS UNIVERSITY OF TECHNOLOGY* (2014).
- [29] S. Lardeau and F. Billard. “Development of an elliptic-blending lag model for industrial applications”. In: *54th AIAA Aerospace Sciences Meeting* (2016).
- [30] M. Cable. “An Evaluation of Turbulence Models for the Numerical Study of Forced and Natural Convective Flow in Atria”. In: *Queen’s University Kingston, Ontario, Canada* (2009).
- [31] H.K. Versteeg and W. Malalasekera. *An introduction to Computational Fluid Dynamics*. Pearson Education Limited, Second edition, 2007.
- [32] L. Davidson. “Numerical Methods for Turbulent Flow, Old Lecture Notes”. In: *Division of Fluid Dynamics, Department of Applied Mechanics* (2005).
- [33] T. van den Boom and B. De Schutter. “SC42055, Optimization in System and Control”. In: *Optimization in System and Control Course Reader, TU Delft* (2015).
- [34] ESTECO. *modeFRONTIER*. URL: <http://www.esteco.com/modelfrontier>.
- [35] ESTECO. *modeFRONTIER, Help, Theory and Tutorials*.
- [36] A. Babajimopoulos. *Technical Expert, Fluid Dynamics and Heat Transfer, Volvo Cars Corporation*. Interview and Discussions. 2018.
- [37] M. Cavazzuti. “Optimization Methods”. In: *From Theory to Design Scientific and Thechnological Aspects in Mechanics* (2013).
- [38] Webinar EnginSoft. *modeFRONTIER & RSMs: Exploit Your Data and Speed Up Your Optimization*. URL: <https://www.youtube.com/watch?v=UM1hsEAuLIQ>.
- [39] Jim Frost. *How To Interpret R-squared in Regression Analysis*. URL: <http://statisticsbyjim.com/regression/interpret-r-squared-regression/>.
- [40] A. Folkesson. *Separator Part Template, Powerpoint Slides*. Internal document. 2018.

Appendix A

Separator degas performance Test Report

Issuer/CDS ID	J. Forsgren, D. Winqvist
Issue Date	2018-03-27
Issue	1
File name	Separator degas performance
Security Class	Thesis work

Appendix A

Organization	Type of document		
Thesis work, Department for cooling system	Test report		
Name of document	Issue	Issue date	Page
Separator degas performance	1	2018-03-27	2

Appendix A

Type of document		Page
Test Report		3 (17)
Name of document	Issue	Date
Separator performance	1	2018-03-27
Issuer (dept.name,CDS-id)		Appendix
Johan Forsgren, David Winqvist		

Table of Contents

1. REVISION HISTORY	4
2. INTRODUCTION	4
3. MATERIALS	4
3.1. Outer Circuit	4
3.2. Inner Circuit	4
4. TEST EQUIPMENT	5
5. TEST RIG DESIGN	5
5.1. Schematic test set up	6
5.2. Test rig	7
6. TEST PERFORMANCE	10
6.1. Step by step performance	11
6.2. Test schedule	12
7. RESULTS	12
7.1. General visual findings	12
7.2. Visual findings from A	13
7.2.1. Test A1	13
7.2.2. Test A2	13
7.2.3. Test A3	13
7.2.4. Test A4, A5	13
7.3. Visual findings from B	14
7.3.1. Test B1	14
7.3.2. Test B2	14
7.3.3. Test B3	14
7.3.4. Test B4, B5	14
7.4. Measured findings	14

Appendix A

Type of document Test Report		Page 4 (17)
Name of document Separator Performance	Issue 1	Date 2018-03-27

1. Revision History

Version	Date	Author(s)	Revision Notes
1	20180327	J.Forsgren, D.Winqvist	

2. Introduction

This test is designed to evaluate the performance of the degas separator placed in the LT part of the cooling system. The test is designed in order to replicate the true environment as good as possible and will be used to validate a computational model of the separation. The test is a part of the master's thesis *Testing and Modeling of Air Elimination in Automotive Cooling System*.

3. Materials

In this section, all the material and equipment used are listed. The test rig is designed having an outer and an inner circuit. The materials used are listed accordingly.

3.1. Outer Circuit

Number:	Part:	Data or Comment:
1	Test frame	
1	Outer tube	Ø: 0.02[m], L: 6[m], reinforced tube
4	T-Couplings	
2	Taps	
1	Valves	
1	Pump	AISIN 09040-48020, 0C130978

3.2. Inner Circuit

Number:	Part:	Data or Comment:
1	Separator outlet tube	Ø: 0.02[m], L: 0.5[m], transparent
1	Separator inlet tube	Ø: 0.018[m], L: 0.5[m], transparent
1	Separator-measurement connection tube	Ø: 0.018[m], L: 0.4[m], transparent
2	Valves	
2	Pressure gauge connectors	
1	Temp. gauge connector	
1	Separator	[CAD-File, or reference to appendix], Transparent
1	Graded measurement tank	250 [ml]

Appendix A

Type of document Test Report		Page 5 (17)
Name of document Separator Performance	Issue 1	Date 2018-03-27

4. Test Equipment

Number:	Part:	Data or Comment:
1	Volume flow sensor	SIEMENS SITRANS F M 1100 F sensor with SIEMENS SITRANS F M MAG 6000 transmitter
2	Pressure sensors	-BELL&HOWELL BHL-4045 -TRANS BHL-4100-05
1	Measurement module	M-SENS DPS 4*1B
1	Measurement module amplifier	SIM-STG
1	Measurement model thermo elements	SIM-THERMO 16
1	Waveform generator	KEYSIGHT TECHNOLOGIES, 33521B Series
1	Direct current power supply	MASCOT 9522
1	Computer	HP, ZBook 15 3G Programs: - VECTOR VN1610
2	Cameras	- GOPRO HERO5 - CANON EOS 100D

5. Test Rig Design

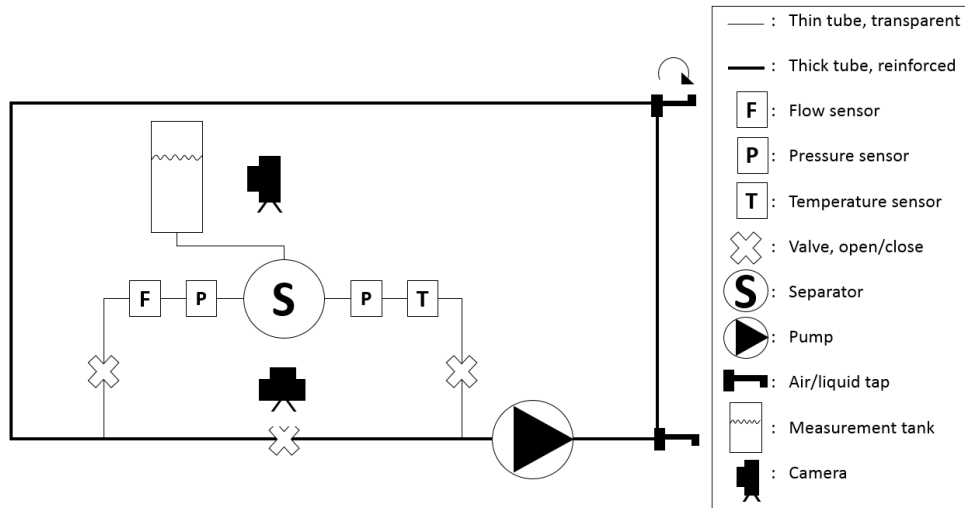
The test rig was built according to the figures in the coming sections. There are both a schematic image of the test as well as pictures of the actual set up. In the outer circuit, a thicker tube is used in order to reduce the total length of the tube, keeping the volume at approximately 3.5 litres. In the inner part, tubes are used in order to fit the size of the inlet/outlet of the separator. The rig is controlled via valves so that the inner circuit can either be connected or disconnected. In the outer circuit there are one tap in the bottom and one in the top. This feature is used when removing a known amount of liquid from the system and replacing with air resulting in a known volume fraction of air in the system. The top tap can also be rotated so that no air is caught in the geometry of the tap. The air can then be evenly distributed in the outer circuit by letting the pump drive the flow for a few revolutions. When the air is properly distributed and flowing with the correct velocity, the inner circuit can be connected, forcing the flow to go via the separator. In this part of the circuit, the flow temperature, volume flow rate and pressure are measured. The pressure is measured before and after the separator so that the pressure drop can be found. The quality of the separator is evaluated through measuring the amount of air leaving the system over time. The separator is pushing the air to the top where it is changing position with the coolant in the measurement tank. During the test, two cameras are used to record the amount of air leaving the separator as well as studying the process in the transparent separator.

The test is performed in two test sections. One where the inlet and outlet are set according to the current configuration used in the car and the other one where the two have swapped place. These two test runs have been named A and B respectively.

Appendix A

Type of document Test Report	Page 6 (17)	
Name of document Separator Performance	Issue 1	Date 2018-03-27

5.1. Schematic test set up



Appendix A

Type of document	Page	
Test Report	7 (17)	
Name of document	Issue	Date
Separator Performance	1	2018-03-27

5.2. Test rig

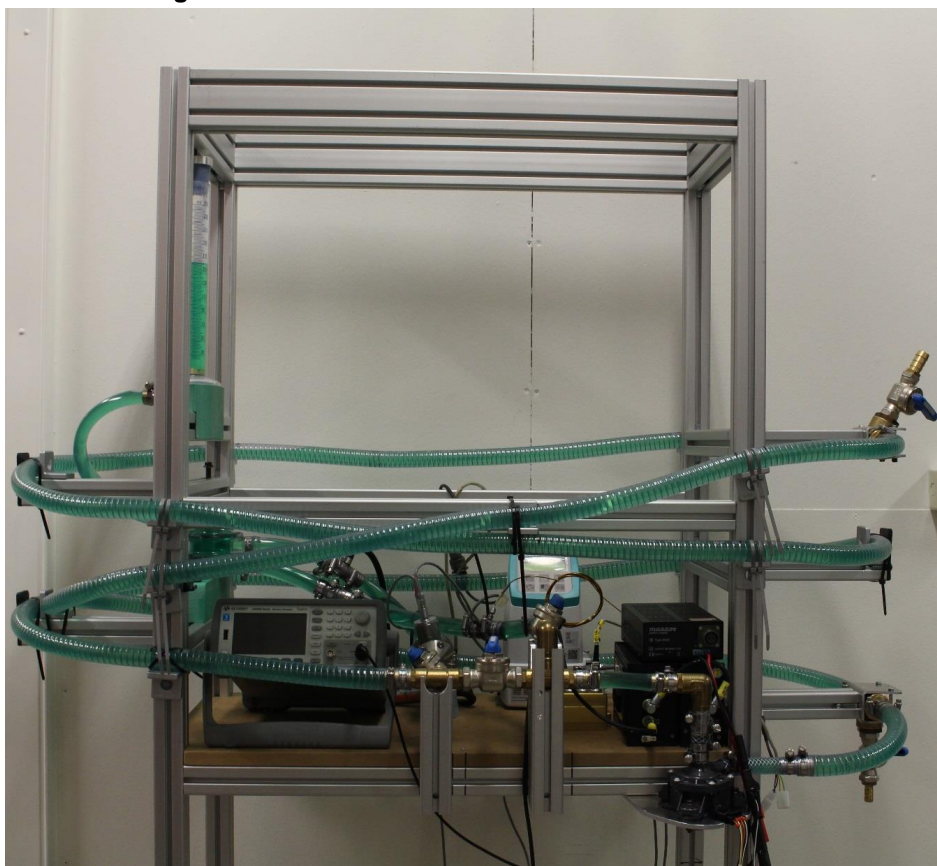


Figure 1: Test rig.

Appendix A

Type of document	Test Report		Page	8 (17)	
Name of document	Separator Performance	Issue	1	Date	2018-03-27



Figure 2: Separator mounted in test rig. In the lower right corner the connections for the pressure sensors are visible.

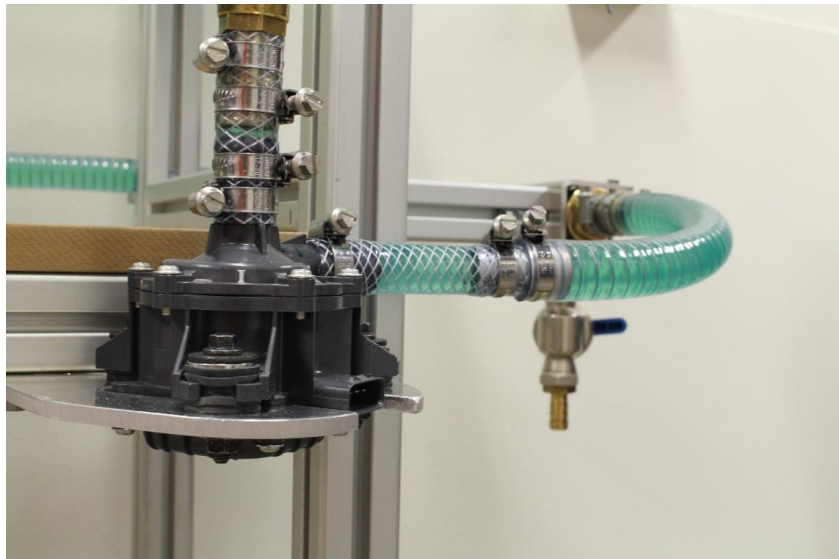


Figure 3: 30 W electric pump to drive the flow.

Appendix A

Type of document	Page	
Test Report	9 (17)	
Name of document	Issue	Date
Separator Performance	1	2018-03-27

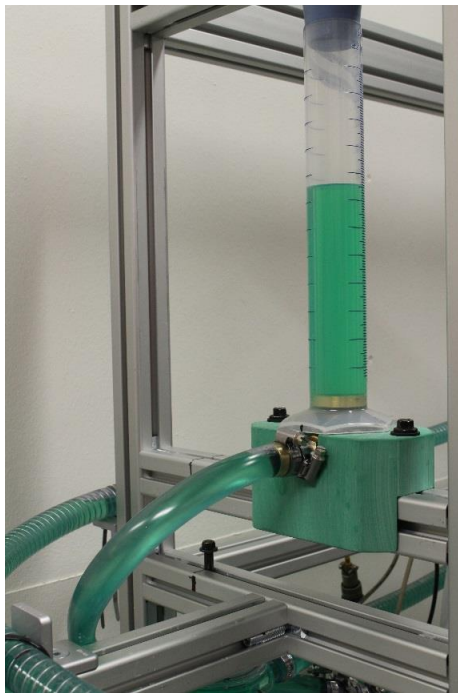


Figure 4: Graded cylinder to measure volume of separated air. The connecting hose is in direct connection to the separator gas outlet.

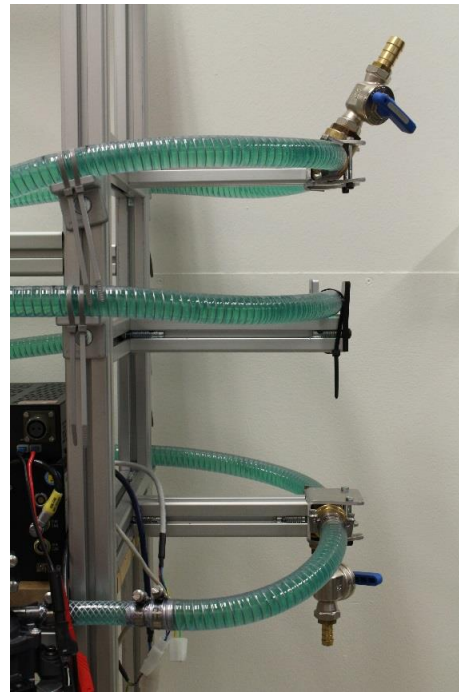


Figure 5: Taps on the outer circuit used to drain coolant and evacuate air when filling the system.

Appendix A

Type of document	Page	
Test Report	10 (17)	
Name of document	Issue	Date
Separator Performance	1	2018-03-27



Figure 6: Valves to open and close the inner circuit.



Figure 7: Hoses in the inner circuit leading up to the separator. Flow meter, temperature sensor and pressure sensors are connected to the circuit.

6. Test Performance

Appendix A

Type of document		Page
Test Report		11 (17)
Name of document	Issue	Date
Separator Performance	1	2018-03-27

6.1. Step by step performance

Filling the system:

1. Open all valves.
2. Close the bottom tap.
3. Open top of measurement tank.
4. Open the top tap.
5. Fill the system gently from the measurement tank until the system is full. i.e. the coolant starts spilling out from the top outlet.
6. Run the pump and try to remove all air from the pump.
7. Repeat stage 5.
8. Close top inlet.
9. Note the amount of coolant filled.
10. Fill gas meter to reference level.
11. Close top of measurement tank.

Calibrating the system:

1. Calibrate pressure sensor, temperature sensor and flow meter.
2. Ramp the pump with the separator system connected. Note at what pump effect the wanted volume flow rate occurs. In this way it is known what pump effect to use for the test.

Introducing the air:

1. Close the two valves to the inner circuit.
2. Open the top outlet.
3. Place a graded cylinder under the bottom tap and open the tap.
4. Empty the same amount of water as you want air into the system.
5. Close the bottom tap.
6. Close the top tap and turn the tap downwards.

Running the test:

1. Start the pump to spread the air in the system. Check visually.
2. Set pump to achieve wanted flow rate.
3. Place the camera so that it clearly sees the measurement tank and separator.
4. Start the cameras.
5. Show the cameras what test it is.
6. Open the two valves to the separator circuit.
7. Close valve for outer circuit.

Data collection:

1. Record the pressure on both sides of the separator.
2. Record and monitor the temperature to ensure no large variations occur.
3. Note the volume flow rate in the separator circuit.
4. Analyse the film and make graphs for the de-gas performance.

Appendix A

Type of document Test Report		Page 12 (17)
Name of document Separator Performance	Issue 1	Date 2018-03-27

Preparing for the next test:

1. Open all valves in the system and the top tap.
2. Open top of measurement tank.
3. Fill the measurement tank to reference value, use the liquid removed from previous test.
4. Close all valves and top of measurement tank.
5. Remove coolant from the system until the 4% level is once again reached.
6. Run the next test.

6.2. Test schedule

There were three tests performed on the volume flow rate of 8.4 l/min since this is the maximum flow rate which is found in the cooling system circuit. Also three tests were performed for 12.6 l/min in the A tests, but in the B tests only two test runs were done since the results were stable and showed repeatability. A lower flow rate proved to not be able to move the air through the system, hence these could not be tested for other aspects than the pressure. The test showed that the results for higher flow rates were very stable and hence there was no need to perform many tests.

Test ID:	Volume fraction:	Volume flow rate:
A1.1	4%	8.4 l/min [0.14 l/s]
A1.2	4%	8.4 l/min [0.14 l/s]
A1.3	4%	8.4 l/min [0.14 l/s]
A2.1	4%	12.6 l/min [0.21 l/s]
A2.2	4%	12.6 l/min [0.21 l/s]
A2.3	4%	12.6 l/min [0.21 l/s]
A.3	4%	16.8 l/min [0.28 l/s]
A.4	4%	4.2 l/min [0.07 l/s]
A.5	4%	2.5 l/min [0.042 l/s]

Test ID:	Volume fraction:	Volume flow rate:
B1.1	4%	8.4 l/min [0.14 l/s]
B1.2	4%	8.4 l/min [0.14 l/s]
B1.3	4%	8.4 l/min [0.14 l/s]
B2.1	4%	12.6 l/min [0.21 l/s]
B2.2	4%	12.6 l/min [0.21 l/s]
B.3	4%	16.8 l/min [0.28 l/s]
B.4	4%	4.2 l/min [0.07 l/s]
B.5	4%	2.5 l/min [0.042 l/s]

7. Results

7.1. General visual findings

Appendix A

Type of document		Page
Test Report		13 (17)
Name of document	Issue	Date
Separator Performance	1	2018-03-27

When the flow rate was low, the system proved not to be able to move all the air in the system but large bubbles of air collected in the top parts of the system. However, when the large bubbles reached the separator, the degassing worked very well for these large bubbles.

When starting the system, the flow was abruptly stopped in the outer circuit to start going through the inner one. This caused some delay in the system and it was clear that the pump got affected by the sudden change in volume fraction (when connecting the separator part, liquid without gas firstly entered the pump). Also, the pump had to accelerate the quiescent fluid in the inner circuit. The effect was that the flow seemed to slow down for a couple of seconds, which might have led to that bubbles had the time to gather in larger groups. The results directly at the start of the test might therefore not be as trustworthy as the values later.

Throughout the test it was found that the separator did gather the air in the center and towards the top of the outlet. This effect did however vary with the flow rate. When reaching the top, the bubbles did not seem to be able to find its way out due to the shape of the gas outlet. When increasing the velocity, barely any air could find its way out since there seemed to be turbulence in the outlet, dragging with it all air through the liquid outlet. For lower velocities, the air seemed to gather in larger bubbles and thereafter it left the separator and went up to the measuring tank.

The bubble size is clearly decreased when increasing the velocity of the flow.

There seem to be a vortex at the entrance of the gas outlet which is working 90 deg from the vortex in the separator. This appears to have the effect that it is blocking degassing of the separator slightly.

7.2. Visual findings from A

It could be seen that the vortex in the separator did not align very well with the outlet of the separator. The vortex had its top center a little bit to the side of the outlet and therefore not directing the air very well.

7.2.1. Test A1

The air gathered in the separator top somewhat good but had troubles getting out of there.

7.2.2. Test A2

The effect of increasing the velocity is clearly negative. Much of the air that enters the separator is just directly flushed out again. There is a bubble in the top of the separator which is basically "in the way" for the rest of the air. It is also clear that the bubble size is much smaller for a higher velocity

7.2.3. Test A3

Similar results as the A2 but even smaller bubbles and an even lower efficiency. There is a continuous flow of small bubbles to the measuring tank but they are so small that there is no strong efficiency. There seem to be turbulence in the gas outlet which makes coalescence harder.

7.2.4. Test A4, A5

Flow velocity was too low. The air gathered in big bubbles and therefore this test is not representative for other than the pressure drop. In this test the centrifugal effect of the separator did not show but the separator worked as a gravitational one. This can however be the case in an actual cooling system as well where the shape of the system is similar. One could with this information argue that the separator should work best for a higher flow velocity because this is

Appendix A

Type of document		Page
Test Report		14 (17)
Name of document	Issue	Date
Separator Performance	1	2018-03-27

when the air is brought along with the flow. For lower velocities it works as a gravitational separator when the air reaches it.

7.3. Visual findings from B

A clear increase in efficiency could be found when changing the inlet and outlet. Especially for the lower velocities (8.4 l/min). It could also be seen that the vortex was standing in a better position and was gathering the bubbles more central in the separator and was better aligned with the separator outlet.

7.3.1. Test B1

The best efficiency of all the tests was found for this value. The bubbles shoot to the top and therefore the efficiency is good. Only a visually small amount of smaller bubbles leave through the liquid outlet.

7.3.2. Test B2

Does not show equally amount of improvement from the A design. However it seems slightly better. The vortex is strong and it tries to gather the bubbles. The top of the separator does not let much out. The vortex effect does not seem good enough to separate the flow by itself. In the outlet there is a vortex in the other direction, sideways so to say.

7.3.3. Test B3

Very similar to the A3. The bubbles are very small and the vortex does not seem able to separate them from the flow. Some small bubbles do leave the separator in a continuous flow, but due to the size of the bubbles the amount of air that they contain is very small. Hence, the efficiency is also bad.

7.3.4. Test B4, B5

These test were not filmed or measured since it was found in previous test that this result would not give any valuable data. Therefore only the pressure difference was collected.

7.4. Measured findings

Pressure, temperature and air elimination data were collected during the tests. The volume flow rate was not recorded throughout the tests but was instead monitored via a physical display to ensure a correct flow rate was held during each test run. In Figure 8 the instantaneous pressure drops for the different tests are shown. In the tests where two or three runs were performed, a mean value has been used. Note that there are some differences in how many samples were taken in each test, especially for A5 which was only recorded for a short period of time. As suspected, the pressure drop increases with increasing volume flow rate and it can also be noticed that the pressure drops in the A and B tests are somewhat similar. Hence, swapping places for in- and outlet has no large effect with respect to pressure drop.

During the tests it was important to make sure the temperature of the coolant did not increase too much due to friction and the pump impeller work. Large variations in temperature would affect the properties of the coolant and make the tests non comparable. In Figure 9 the mean temperature from each test run is plotted. The temperature was kept stable at approximately 23 °C making the variations non-significant for.

Appendix A

Type of document	Test Report		Page	15 (17)	
Name of document	Separator Performance	Issue	1	Date	2018-03-27

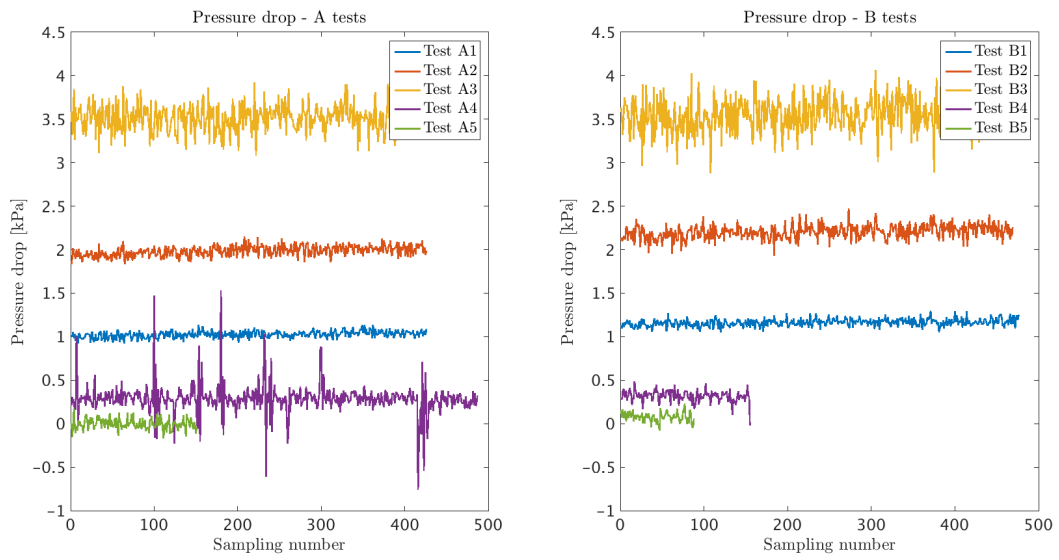


Figure 8: Pressure drop plots from experimental data.

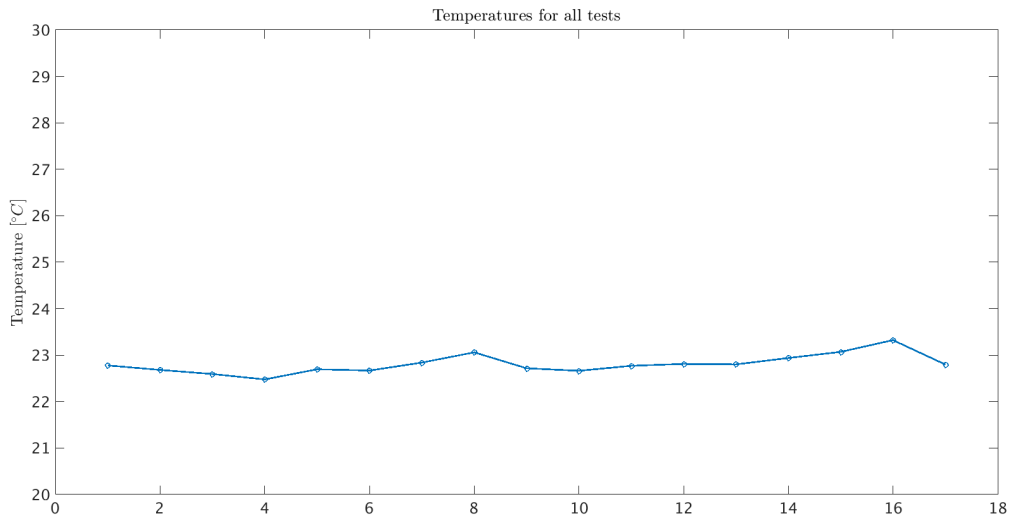


Figure 9: Mean temperature values for all test runs.

Appendix A

Type of document Test Report		Page 16 (17)
Name of document Separator Performance	Issue 1	Date 2018-03-27

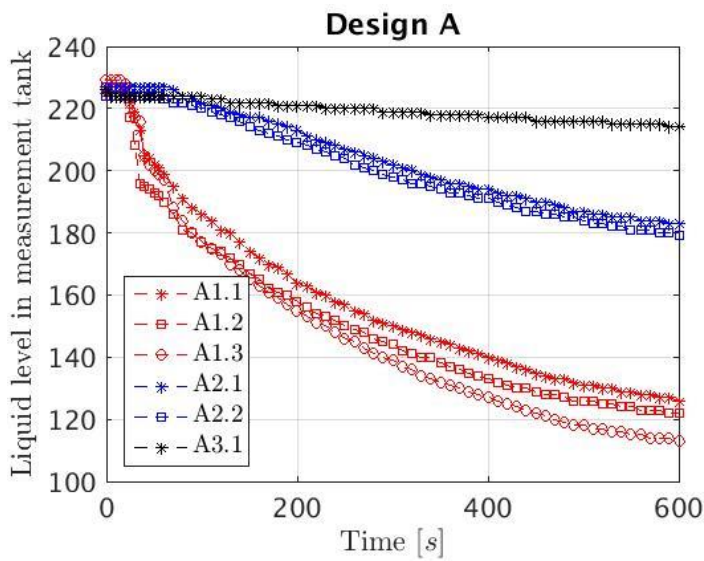


Figure 10: Separator degas performance measurements from tank over time, Design A [Raw data]

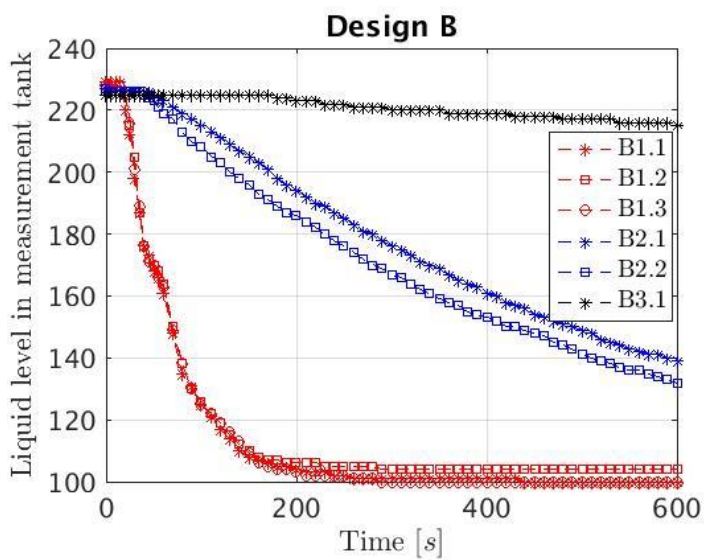


Figure 11: Separator degas performance measurements from tank over time, Design D [Raw data]

Appendix A

Type of document		Page
Test Report		17 (17)
Name of document	Issue	Date
Separator Performance	1	2018-03-27

8. Discussion and sources of error

8.1. Sources of error

- When connecting the inner circuit, there was a tendency of the flow to slow down for a few seconds. This might have caused some of the bubbles to gather into larger ones, resulting in an unnaturally high efficiency of the separator at the initial stages.
- The pressure sensors are known to have a level of tolerance which is quite high. Therefore this should be taken into account when reviewing measurements.
- When the air left the separator into the measurement tank, there was a bubble standing at the entrance of the measurement tank. Therefore this led to a slight delay of the bubble rising to the top. In one test, the bubble was accidentally removed when filling the system. Therefore there is a delay before any air is entering the measurement tank for this test.
- There is an overall delay when the bubbles leave the separator until they reach the measurement tank and can change the level of the liquid surface.